ABSTRACT

Comets are small bodies in the solar system that consist of icy and dusty materials. The heart of the comet, called the cometary nucleus, is a remnant of icy planetesimals formed in the solar nebula 4.6 Gyrs ago. Once the cometary nuclei had formed, they were scattered into two current dynamical reservoirs of comets (the Oort cloud and the Kuiper belt) and into other places (inner and outer parts of the solar system) by the gravitational scattering caused by the migration of planets in the early solar system. After scattering to current dynamical reservoirs, comets have spent most of their lifetime in low-temperature regions far from the sun, where no interior modifications can occur. Therefore, comets are considered to contain information about the solar system formation. However, their physico–chemical properties (e.g., the chemistry of their icy materials, their nuclear structure, and the mineralogy of their dust grains) have not been definitively interpreted. Because the information of the previous formation environment should be preserved in the abundance ratio of nuclear spin isomers (or the ortho-to-para abundance ratio; OPR) and the isotopic ratios of cometary volatiles, we study the OPRs and the nitrogen isotopic ratios of the cometary volatiles, thereby reveal the physic–chemical conditions in the solar nebula or in the presolar molecular cloud. Our scientific goal is to understand the origin of cometary volatiles based on these properties.

We developed a method that estimates the OPRs of cometary ammonia from the emission spectra of NH_2 more precisely than previous estimates (Shinnaka et al., 2010) and increased the number of investigated comets by three times or more, relative to the previous investigation (Shinnaka et al., 2011). We obtained high-dispersion optical spectra of 18 comets using the Subaru/HDS, VLT/UVES, and other telescopes/instruments. We also developed another technique that estimates the OPRs of cometary water from the emission spectra of water ions (Shinnaka et al., 2012). Moreover, we reported the nitrogen isotopic ratio of ammonia in a single comet for the first time (Shinnaka et al., 2014).

The OPRs of cometary water and ammonia in comets cluster around a

value corresponding to the nuclear spin temperature of ~30 K. The OPRs of cometary volatiles may not reflect their original formation conditions in the solar nebula or in the interstellar molecular cloud but rather the environment in the inner coma. Sole water molecules might chemically react with the water clusters that formed during the expansion of ejected gas and dust, accelerating the ortho–para conversion of water in the inner coma.

We found that the nitrogen isotopic ratios of the cometary ammonia from two single comets were fractionated of ^{15}N by at least twice that of the proto-solar ratio. ^{15}N-fractionations are very uncommon once the cometary nucleus has formed, so the nitrogen isotope ratio conserves preformation information. According to theoretical studies, ^{15}N-fractionation of cometary molecules could arise by chemical reactions related to para-H_2 under the extremely low-temperature environments (~10 K) of dense cloud cores. This suggests that cometary ammonia formed in the molecular clouds at ambient temperatures around 10 K. This temperature is lower than previously estimated from the OPRs ratios (~30 K).

We conclude that most cometary organics (at least ammonia molecule) were formed in the natal molecular cloud at ~10 K, although cometary water originates from both the molecular cloud and the solar nebula.

CONTENTS

1. GENERAL INTRODUCTION

1.1. SCIENTIFIC GOALS IN COMET SCIENCES

My scientific goal is to understand the formation environment of solar system matters. The solar system is a star-and-planetary system whose components (such as planets, satellites, asteroids, and comets) have been investigated to high accuracy in *in situ* explorer observations. Moreover, solar system objects have been extensively observed from space and ground-based observatories. By understanding our solar system in detail, we acquire a general understanding of how star-and-planetary systems form and evolve. The conditions of the early solar system (such as temperature, density, and composition) are especially important for understanding the chemical evolutions therein.

The solar system formation process in molecular clouds was summarized by Shu et al. (1987).

(1) Some 4.6 Gyrs ago, a region of relatively dense interstellar matter (called the molecular cloud) formed under some gravitational influences. The original matter may have been sourced from supernova explosions, nova explosions, supply from AGB stars, etc. Various chemical reactions occurred in the molecular cloud.

(2) Distributions of density, temperature, and ionization degrees in the molecular cloud were inhomogeneous. The higher density regions are known as the molecular cloud core.

(3) When the pressure at the molecular cloud core exceeded the critical density (t_{SS} = 0 yrs; t_{SS} denotes the age of the solar system), the proto–sun formed at the center of the molecular cloud core by gravitational collapse (t_{SS} = ~10^4 yrs). That is, the stages of a molecular cloud and a molecular cloud core are before the star formation (t_{SS} <0 yrs).

(4) Governed by the angular momentum of the whole molecular cloud core, gas and dust materials in the molecular cloud accreted around the proto–sun, forming a disk (called the solar nebula; t_{SS} = 10^5–10^6 yrs). Many kinds of chemical reactions in the solar nebula were

proceeded, depending on the spatially and temporally varying temperature, abundances, density, and ionization degree in the solar nebula.

(5) The solid materials in the solar nebula aggregated into planetesimals, the building blocks of planets (t_{SS} = 10^4–10^7 yrs). Rocky planetesimals formed within the snowline (defined as the boundary between the gaseous and solid phases) of water, whereas icy planetesimals (including the icy and dust materials) formed far from the snowline of water.

(6) Once the icy and rocky planetesimals had formed in the solar nebula, the planetesimals continued to aggregate and eventually grew into planets (t_{SS} <10^7 yrs). Planetesimals not captured by planetary growth were scattered into the Oort cloud, Kuiper belt, and other places (inner and outer parts of the solar system) by planetary migration. Today's cometary nuclei are the surviving icy planetesimals that form the coma and the tail when approaching the Sun.

(7) Stages (1)–(6) led to the establishment of the current solar system (t_{SS} <10^9 yrs). Cometary nuclei spend much of their lifetimes far from the Sun. In such low-temperature environments, comets undergo no interior evolution, and therefore conserve the solar system's primordial properties.

Cometary nuclei retain pristine materials as mentioned above, providing clues on the physical conditions of the early solar system. Rocky or icy planetesimals formed in the solar nebula, depending on their distance from the Sun. The icy planetesimals formed in the outer region (approximately 3 to 30 AU), beyond the snowline of water. It is thought that some of the icy planetesimals scattered into the Kuiper belt (50–~300 AU) or the Oort cloud (~10^4–10^5 AU) regions as cometary nuclei. Planetesimals and gases not captured into planets were ejected into regions far from the Sun by close encounters with giant migrating planets (Grand Tack model: Walsh et al., 2011; and references therein, Nice model: Tsignis et al., 2005; and references

therein). Since the temperature in these regions (<10 K) is below the sublimation temperatures of the volatiles contained in the cometary nuclei, chemical reactions are blocked in the nuclei interiors. Therefore, comets are considered as the most pristine icy bodies in the solar system. The materials of cometary ices can be investigated by observing the coma and tail formed by the sublimated icy components as the cometary nucleus approaches the Sun. However, the real meanings of some observed metrics are still being debated.

The physical parameters related to the chemical reactions (such as temperature, density, chemical abundance, and ionization degree) can be inferred from observations of cometary volatiles. Temperature is the most important parameter because it controls the chemical reactions in the solar nebula and/or the presolar molecular cloud. Note that the physico–chemical properties of comets reflect their different environments. For example, the chemical compositions of existing ices might reflect the chemical compositions of the environment in which the cometary nuclei formed (Muuma & Charnley, 2011 and references therein); the isotopic ratios of cometary volatiles might reflect the temperature and number density of the gas in which the molecules formed (Balsiger et al., 1995; Manfroid et al., 2009; Lis et al., 2013; Rousselot et al., 2014; Shinnaka et al., 2014; and references therein); the composition of the dust components might reflect the temperature of the inner solar nebula and the strength of turbulent mixing (in the radial and vertical directions) in the solar nebula (Wooden et al., 1999; Gail et al., 2001; Bockelée–Morvan et al., 2002).

Moreover, our solar system is located ~8 kpc from the galactic center of the Milky Way Galaxy. Its rotation period around the galactic center is ~2 × 10^8 years (Honma et al., 2012). Since the solar system formed from materials ~8 kpc distant from the galactic center, cometary materials provide information on the intergalactic matter that existed 4.6 Gyrs ago. Furthermore, the distribution of cometary orbits in the Oort cloud has been affected by nearby attractors in the Galaxy, such as other stars and giant molecular clouds that encounter the solar system.

1.2. PREVIOUS STUDIES ABOUT COMETARY PRISTINE PROPERTIES

Here, we briefly summarize the progress made in comet science during the last decades. Cometary studies can be classified into volatile and refractory studies which investigate the volatile and dust cometary materials, respectively.

To infer information of the early solar system, researchers focus on the following properties of cometary volatiles:

(V.1) Chemical abundances of cometary ices (see Section 1.2.1).

(V.2) OPRs of the cometary volatiles (see Section 1.3).

(V.3) Isotopic ratios of the major elements in the cometary volatiles (such as hydrogen, nitrogen, carbon, oxygen, and sulfur; see Section 1.2.2).

To investigate the physical condition in the early solar system, the following properties of the dust components are investigated:

(D.1) The structures of cometary dust grains, such as the abundance ratio of dust materials, size distributions, shapes, and fluffiness. These parameters may be related to radial and vertical mixing and the temperature distributions in the solar nebula.

(D.2) The crystalline-to-amorphous ratio of cometary silicates is related to phenomena, such as radial mixing, dynamical evolution, and the temperature distributions in the solar nebula. The existence of crystalline silicate in a cometary nucleus is regarded as evidence of large-scale radial mixing in the solar nebula. The abundance ratio of crystalline to amorphous silicate grains is quite small in interstellar matters (Waters et al., 1999; Justtanont et al., 1997; and references therein). Amorphous silicate is crystallized by high-temperature (> 1000 K) annealing close to the proto–sun, yet comets are formed far from the Sun under low-temperature conditions (<150 K, corresponding to the sublimation temperature of water).

The remainder of this thesis concentrates on the cometary volatiles, with a view of understanding their chemical evolution and formation conditions in the solar nebula and/or in the presolar molecular cloud.

1.2.1. CHEMICAL ABUNDANCES

Active comets have been assigned to the Oort cloud, Kuiper belt, and other reservoirs based on their orbital properties. However, dynamical evolution models of planetesimals now suggest that these reservoirs formed in a common region, or at least in overlapping regions (Walsh et al., 2011; Tsignis et al., 2005). Moreover, a large fraction of the comets now occupying the Oort cloud may have been captured from stars in the Sun's birth cluster, before the cleaning of gas in the molecular cloud that formed the Sun (Levison et al., 2010).

Cometary volatiles (and their fragments and ions) are characterized by their spectroscopic and photometric observations at UV to radio wavelengths. Especially, optical observations have been performed since the earliest times of the astronomical era. Rotational, vibrational, and electronic transitions (collectively called "rovibronic" transitions) of daughter species resulting from photodissociation of volatiles released directly from the nucleus (called the "parent" species or "parent" molecules) predominantly emit at optical wavelengths. Many volatiles (such as CN, C_2, C_3, CH, [OI], NH_2, and NH), ions (such as CO^+, H_2O^+, CO_2^+), and atoms (sodium, oxygen) have been recognized in the optical wavelength region. A'Hearn et al. (1995) reported on 85 comets observed by optical spectrophotometry and found that C_2 and/or C_3 are depleted relative to CN in short-period comets. Fink (2009) also summarized a low-dispersion optical spectroscopic survey of 92 comets and proposed four taxonomic classes based on the abundance ratios of cometary C_2, NH_2, and CN.

Infrared instruments developed in the first half of the 1990s enabled high-dispersion spectroscopic observations in the near-infrared region by several telescopes. In the 1990s, two bright comets (C/1996 B2 (Hyakutake) and C/1995 O1 (Hale–Bopp)) approached the Sun, and their emission lines associated with ro-vibrational transitions of H_2O, HCN, C_2H_2, CH_4, C_2H_6, and CO were detected by the IRTF telescope installed with a CSHELL spectrometer in L-band (~3 μm) and M-band (~5 μm) (Greene et al., 1993). Chemical compositions of these species relative to water were summarized (DiSanti and Mumma, 2008; Mumma & Charnley, 2011; and references

therein). Other telescopes/instruments, such as the Subaru/IRCS (Kobayashi et al., 2000), Keck II/NIRSPEC (McLean et al., 1998), and VLT/CRIRES (Käufl et al., 2004), have also conducted cometary observations.

The transition between the hyperfine structure of OH (the socalled "18 cm line"), which emits at radio wavelengths, has been monitored by the Nançay radio telescope (Crovisier et al., 2002 and references therein) and has sometimes been observed by other radio telescopes. The Odin satellite and the Herschel Space Telescope have proven useful for monitoring cometary H_2O, $H_2{}^{18}O$, and NH_3 in far-infrared or sub-mm regions (Biver et al., 2007; Bockelée–Morvan et al., 2012). Moreover, ground-based radio telescopes can observe the emission lines of pure rotational transitions of CO, CH_3OH, H_2CO, HCN, HNC, and other complicated volatiles (e.g., Corivisier et al., 2009) and also the inversion transitions of NH_3 (Bird et al., 1997). Recently, the distributions of HCN, HNC, H_2CO, and dust within the coma have been observed at high spatial resolution by the Atacama Large Millimeter/submillimeter Array (ALMA) (Cordiner et al., 2014).

In summary, multi-wavelength observations have revealed various chemical species and compositions of cometary ices. The observed parent volatiles and their abundances (relative to H_2O) are summarized in Figure 4 of Mumma & Charnley (2011).

1.2.2. THE ISOTOPIC RATIOS OF COMETARY VOLATILES

The isotopic ratios in primary volatiles are considered as conserved parameters of formation processes. This dissertation focuses on the isotopologues of nitrogen ($^{14}N/^{15}N$) in cometary ammonia (see Section 1.4). The nitrogen isotopic ratios have been determined in cometary CN and HCN (Manfroid et al., 2009; Bockelée–Morvan et al., 2008). The isotopic ratios of hydrogen (D/H), carbon ($^{12}C/^{13}C$), oxygen ($^{16}O/^{18}O$), and sulfur ($^{32}S/^{34}S$) in some primary volatiles are briefly described below. Observed cometary isotopes are well summarized in Bockelée-Morvan et al. (2015).

Before 2011, the D/H ratio in the cometary water of seven comets had been measured (six comets originating from the Oort cloud, one originating

from the Kuiper belt). The average D/H ratio of the Oort cloud comets (~3.0 × 10^{-4}) was double that of the Earth's oceans (VSMOW, D/H = 1.56 × 10^{-4}; Hartogh et al., 2011) and approximately 15 times the protosolar value ((2.1 ± 0.5) × 10^{-5}; Lellouch et al., 2001). In contrast, the D/H ratio of three Jupiter-family comets ((1.61 ± 0.24) × 10^{-4} for 103P/Hartley 2: Hartogh et al., 2011; (<2 × 10^{-4} for 45P/Honda–Mrkos–Pajdusáková; Hartogh et al., 2011, (5.3 ± 0.7) × 10^{-4} for 67P/Churymov–Gerasimenko; Altwegg et al., 2015) might have large variation. This indicates that (relative to protosolar water) cometary water has been largely fractionated into deuterium. The D/H ratios of the six Oort cloud comets are similar, implying either that these comets formed in a similar region of the solar nebula, or that the radial distribution of the D/H ratios in the solar nebula ices was quite uniform over the range of heliocentric distances that sourced most of the Oort cloud comets.

The cometary D/H ratio was first inferred from the mass-resolved ion spectra of H_3O^+ and H_2DO^+ in 1P/Halley, observed by the Ion Mass Spectrometer (IMS) and Neutral Mass Spectrometer (NMS) instruments onboard the Giotto spacecraft (IMS: Balsiger, Altwegg, & Geiss, 1995; NMS: Eberhardt et al., 1995). Cemetary HDO was first detected in the 1_{00}–0_{00} rotational line emissions from C/1996 B2 (Hyakutake) and C/995 O1 (Hale–Bopp), recorded at 465 GHz by ground-based observatories (Bockelée-Morvan et al., 1998; Meier et al., 1998). The derived D/H ratios were consistent with those of 1P/Halley. The D/H ratio in cometary water was also estimated from the optical spectra of OD and OH ((2.5 ± 0.7) × 10^{-4}; Hutsemékers et al., 2008), the UV spectra of H and D ((4.6 ± 1.4) × 10^{-4}; Weaver et al., 2008), and the infrared spectra of H_2O and HDO ((4.0 ± 1.4) × 10^{-4}; Villanueva et al., 2009). The D/H ratios obtained by these new methods lie within the uncertainties of previous measurements of the same comets. Assuming water formed in gas-phase chemistry, a formation temperature can be estimated from a D/H ratio in water (Millar et al. 1989). The range of water D/H ratio in comets corresponds to the temperatures from 28 K to 40 K as formation temperature of cometary water. This is one possible interpretation of observed water D/H ratios in comet. Grain surface

chemistry and mixing of materials formed in low and high temperature environments may lead to different conclusions (Cleeves et al., 2014).

Given that deuterium fractionation is precluded in the coma (Rodgers & Charnley, 2002), the D/H ratios in volatiles other than H_2O can uniquely reveal the formation temperatures of cometary primary volatiles. For instance, comet Hale–Bopp demonstrates higher deuterium enrichment of HCN than of water (Meier et al., 1998b). The upper limit of D/H ratios of other volatiles have also been reported for Hale–Bopp: H_2CO ($<2 \times 10^{-2}$; Balsiger et al., 1995), CH_3OH ($<\sim 1 \times 10^{-2}$; Eberhardt et al., 1994), NH_3 and CH (NH_3: $<6 \times 10^{-3}$; CH: $<3 \times 10^{-2}$; Meier et al., 1998c). For methane, the first trial to detect a monodeuterio–methane (CH_3D) in the comet 153P/Ikeya–Zhang obtained a 2σ upper limit of the D/H ratio of <0.075 (Kawakita & Watanabe, 2003). Upper limits of the methane D/H ratios in other comets were reported (C/2001 Q1 (NEAT): <0.01; Kawakita et al., 2005, C/2004 Q2 (Machholz): <0.003 (3σ) and 0.005 (3σ); Kawakita & Kobayashi, 2009 and Bonev et al., 2009, respectively, C/2008 N3 (Lulin): <0.07 (3σ); Gibb et al., 2012). The predicted D/H ratio in cometary methane is obtained as 0.1–0.2 by the theoretical calculation based on gas-phase chemical reactions at 10 K by Aikawa & Herbst (1999). Meanwhile, an upper limit of the D/H ratio in methane in the early solar nebular was inferred as $\sim 3 \times 10^{-4}$ from the methane D/H ratio observed in the atmosphere of Titan (Mousis et al., 2002). Upper limits obtained in comets cannot be explained by the deuteration in methane at such low temperatures, ~10 K.

The carbon isotopic ratios ($^{12}C/^{13}C$) of the cometary volatiles HCN, CN, and C_2 have been determined from 2, 21, and 4 samples, respectively (HCN: Bockelée–Morvan et al., 2008; CN: Manfroid et al., 2009; C_2: Wyckoff et al., 2000). The average carbon isotopic ratio of cometary CN (91.0 ± 3.6) is consistent with the telluric value (88.99; Anders & Grevesse, 1989) and with the cosmic ratio in the solar neighborhood (70–90; Wilson & Rood, 1994; Milam et al., 2005). In contrast, the nitrogen isotopic ratio in cometary CN (147.8 ± 5.7), reported by Manfroid et al. (2009), is almost one third the protosolar value (441 ± 5; Marty et al., 2011). Therefore, the origin of the nitrogen isotopic ratio of cometary volatiles remains debatable.

The oxygen isotopic anomaly in meteorites can be explained by several scenarios (Busemann et al, 2006; Alexander et al., 2007). The most likely of these scenarios could be elucidated from the oxygen isotopic ratios ($^{16}O/^{18}O$) of cometary volatiles. Several $^{16}O/^{18}O$ measurements have been performed on the constituents of cometary water: H_2O (520 ± 25; Biver et al., 2007), OH and H_3O^+ (OH: 425 ± 55; H_3O^+: 425 ± 55; Hutsemékers et al., 2008), and their ^{18}O counterparts. However, the $^{16}O/^{18}O$ values obtained by current methods are too uncertain (typical errors are 10%) for understanding their significant deviation from the VSMOW value of 498.7 (Hartogh et al., 2011). Some comets are hypothesized to become depleted in ^{18}O and enriched in other cometary volatiles (Hutsemékers et al., 2008). More precise measurements are needed to resolve these problems.

The sulfur isotopic ratios ($^{32}S/^{34}S$) of various cometary volatiles have also been measured: S^+ (23 ± 6; Altwegg, 1996), CS (27 ± 3; Jewitt et al., 1997), and H_2S (17 ± 4; Crivisier et al., 2004). These values are reasonably consistent with the solar system ratio (22.5; Anders & Grevesse, 1989), except for H_2S. The marginal ^{34}S enrichment in H_2S, reported by Crovisier et al. (2004), requires further confirmation. Meanwhile, the primitive matters contained in IDPs and carbonaceous meteorites exhibit much smaller anomalies in their sulfur isotopic compositions (Busemann et al., 2006; Floss et al., 2006).

1.3. ORTHO-TO-PARA ABUNDANCE RATIOS OF COMETARY VOLATILES

The OPR is useful for understanding the very low temperatures at which cometary volatiles formed. Molecules with two or more hydrogen atoms (fermions), such as H_2O (water), NH_3 (ammonia), and CH_4 (methane), can be classified by the nuclear spin states of their hydrogen atoms (the socalled nuclear spin isomers). The entire wave function of these volatiles should change sign when equivalent hydrogen atoms are exchanged. For example,

hydrogen exchange in an H_2 molecule (the simplest volatile) causes the entire wave function Ψ_{H2} of the H_2 molecule to switch as:

$$\Psi_{H2} \rightarrow -\Psi_{H2}.$$

The entire wave function of a general molecule ($\Psi_{molecule}$) can be expressed wave function of each component by the Born–Oppenheimer approximation:

$$\Psi_{molecule} = \Psi_{trans.}\Psi_{elec.}\Psi_{vib.}\Psi_{rot.}\Psi_{ns},$$

where $\Psi_{trans.}$, $\Psi_{elec.}$, $\Psi_{vibr.}$, $\Psi_{rot.}$, and Ψ_{ns} denote the wave functions of the translational motion, electronic state, vibration of the atomic nuclei, molecular rotational motion, and the total nuclear spin state, respectively. Moreover, the nuclear spin can be written as the product of the wave functions of the nuclear spins of the individual atoms (e.g., the nuclear spin of the H_2O molecule can be expressed as Ψ_{ns} = Ψ_{ns} (hydrogen) Ψ_{ns} (hydrogen) Ψ_{ns} (oxygen)).

The H_2 wave function switches sign under hydrogen atom exchange because of the inverse of the signs between the rotational ($\Psi_{rot.}$) and nuclear spin (Ψ_{ns}) wave functions. Since the nuclear spin of hydrogen is +1/2 (α) or–1/2 (β) and the atomic nuclei of hydrogen are numbered 1 and 2, there are four possible wave functions of H_2 nuclear spin:

(A) $\alpha(1)\beta(2)$ (C) $1/\sqrt{2}(\alpha(1)\beta(2) + \alpha(2)\beta(1))$

(B) $\alpha(2)\beta(1)$ (D) $1/\sqrt{2}(\alpha(1)\beta(2) - \alpha(2)\beta(1))$

Wave functions (A), (B), and (C) are invariable (symmetric) under hydrogen atom exchange. On the other hand, wave function (D) changes sign under hydrogen exchange (that is, (D) is antisymmetric). Molecules possessing symmetric and antisymmetric nuclear spin wave functions are called ortho-H_2 and para-H_2 molecules, respectively. Thus, the total nuclear spin of hydrogen I is 1 (↑↑ or ↓↓) if the H_2 molecule is an ortho-species, and is 0 (↑↓ or ↓↑) if the molecule is a para- species. Here because the wave function of the entire molecule switches sign when the hydrogen atoms are exchanged, Ψ_{rot} must be anti-symmetric (symmetric) when the molecule is symmetric (anti-symmetric). Thus, ortho- and para-species are characterized by specific

rotational states. In other words, the ortho- and para-species behave as different molecules because ortho–para conversion is forbidden by radiative and collisional transitions (Miani & Tennyson, 2004). Cometary volatiles might retain their original ortho or para states over long periods (Mumma et al., 1993 and references therein). If this is true, we could estimate the formation temperatures of cometary volatiles (such as H_2O, NH_3, and CH_4) from their observed OPRs. The OPR of water is 3.0 under high-temperature conditions (>50 K). Similarly, the thermal equilibrium OPR of ammonia has been determined as 1.0. At thermal equilibrium, the OPR of volatiles is a function of temperature; thus, assuming that the species follow the Boltzmann distribution, we can calculate the abundance ratios of the total numbers of ortho- and para-species at a given temperature as follows:

$$OPR = \frac{(2I_O + 1)\sum_{Olevels.}(2J+1)\exp(\frac{E}{kT_{spin}})}{(2I_P + 1)\sum_{Plevels.}(2J+1)\exp(\frac{E}{kT_{spin}})},$$

where OPR, I, J, and E indicate the OPR, the total nuclear spin of the hydrogen atoms (statistically weighted by $2I_O + 1$ for the ortho-species and $2I_P + 1$ for the para-species), the rotational quantum number, and the energy of each state, respectively. The subscripts "O" and "P" indicate the ortho- and para-species, respectively. The temperature parameter that reproduces the observed OPR, called the nuclear spin temperature (T_{spin}), possibly reflects the formation temperature of the cometary volatiles (Mumma et al., 1993). Therefore, the formation temperature of cometary volatiles should be estimable from the observed OPRs of cometary volatiles.

Water molecules are the most important volatiles in comets because both of their OPRs alter at around 10–50 K under the thermal equilibrium condition (the estimated temperature range of the early solar system). Moreover, water is the most abundant volatile in cometary nuclei (>80%). Therefore, understanding the formation conditions of water is crucial to understand the origin of icy materials in comets.

The OPR of cometary water was first determined in the comet 1P/Halley by the Kuiper Airborne Observatory in 1987 (Mumma et al., 1987). From the obtained OPR of the cometary water (2.73 ± 0.37), the T_{spin} of water was estimated as 35 +9/–5 K. Until 1999, the OPRs of cometary water were determined from the ν_1 and ν_3 fundamental bands of water, which appear around 2.7 microns. These bands cannot be observed by ground-based telescopes because they are heavily absorbed by telluric water vapor, which severely limits their sampling size. Thus, to determine the OPRs of cometary water by this technique, the telescope must be airborne or orbiting in space. To remove this difficulty, Dello Russo et al. (2004) developed a method using the water hot-band which is emitted at around 2.9 microns and hence observable by ground-based observatories. In the second half of the 2000s, ten or more samples of OPRs of cometary volatiles were obtained by this method (based on high-dispersion near-infrared spectroscopic observations of the water hot-band; Bonev et al., 2007). These previous results obtained similar T_{spin}s of cometary water (~30 K). However, only bright comets yield sufficiently high-S/N spectra of water lines; moreover, to precisely measure the OPR of cometary water, the radial velocity of the comet (relative to Earth) should be needed (>20 km/s, corresponding to a spectral resolution of 20,000) to avoid the absorption of the cometary lines by the telluric atmosphere. Therefore, an alternative technique is necessary to improve the OPR sampling size of cometary volatiles.

Ammonia molecules are also important species of cometary volatiles because both of their OPRs alter at around 10–50 K and ammonia is the most abundant nitrogen-bearing volatile. However, the OPRs of cometary ammonia are difficult to measure with high accuracy, because ammonia has a narrow existence region in the cometary coma. On account of its short lifetime, ammonia cannot be observed to the required spatial resolution by current observational facilities. A method for estimating the OPRs of cometary ammonia from the high-dispersion optical spectrum of NH_2 was developed in 2001 (Kawakita et al., 2001). Most of the cometary ammonia photodissociates into NH_2 under solar UV radiation (the branching ratio of NH_3 is ~95 %; Huebner, 1992). Fortunately, we can easily obtain high-S/N

spectra of NH_2, because the ro-vibronic transitions of NH_2 strongly emit in the optical; in addition, there are many high-resolution optical spectrographs mounted on large telescopes across the world. To more accurately determine the ammonia OPRs, the method could conceivably be improved by (1) considering the influence of the telluric absorption lines, (2) removing the C_2 Swan band lines that contaminate the NH_2 lines, and (3) measuring multiple vibronic bands of NH_2. By correcting for these influences, Shinnaka et al. (2010) successfully reduced the measurement errors in the OPRs of cometary ammonia; typically by more than half for a given comet. However, the statistical behavior of the OPR of cometary ammonia remained obscure because insufficient samples had been recorded in 2010. Since then, we have investigated the statistical behavior of OPRs of cometary ammonia. The results are reported in Section 2 of this dissertation.

Moreover, 30 K is the approximate nuclear spin temperature, estimated from the *E:F:A* ratios of CH_4 (Kawakita et al., 2006). The nuclear spin temperatures of water, ammonia, and methane are nicely consistent in comet C/2001 Q4 (NEAT) (Kawakita et al., 2006).

Although the OPRs of water have been determined in ten or more comets (Bonev et al., 2007, cited in Mumma & Charnley, 2011), the OPRs of cometary ammonia and methane have been sampled less frequently. Furthermore, the real meaning of the OPRs of cometary volatiles is still being debated (Bonev et al., 2009; Cacciani et al., 2009; Crovisier et al., 2008; Dello Russo et al., 2005; Jehin et al., 2009; Kawakita et al., 2007; Kawakita & Kobayashi, 2009; Shinnaka et al., 2011; Woodward et al., 2007; and references therein).

1.4. NITROGEN ISOTOPIC RATIOS OF COMETARY VOLATILES

The nitrogen isotopic ratio is important for understanding the formation conditions of cometary volatiles. In general, ^{15}N-fractionation occurs in chemical reactions under very low-temperature conditions because the energy diagram of heavy isotopes (including ^{15}N) is highly stable. Arpigny et al. (2003) investigated the CN (0-0) band (around 388 nm) and reported a

twofold enrichment of heavy nitrogen in cometary CN relative to the protosolar value. Manfroid et al. (2009) extended the sampling size of the nitrogen isotopic ratios of cometary CN to 23 comets and found that these ratios were independent of heliocentric distance and dynamical class. Previously, the nitrogen isotopic ratios of cometary volatiles have been determined from the cometary HCN (Bockelée-Morvan et al., 2008, Lis et al., 2013) and CN (dominant photodissociation product of HCN in the coma; Arpigny et al., 2003, Manfroid et al., 2009). The transitions of HCN strongly emit at submillimeter wavelengths ($H^{12}C^{14}N$: 265.9 GHz; $H^{12}C^{15}N$: 259.0 GHz), whereas CN exhibits a strong electronic band in the optical region (0-0 band around 388 nm). However, the nitrogen isotopic ratios of ammonia in comets have not been previously reported, despite ammonia being the dominant nitrogen-bearing volatile in comets (Section 4).

1.5. FORMATION PROCESSES OF WATER AND AMMONIA

At very low-temperatures (<50 K), molecules may form by one of two mechanisms.

Ion–molecule reactions dominate in low-gas-density environments, such as molecular clouds and the outer regions of solar nebulae, because the probability of collisions between molecules (or atoms) is very small. Under such low-density conditions, molecules can form by gas-phase ion–molecule reactions or by surface reactions on cold grains. Whereas water can form by both reactions, ammonia is generally formed by grain surface reactions. The gas-phase formation of ammonia is inefficient because it involves endothermic processes.

In a gas-phase chemistry, H_3^+ ions are the most important volatiles for chemical reactions under low-density conditions, because they are stable and were abundant in the molecular cloud and the solar nebula. In the gas-phase, water predominantly formed by the following reaction chain:

$H_3^+ + O \rightarrow OH^+ + H_2$,

$OH^+ + H_2 \rightarrow H_2O^+ + H$,

$H_2O^+ + H_2 \rightarrow H_3O^+ + H$,

$H_3O^+ + e^- \rightarrow H_2O + H$.

Similarly, ammonia in the gas-phase is predominantly formed as follows:

$N^+ + H_2 \rightarrow NH^+ + H$,

$NH^+ + H_2 \rightarrow NH_2^+ + H$,

$NH_2^+ + H_2 \rightarrow NH_3^+ + H$,

$NH_3^+ + H_2 \rightarrow NH_4^+ + H$,

$NH_4^+ + e^- \rightarrow NH_3 + H$.

When the density and temperature are both low (temperature <~30 K), molecular formation also depends on the grain surface chemistry; first, grains operate as a heat bath (that is, they absorb the heat generated by exothermic reactions); second, grains easily collide because their collisional cross-sections are much larger than those of molecules and atoms. The hydrogen addition reaction on grain surfaces is especially efficient at 10 K because of the high absorbance rate of hydrogen by the grain surface (Hama et al., 2011). Thus, if water and ammonia were formed by the hydrogen addition reaction on grain surfaces, we can infer the temperature of the grain surfaces as <10 K.

Water is formed by the hydrogen addition reaction on low-temperature grain surfaces as follows:

$O + H \rightarrow OH$,

$OH + H \rightarrow H_2O$.

Similarly, ammonia is formed as follows:

$N + H \rightarrow NH$,

$NH + H \rightarrow NH_2$,

$NH_2 + H \rightarrow NH_3$.

1.6. SCIENTIFIC GOALS IN THIS DISSERTATION

Section 1.3 highlighted several unclarified issues regarding the OPRs of cometary volatiles. Accurate determination of the OPRs of water is hampered by the limited number of suitable targets, and the OPRs of cometary ammonia have been rarely sampled. Moreover, as mentioned in

Section 1.4, the $^{14}N/^{15}N$ ratios in cometary ammonia have never been sampled. The scientific goal of my dissertation is to resolve these issues and thereby understand the origin of cometary volatiles. Section 2 summarizes the ammonia OPRs in 18 comets and compares them with other primordial cometary properties, such as the gas production rates of volatiles relative to water (as abundance ratios of solid-phase into the cometary nucleus) and the nitrogen isotopic ratios of CN. Section 3 describes the development of our new technique by which we inferred the water OPR from the high-dispersion optical spectra of water ions in three comets. Section 4 presents the first measurement of the nitrogen isotopic ratio of ammonia, obtained from the NH_2 in a single comet (comet C/2012 S1 (ISON)). In section 5, we discuss the possibility of ortho–para conversion in the cometary coma and the formation environments of cometary volatiles. This discussion is based on our own and other recent results. Section 6 concludes my dissertation and suggests some future directions of cometary studies.

2. ORTHO–TO–PARA ABUNDANCE RATIO (OPR) OF AMMONIA IN 18 COMETS: OPRS OF AMMONIA VERSUS $^{14}N/^{15}N$ RATIOS IN CN

ABSTRACT

The Ortho–to–Para abundance Ratio (OPR) of cometary molecules is considered to be one of the primordial characteristics of cometary ices. We present OPRs of ammonia (NH_3) in 18 comets based on optical high–dispersion spectroscopic observations of NH_2, which is a photo–dissociation product of ammonia in the gaseous coma. The observations were mainly carried out with the VLT/UVES. The OPR of ammonia is estimated from the OPR of NH_2 based on the observations of the NH_2 (0,9,0) vibronic band. The absorption lines by the telluric atmosphere were corrected and the cometary C_2 emission lines blended with NH_2 lines were removed in our analysis. The ammonia OPRs show a cluster between 1.1 and 1.2 (this corresponds to a nuclear spin temperature of ~30 K) for all comets in our sample except for 73P/Schwassmann–Wachmann 3 (hereafter 73P/SW3). Comet 73P/SW3 (both B– and C–fragments) shows the OPR of ammonia consistent with nuclear spin statistical weight ratio (1.0) that indicates a high–temperature limit as nuclear spin temperature. We compared the ammonia OPRs with other properties ($^{14}N/^{15}N$ ratios in CN, D/H ratios of water, and mixing ratios of volatiles). Comet 73P/SW3 is clearly different from the other comets in the plot of ammonia OPRs versus $^{14}N/^{15}N$ ratios in CN. The ammonia OPRs of 1.0 and lower ^{15}N–fractionation of CN in comet 73P/SW3 imply that icy materials in this comet formed under warmer conditions than other comets. Comets may be classified into two groups in the plot of ammonia OPRs against $^{14}N/^{15}N$ ratios in CN.

2.1. INTRODUCTION

Our solar system was formed from interstellar matter 4.6 Gyrs ago. After the gravitational collapse of a molecular cloud core, the solar nebula (protoplanetary disk of the Sun) was formed. The planetesimals of ~km size,

the building blocks of the planets, were accreted as rocky small bodies in the inner region of the solar nebula (asteroids) while they were mostly made of ice (but with dust grains) in the outer region. Remnants of those icy planetesimals are currently observed as comets.

Comets are defined as solar system small bodies that exhibit activities of out–gassing and/or of mass loss (ejection of dust grains). The chemical composition of the gaseous "coma" (expanding atmosphere formed by sublimating ices from the nucleus) provides precious information to link the interstellar matter and the formation of our solar system. Similarity in chemistry between interstellar and cometary ices indicates that the comets incorporated the interstellar ices without any significant (or with very small) chemical alteration. However, the physical conditions of the pre–solar molecular cloud and their evolution are unclear so far.

Like the chemical composition of the cometary ice (usually we refer to relative abundances of molecular species with respect to water that is the most abundant molecule in cometary ice), isotopic ratios and abundance ratios of nuclear spin isomers for some molecular species also give information about the formation conditions of the cometary molecules. In this Section, we concentrate on the abundance ratios between nuclear spin isomers of NH_3 in comets (ortho– and para–species for I=1/2 and I=3/2 where I denotes the total nuclear spin of identical H–atoms).

Ortho to para abundance ratio (OPR) of ammonia (NH_3) in comets, were first measured in 2001. The OPR of water was determined from near–infrared spectroscopic observations in 1986 in comet 1P/Halley (Mumma et al., 1987) for the first time, the determination of OPR for NH_3 came later due to the difficulty of observing cometary NH_3 from ground–based observatories (until 1990s, firm detections of NH_3 lines in the radio range were reported in the case of two bright comets only, comet Hyakutake and comet Hale–Bopp). Although NH_3 lines were also detected by the near–infrared high–dispersion spectroscopic observations in this decade, the S/N ratios of the measurements were not enough to determine the meaningful OPR of NH_3 in comets (Dello Russo et al., 2006). On the other hand, Kawakita et al. (2001) developed the new method to estimate the OPR

of NH_3 from the high–dispersion optical spectrum of NH_2. Thereafter, our group has reported the OPRs of NH_3 in several comets (Kawakita et al., 2001, 2002, 2004, 2006, 2007; Jehin et al., 2008, 2009a; Shinnaka et al., 2010). However, the number of comets sampled was still small.

The statistical weight ratio for nuclear spin species is unity for NH_3 in thermal equilibrium at the high temperature limit, but the OPR of cometary NH_3 show a cluster between 1.1 and 1.2. The real meaning of the OPR of NH_3 (as well as of water, methane, and other molecules) is still in debate (e.g., Bockelée–Morvan et al., 2009; Bonev et al., 2007, 2009; Crovisier et al., 2006, 2007, 2008; Cacciani et al., 2009; Dello Russo et al., 2005; Jehin et al., 2008, 2009a, 2009b; Kawakita et al., 2002, 2004, 2005, 2006, 2007; Kawakita & Kobayashi 2009; Pardanaud et al., 2007, Woodward et al., 2007). One possible interpretation for the observed OPRs is "a nuclear spin temperature" (Mumma et al., 1987). The nuclear spin temperature (T_{spin}) and rotational excitation temperature (T_{rot}) can differ. A T_{spin} indicates the relation of populations between spin ladders while T_{rot} indicates the populations within the ladders.

Most measurements of NH_3 OPR indicate ~30 K as nuclear spin temperatures. Surprisingly, nuclear spin temperatures also cluster around 30 K in the case of water. This temperature, ~30 K, seems to be a critical value for the formation of cometary molecules.

In this Section, we present a larger sample with the OPRs of NH_3 measured in 18 comets. We corrected the spectra for the influence of telluric transmittance (i.e., telluric absorption lines overlapped with the NH_2 lines) and removed the contamination of NH_2 lines by the C_2 Swan bands (such a correction was not considered in previous works). We discuss the real meaning of OPR based on the relationship between the OPRs and other properties.

2.2. THE DATA MATERIALS

In order to determine the OPR of cometary NH_3, we observe NH_2 lines in the optical region and determine OPRs of NH_2. The NH_2 radical is formed in

the coma through the photo–dissociation of NH_3 by the solar UV radiation. Since the NH_2 radical has strong rovibronic transitions in the optical region (the $\tilde{A}-\tilde{X}$ system) caused by the solar fluorescence excitation mechanism, it is easy to obtain high signal–to–noise (S/N) ratio spectra of NH_2 in the coma. Here we assume that NH_3 is the only parent of NH_2 in the coma (Kawakita & Watanabe, 1998). Another possible parent of NH_2 (formamide (NH_2CHO)) was discovered in comet Hale–Bopp but with an abundance of only 1% – 2% relative to the NH_3 abundance (Bockelée–Morvan et al., 2000; Bird et al., 1997). Hydrazine (N_2H_4) and Methylamine (CH_3NH_2) may be other potential parents. However, we do not consider these potential parents here because these species have never been detected in cometary comae (Feldman et al., 2004). We can then assume that its contribution to the NH_2 production is negligible. In this case, the OPR value of NH_2 is related to that of NH_3 via the nuclear spin selection rules that are applied to the photo–dissociation reaction (Uy et al., 1997; Quack, 1977). Thus, we can determine OPRs of NH_3 in comets from the observations of NH_2.

The NH_2 $(0,9,0)^{*1}$ band has been used to determine the OPR of NH_2 since this band is the strongest in the optical region for comets around 1AU from the Sun and since it is not significantly affected by telluric absorption lines. Even though the NH_2 (0,9,0) band is partially overlapped with the C_2 Swan sequence ($\Delta v = -2$), we can correct the contaminated NH_2 lines by using the fluorescence model of C_2 as demonstrated by Shinnaka et al. (2010). Detail of the fluorescence excitation model of NH_2 is described in Section 2.3.

High–dispersion spectroscopic observations in the optical region were performed with different telescopes and instruments as follows:

(A) the Ultraviolet and Visual Echelle Spectrograph (UVES; Dekker et al., 2000) mounted on the UT2 of the VLT at ESO Paranal, Chile,

(B) the High Dispersion Spectrograph (HDS; Noguchi et al., 1998) mounted on the Subaru Telescope atop of Mauna Kea, Hawaii,

(C) the cross–dispersed echelle spectrograph SARG (Gratton et al., 2001) mounted on the 3.5 m Telescopio Nazionale Galileo (TNG) at La Palma, Canary Islands, and

(D) the Coudé Echelle Spectrograph (CES; Zhao & Li, 2001) mounted on

the Xinglong 2.16 m Telescope at Beijing Astronomical Observatory. The details of the various observing runs of the 15 comets discussed here are summarized in Table 2.1.

Table 2.1: Observational log

Comets	Telescope/ Instruments	Number of observations	R_h [AU]	Δ [AU]
C/1995 O1 (Hale–Bopp)[a]	D	1	0.92	1.33
C/1999 S4 (LINEAR)[b]	B	1	0.86	0.82
C/2001 A2 (LINEAR)[c]	B	1	1.39	0.46
153P/Ikeya–Zhang[d]	C	1	0.89	0.43
C/2000 WM_1 (LINEAR)[e]	A	8	1.08 – 1.34	1.24
C/2002 V1 (NEAT)[f]	A	5	1.01 – 1.22	0.83–1.63
C/2002 X5 (Kudo–Fujikawa)[f]	A	6	0.70 – 1.07	0.86–0.99
C/2002 Y1 (Juels–Holvorcem)[f]	A	4	1.14 – 1.16	1.55 – 1.56
88P/Howell[g]	A	11	0.89 – 1.44	1.62 – 1.68
C/2001 Q4 (NEAT)[h]	A	10	0.97 – 0.98	0.32 – 0.32
C/2002 T7 (LINEAR)[f]	A	3	0.68 – 0.94	0.41 – 0.61
C/2003 K4 (LINEAR)[f]	A	1	1.20	1.51
9P/Tempel 1[i]	A	10	1.51	0.89 – 0.94
73P–B/SW3[j]	A	1	0.94	0.25
73P–C/SW3[j]	A	1	0.95	0.15
8P/Tuttle[k]	A	3	1.03 – 1.04	0.36 – 0.62
103P/Hartley 2[m]	B	1	1.07	0.12
C/2012 S1 (ISON)[m]	B	1	0.60	0.90
C/2013 R1 (Lovejoy)[m]	B	1	1.07	0.41

References: [a]Kawakita et al. (2004), [b]Kawakita et al. (2001), [c]Kawakita et al. (2002), [d]Capria et al. (2002), [e]Arpigny et al. (2003), [f]Manfroid et al. (2009), [g]Hutsemékers et al. (2005), [h]Manfroid et al. (2005), [i]Jehin et al. (2006), [j]Jehin et al. (2008), [k]Jehin et al. (2009b), [m]This work

Telescope/Instruments: A: VLT/UVES, B: Subaru/HDS, C: TNG/SARG, D: Xinglong 2.16 m Telescope/CES

2.3. ANALYSIS AND MODELS

2.3.1 FLUORESCENCE EXCITATION MODEL OF NH_2

We used the fluorescence excitation model of NH_2 in the optical (Kawakita, Ayani, & Kawabata, 2000; Kawakita et al., 2000, 2001, 2004, 2006) to derive OPRs of NH_2 in the comets from their spectra of the NH_2 (0,9,0) band. In the model we take into account,

(1) the rovibronic transitions between $\tilde{A}$ (0,v_2',0) and $\tilde{X}$ (0,0,0), v_2' = 1–18,

(2) the rovibrational transitions of $\tilde{X}$ (0,v_2',0) – $\tilde{X}$ (0,0,0), v_2' = 8–13,

(3) the rovibrational transition of $\tilde{X}$ (1,0,0) – $\tilde{X}$ (0,0,0) and $\tilde{X}$ (0,0,1) – $\tilde{X}$ (0,0,0),

(4) the pure rotational transitions in $\tilde{X}$ (0,0,0), and

(5) the fine structure of the energy levels (i.e., both F_1 and F_2 levels).

The fluorescence equilibrium is assumed for NH_2. More detailed information about the fluorescence excitation model of NH_2 is described in references listed above. Regarding the vibronic and vibrational transition moments of NH_2, these were recently recalculated by Jensen, Kraemer, and Bunker (2003), and updated in our model. The OPR of NH_2 is a free parameter in the model, and is determined from a χ^2 fitting between observed and modeled spectra.

2.3.2 FLUORESCENCE EXCITATION MODEL OF C_2

C_2 is one of the radicals that usually show prominent lines in the optical spectra of comets. The C_2 radical is a homo–nuclear diatomic molecule, and it is considered to be a daughter species (a photo–dissociation product) of more complex molecules (e.g., C_2H_2, etc.). There are some strong emission bands around 4000 – 6000 Å (a.k.a., the Swan band sequences corresponding to the $d^3\Pi_g$–$a^3\Pi_u$ electric transition). The C_2 Swan sequence ($\Delta v = -2$) is recognized in the NH_2 (0,9,0) band region (~6000 Å). The contamination of NH_2 lines by C_2 lines should be removed to determine the OPR of NH_2 more accurately even if the C_2 lines are much weaker than the NH_2 lines.

We used the fluorescence excitation model of C_2 to remove the contamination of the NH_2 lines by the C_2 lines in the observed spectra. In

this model, the Swan band sequences of $d^3\Pi_g$–$a^3\Pi_u$ are taken into account. For simplicity we assume (1) the Boltzmann distribution at a given temperature (T_{rot}) in the lower state ($a^3\Pi_u$), (2) the statistical equilibrium for the fluorescence excitation from the lower to the upper state ($d^3\Pi_g$). T_{rot} is determined by fitting the modeled spectra with the observations. The fluorescence excitation model of C_2 is also explained in Shinnaka et al. (2010).

2.3.3. ANALYSIS

Data reduction was performed by the pipeline software customized for the instrument (in the case of UVES) and/or by the IRAF software package distributed from the NOAO[*2]. The details for the reduction and calibration of the data obtained with VLT/UVES were described in Arpigny et al. (2003) and Jehin et al. (2004). The details for the reductions and calibrations of the data obtained with Subaru/HDS, TNG/SARG, and Xinglong 2.16 m Telescope/CES were described in Kawakita et al. (2004). After the spectra are calibrated, we have to subtract the continuum component (the sunlight reflected by cometary dust grains) from the calibrated spectra. Since the continuum component is convolved with the telluric absorption lines of the atmosphere, we used the high–dispersion solar spectrum without telluric absorption lines (Kurucz, 2005) and the synthesized telluric transmittance spectrum calculated by the LBLRTM code (Clough & Iacono, 1995). We fitted the modeled transmittance with the observed spectra in the wavelength region where the continuum component is almost free from cometary lines. The fully–resolved transmittance spectrum was convolved with a Gaussian function as the instrumental profile. The modeled continuum (the solar spectrum convolved with both the telluric transmittance and a reflectivity of dust grains) was fitted with the observations and then was subtracted from the observed spectrum.

We measured the emission flux of the NH_2 lines after removing all contamination by the C_2 lines based on the synthesized spectrum of the C_2 radical (Shinnaka et al., 2010) as described in the previous section. Then, we corrected the NH_2 flux for the telluric transmittance at the wavelength

where each NH_2 line was observed. Note that the NH_2 (0,9,0) band is not severely affected by the telluric features. Figure 2.1 shows an example of both observed and modeled (best–fit) spectra of NH_2 in the case of C/2001 Q4 (NEAT). Finally, the OPR of ammonia could be estimated from the OPR of NH_2 determined from the comparison between observed and modeled spectra. Details of the analysis are described elsewhere (Shinnaka et al., 2010; Kawakita et al., 2006, 2004, 2002, 2001).

The OPRs of both NH_2 and NH_3 determined from the observations are listed in Table 2.2. The weighted mean value and estimated errors of OPRs of NH_3 for each comet are given in Table 2.3.

[FOOTNOTES]

*1 The linear notation is employed for Ã state here.

*2 IRAF is distributed by the National Optical Astronomy Observatory, which is operated by the Association of Universities for Research in Astronomy (AURA) under cooperative agreement with the National Science Foundation.

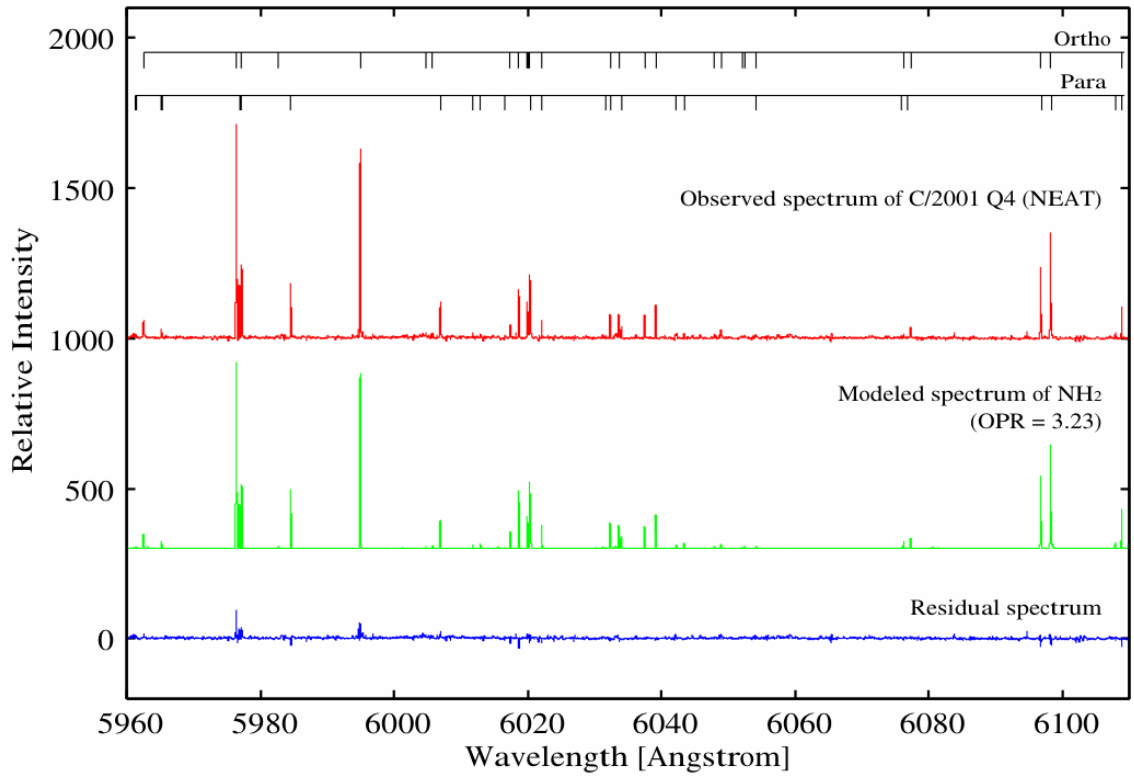

Figure 2.1: Comparison between observed and modeled (best–fit) spectra of NH_2 in C/2001 Q4 (NEAT). Observed and modeled spectra are with offsets of 1000 and 300, respectively. These spectra are in good agreement (the residual spectrum between them is also plotted in the Figure). The ortho– and para–NH_2 lines are labeled in these spectra. Although the line intensity of C_2 Swan band ($\Delta v=-2$) is much weaker than NH_2 lines in the (0,9,0) band, many weak lines of C_2 are recognized in the residual spectrum (not noise).

2.4. RESULTS

2.4.1. C/1995 O1 (HALE–BOPP)

The OPR of NH_3 in comet C/1995 O1 (Hale–Bopp) had already been reported in our previous study (Kawakita et al., 2004). The previous OPR of NH_3 was 1.21 ± 0.15 while the revised value is 1.17 ± 0.13 in this work. The small difference was caused by improvement in method for the data analysis. In the case of C/1995 O1 (Hale–Bopp), the dust–to–gas ratio is very high and the accuracy of the continuum subtraction is especially important for the measurements of the emission lines. In our analysis the continuum component is modeled by convolving the solar spectrum with the synthesized telluric transmittance curve adjusted to the observational conditions. The T_{spin} is derived to be 28 +12 / –4 K for NH_3. This value is consistent with T_{spin} of 28 ± 2 K derived from water lines in the same comet reported in Crovisier (1997).

2.4.2. C/1999 S4 (LINEAR)

Comet C/1999 S4 (LINEAR) broke into many fragments and disappeared before its perihelion passage during the 2000 apparition (Weaver et al., 2001). This comet was depleted in highly volatile species and it might have formed in a warm region of the solar nebula, probably near Jupiter's orbit (Mumma et al., 2001a). Kawakita et al. (2001, 2004) had reported the OPR of NH_3 in this comet as 1.19 ± 0.06 while the revised value in this work is OPR = 1.16 ± 0.05 indicating a T_{spin} = 28 +3 / –2 K. This revised T_{spin} is consistent with the lower limit of T_{spin} for water (30 K) reported by Dello Russo et al. (2005). The depletion in highly volatile species in this comet might be the signature for a formation in a warmer region than other typical comets. However, the T_{spin} of NH_3 determined in our study implies that the materials in this comet formed at a similar environment as others (see discussion in Section 2.5). The T_{spin} may indicate formation conditions corresponding to the formation of molecules in the pre–solar molecular cloud while the chemical abundance ratio of cometary volatiles reflects the temperature at the accretion of cometary nuclei in the solar nebula.

2.4.3. C/2001 A2 (LINEAR)

Comet C/2001 A2 (LINEAR) showed frequent outburst phenomena linked to fragmentations (e.g., Jehin et al., 2002). Near–infrared spectroscopy revealed that the comet was enriched in organics (Magee–Sauer et al., 2008). We also reported the OPR of NH_3 in this comet as 1.25 ± 0.05 (Kawakita et al., 2004) while the revised value is OPR = 1.24 ± 0.06 corresponding to T_{spin} = 25 ± 2 K for NH_3. The NH_3 T_{spin} in this comet is relatively lower than the usual value of ~30 K and this conclusion is consistent with the water T_{spin} derived by Dello Russo et al. (2005) as 23 +4 / –3 K. These lower T_{spin} may be related to the organic–rich chemistry and frequent outbursts (with fragmentations) in this comet.

2.4.4. 153P/IKEYA–ZHANG

Comet Ikeya–Zhang is now in a Halley–type orbit, and thus probably originated in the Oort cloud. The OPR of NH_3 of this comet was reported to be 1.11 ± 0.06 (Kawakita et al., 2004) while the revised value is 1.14 ± 0.05 (corresponding to T_{spin} = 29 +4 / –2 K) in NH_3. Improvement in the method of data analysis changes the results slightly but consistently with previous result. Comet Ikeya–Zhang is a typical comet from the viewpoint of T_{spin}.

2.4.5. C/2000 WM_1 (LINEAR)

OPRs of NH_3 in comet C/2000 WM_1 (LINEAR) were determined based on multiple measurements of OPR of NH_2 (shown in Table 2.3). The weighted mean of the NH_3 OPR is 1.12 ± 0.02 in this comet. The corresponding T_{spin} of NH_3 is 30 ± 1 K. This is consistent with T_{spin} derived for water, OPR = 2.6 ± 0.2 corresponding to T_{spin} ~31 K (28 – 38 K) (Radeva et al., 2010). This comet is also typical in T_{spin}.

2.4.6. C/2002 V1 (NEAT)

In comet C/2002 V1 (NEAT), the weighted mean of the NH_3 OPR is 1.14 ± 0.02 based on multiple observations of the comet (Table 2.3). The T_{spin} of NH_3 is 29 ± 1 K like other comets typical in T_{spin}.

2.4.7. C/2002 X5 (KUDO–FUJIKAWA)

Based on multiple observations of comet C/2002 X5 (Kudo–Fujikawa), we derived the weighted mean of NH_3 OPR to be 1.13 ± 0.02 indicating T_{spin} = 30 ± 1 K for NH_3. This comet is also normal in T_{spin}.

2.4.8. C/2002 Y1 (JUELS–HOLVORCEM)

In comet C/2002 Y1 (Juels–Holvorcem), the weighted mean of NH_3 OPR is 1.13 ± 0.03 (corresponding to T_{spin} = 30 ± 2 K) based on multiple observations. The derived OPR of NH_3 is in the typical range.

2.4.9. 88P/HOWELL

This comet belongs to the Jupiter family comets (JFCs). It was observed at multiple epochs and the determinations of NH_3 OPR led to the weighted mean value of OPR = 1.19 ± 0.02 (T_{spin} = 27 ± 1 K) for NH_3. Since the T_{spin} of this comet is similar to those for the Oort cloud comets (~30 K, see above), icy materials incorporated in the comets now in different reservoirs (the Oort cloud and the Kuiper belt) might be formed in similar environments.

2.4.10. C/2001 Q4 (NEAT)

Comet C/2001 Q4 (NEAT) was observed many times and we derived OPRs of NH_3 for each observation. The weighted mean value of NH_3 OPR is 1.12 ± 0.02 (T_{spin} = 30 ± 1 K) based on the observations with VLT/UVES. In our previous study (Kawakita et al., 2006), the NH_3 OPR = 1.11 ± 0.04 and T_{spin} = 31 +4 / –2 K were derived from the Subaru/HDS observation. These values have been revised recently by Shinnaka et al. (2010), as OPR = 1.12 ± 0.02 and T_{spin} = 30 ± 1 K. These OPRs of NH_3 using the Subaru/HDS observations are consistent with the OPRs derived from the VLT/UVES observations in this work. Furthermore, T_{spin} of water and methane were also derived from the near–infrared high–dispersion spectrum (Kawakita et al., 2005, 2006). All these T_{spin} values (31 +11 / –5 K for water, 30 +2 / –1 K for NH_3, and 33 +2 / –1 K for methane) are consistent with one another in this comet.

2.4.11. C/2002 T7 (LINEAR)

In the case of comet C/2002 T7 (LINEAR), we report the OPR of NH_3 as 1.13 ± 0.03 corresponding to T_{spin} = 30 ± 2 K. This value seems typical of our sample. In this comet, the D/H ratio in OH (photodissociation product of H_2O) is also measured and the typical D/H ratio in water was obtained (~3 x 10^{-4}) by Hutsemékers et al. (2008).

2.4.12. C/2003 K4 (LINEAR)

The OPR of NH_3 in comet C/2003 K4 (LINEAR) is 1.16 ± 0.04. The resultant T_{spin} of NH_3 is 28 +3 / –2 K. This temperature is consistent with T_{spin} in other comets and also consistent with the T_{spin} of water (28.5 +6.5 / –3.5 K) derived by Woodward et al. (2007) based on infrared observations.

2.4.13. 9P/TEMPEL 1

Comet 9P/Tempel 1 is a JFC and was the target of NASA Deep Impact mission (A'Hearn et al., 2005). Although the data were analyzed and already published by Kawakita et al. (2007), we revisited the data and used the improved method for this comet. Since this comet is dust rich in the optical spectra, precise subtraction of the solar continuum would improve the results. We report the OPR of NH_3 as 1.14 ± 0.02 (weighted mean of multiple observations) that is lower than previous values. The T_{spin} of NH_3 is 29 ± 1 K for 9P/Tempel 1 while ~25 K in our previous report (Kawakita et al., 2007). Relatively high dust–to–gas ratio in this comet would be the reason for this change (see the case of C/Hale–Bopp). However, the basic conclusion has not changed; namely, no significant change in OPR of NH_3 was found before and after the Deep Impact on July 4, 2005 (see Figure 2.2). In Figure 2.2, we plotted the obtained OPRs with random errors (not including systematic ones) to check the change in OPR before and at the Deep Impact. Based on this Figure, we conclude that the OPRs did not change after the Deep Impact event with the confidence level of 95%. Anyway, comet 9P/Tempel 1 is similar to Oort cloud comets (and also similar to 88P/Howell as a JFC) from the viewpoint of T_{spin} in our sample.

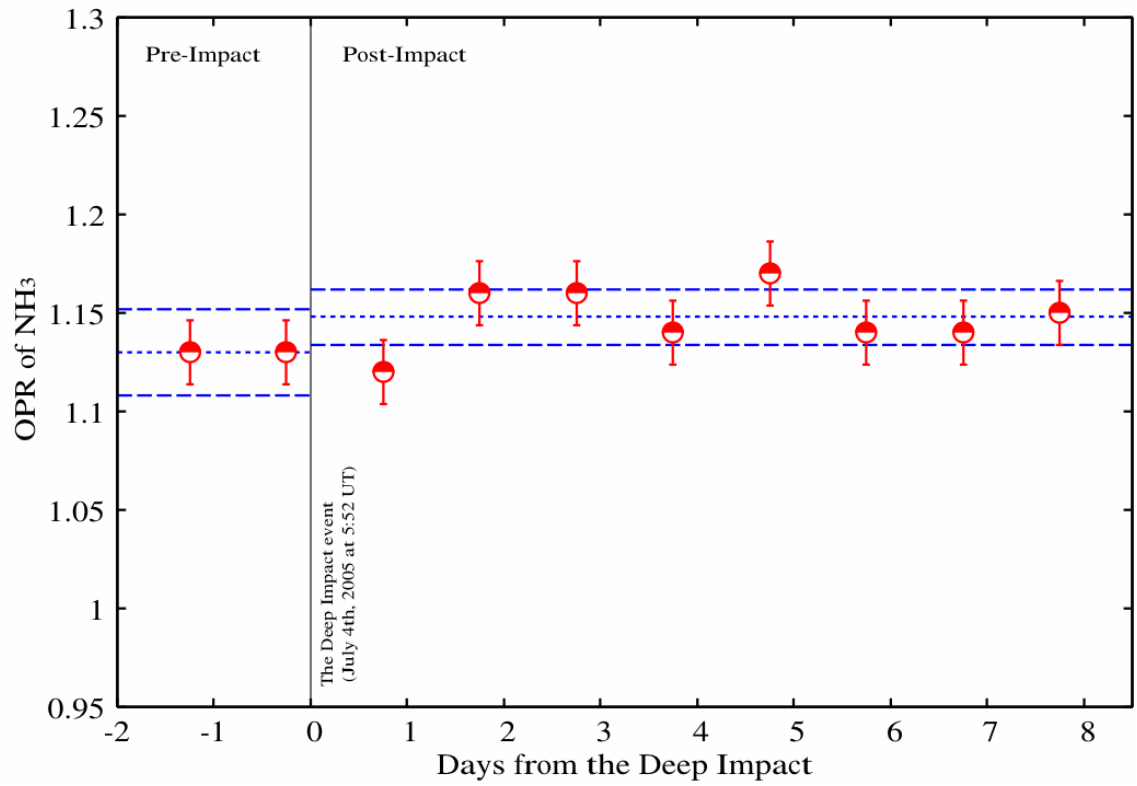

Figure 2.2: Temporal variation of OPRs of NH_3 in comet 9P/Tempel 1 before and after the Deep Impact. We plotted the NH_3 OPRs with their random errors in each measurement and the error bars correspond to ± 1σ error levels. The dotted and dashed lines show a mean values and a 95 % confidence levels of the mean for before and after the impact (1.130 ± 0.022 and 1.147 ± 0.014), respectively. These values overlap within their 95% confidence levels. The disagreement between before and after impact is not significant.

2.4.14. 73P/Schwassmann–Wachmann 3 (B and C fragments)

Comet 73P/Schwassmann–Wachmann 3 is a very peculiar comet that showed fragmentation into many fragments. In the 2006 apparition, it was expected that the fresh icy materials exposed on the new surface (formed by the fragmentations) could be observed. Comparison in chemistry between the main fragments B and C implies that the parent body was homogeneous in chemistry (Biver et al., 2008; Villanueva et al., 2006; Dello Russo et al., 2007; Kobayashi et al., 2007; Schleicher et al., 2008). Jehin et al. (2009a)

pointed out that the parent comet is peculiar from the viewpoint of $^{14}N/^{15}N$ ratio in CN and OPR of NH_3. We reanalyzed the data and found OPR = 1.01 ± 0.03 and 1.02 ± 0.03 for the fragment –B and –C, respectively. These values are far from the typical values in our sample and consistent with the high–temperature limit (1.0) for NH_3. The nuclear spin temperatures are higher than 39 K and 37 K for the fragment–B and –C, respectively. These signatures for high temperatures are consistent with the results derived for water. The lower limits of T_{spin} of water are reported as 42 K and 37 K for B and C fragments (Dello Russo et al., 2007). These results may be related to the strong depletion in highly volatile species (Villanueva et al., 2006, Dello Russo et al., 2007, Kobayashi et al., 2007). We will discuss the peculiarity of 73P/Schwassmann–Wachmann 3 in Section 2.5 and 5.3.

2.4.15. 8P/TUTTLE

Comet 8P/Tuttle is now classified as a Halley–type comet, and thus probably coming from the Oort cloud. The weighted mean of OPR for NH_3 is 1.14 ± 0.02 (corresponding to 29 ± 1 K). This is similar to the other Halley–type comet in our sample, comet 153P/Ikeya–Zhang (and similar to most comets in our database). Our determination of OPR of NH_3 indicates that comet 8P/Tuttle is a typical comet. Near–infrared spectroscopic observations revealed that the chemical composition of 8P/Tuttle is slightly different from that of typical Oort cloud comets (Bonev et al., 2008a, Kobayashi et al., 2010). However, the D/H ratio in water (considered as a sensitive indicator of the temperatures where the molecules formed) is similar to those found in other Oort cloud comets (Villanueva et al., 2008).

2.4.16. 103P/HARTLEY 2

Comet 103P/Hartley is classicied as JFC and the target of NASA's *EPOXI* mission (A'Hearn et al., 2011). Many kind of observation were carried out in this comet from over the wide (Meech et al., 2011). The weighted mean of OPR for NH_3 is 1.08 ± 0.02 (corresponding to 34 +3 / –2 K as T_{spin}). This value is consistent with the water T_{spin} derived by Bonev et al. (2013) as 37 +8 / –4 K. This comet may be little higher value in T_{spin}.

2.4.17. C/2012 S1 (ISON)

Comet C/2012 S1 (ISON) is a sungrazer with its perihelion distance of 0.012 AU (~1,870,000 km) and a long period comet. This comet has approached the Sun for the first time (dynamically new) and broke on the way of approaching the Sun. Our data were taken with the Subaru/HDS 13 days before it broken. The obtained NH_3 OPR is 1.14 ± 0.02 in this comet. The corresponding T_{spin} of NH_3 is 29 ± 1 K like other comets typical in T_{spin}.

2.4.18. C/2013 R1 (LOVEJOY)

Comet C/2013 R1 (Lovejoy) originate from the Oort cloud and is not dynamically new comet (its period of ~12,000 year). The OPR of NH_3 in this comet is 1.13 ± 0.02. The resultant T_{spin} of NH_3 is 30 ± 2 K. The obtained OPR of NH_3 is in the typical range.

Table 2.2: OPR of NH_2 and NH_3 of all observations

Comets	Observational UT Data	Observed R_h [AU]	NH_2 OPR	NH_3 OPR
C/1995 O1 (Hale–Bopp)	March 28th, 1997	0.92	3.33 ± 0.26	1.17 ± 0.13
C/1999 S4 (LINEAR)	July 5th, 2000	0.86	3.31 ± 0.10	1.16 ± 0.05
C/2001 A2 (LINEAR)	July 27th, 2001	1.39	3.47 ± 0.11	1.24 ± 0.06
153P/Ikeya–Zhang	April 20th, 2002	0.89	3.27 ± 0.10	1.14 ± 0.05
C/2000 WM_1 (LINEAR)	March 7th, 2002	1.08	3.25 ± 0.07	1.13 ± 0.04
	March 7th, 2002	1.08	3.22 ± 0.09	1.11 ± 0.05
	March 8th, 2002	1.10	3.19 ± 0.10	1.10 ± 0.05
	March 8th, 2002	1.10	3.24 ± 0.11	1.12 ± 0.06
	March 22nd, 2002	1.33	3.25 ± 0.12	1.13 ± 0.06
	March 22nd, 2002	1.33	3.25 ± 0.08	1.13 ± 0.04
	March 23rd, 2002	1.34	3.26 ± 0.10	1.13 ± 0.05
	March 23rd, 2002	1.34	3.24 ± 0.11	1.12 ± 0.06
C/2002 V1 (NEAT)	January 8th, 2003	1.22	3.30 ± 0.08	1.15 ± 0.04

	January 8th, 2003	1.22	3.25 ± 0.11	1.13 ± 0.06
	January 10th, 2003	1.19	3.31 ± 0.10	1.16 ± 0.05
	January 10th, 2003	1.18	3.28 ± 0.10	1.14 ± 0.05
	March 21st, 2003	1.01	3.25 ± 0.09	1.13 ± 0.05
C/2002 X5 (Kudo–Fujikawa)	February 19th, 2003	0.70	3.29 ± 0.08	1.15 ± 0.04
	February 20th, 2003	0.72	3.25 ± 0.13	1.13 ± 0.07
	February 20th, 2003	0.72	3.22 ± 0.14	1.11 ± 0.07
	March 7th, 2003	1.06	3.27 ± 0.09	1.14 ± 0.05
	March 7th, 2003	1.07	3.21 ± 0.10	1.11 ± 0.05
	March 7th, 2003	1.07	3.28 ± 0.09	1.14 ± 0.05
C/2002 Y1 (Juels–Holvorcem)	May 29th, 2003	1.14	3.25 ± 0.10	1.13 ± 0.05
	May 29th, 2003	1.14	3.27 ± 0.09	1.14 ± 0.05
	May 30th, 2003	1.16	3.24 ± 0.12	1.12 ± 0.06
	May 30th, 2003	1.16	3.19 ± 0.12	1.10 ± 0.06
88P/Howell	April 18th, 2004	1.37	3.39 ± 0.09	1.20 ± 0.05
	April 19th, 2004	1.37	3.42 ± 0.09	1.21 ± 0.05
	April 20th, 2004	1.37	3.35 ± 0.06	1.18 ± 0.03
	April 22nd, 2004	1.37	3.41 ± 0.09	1.21 ± 0.05
	May 2nd, 2004	1.39	3.41 ± 0.11	1.21 ± 0.06
	May 3rd, 2004	1.39	3.37 ± 0.08	1.19 ± 0.04
	May 4th, 2004	1.39	3.31 ± 0.10	1.16 ± 0.05
	May 17th, 2004	1.42	3.45 ± 0.10	1.23 ± 0.05
	May 21st, 2004	1.43	3.45 ± 0.09	1.23 ± 0.05
	May 22nd, 2004	1.44	3.36 ± 0.08	1.18 ± 0.04
	May 24th, 2004	1.44	3.31 ± 0.10	1.16 ± 0.05
C/2001 Q4 (NEAT)	May 5th, 2004	0.98	3.25 ± 0.06	1.13 ± 0.03
	May 5th, 2004	0.98	3.20 ± 0.06	1.10 ± 0.03
	May 5th, 2004	0.98	3.22 ± 0.10	1.11 ± 0.05
	May 5th, 2004	0.98	3.16 ± 0.16	1.08 ± 0.08
	May 5th, 2004	0.98	3.17 ± 0.14	1.09 ± 0.07
	May 5th, 2004	0.98	3.19 ± 0.18	1.10 ± 0.09
	May 6th, 2004	0.98	3.27 ± 0.10	1.14 ± 0.05

	May 6th, 2004	0.98	3.24 ± 0.17	1.12 ± 0.09
	May 6th, 2004	0.98	3.23 ± 0.19	1.12 ± 0.10
	May 7th 2004	0.97	3.29 ± 0.08	1.15 ± 0.04
C/2002 T7 (LINEAR)	May 6th, 2004	0.68	3.24 ± 0.09	1.12 ± 0.05
	May 26th, 2004	0.94	3.25 ± 0.11	1.13 ± 0.06
	May 27th, 2004	0.94	3.28 ± 0.08	1.14 ± 0.04
C/2003 K4 (LINEAR)	November 20th, 2004	1.20	3.32 ± 0.07	1.16 ± 0.04
9P/Tempel 1	July 2nd, 2005	1.51	3.25 ± 0.08	1.13 ± 0.04
	July 3rd, 2005	1.51	3.25 ± 0.08	1.13 ± 0.04
	July 4th, 2005	1.51	3.24 ± 0.09	1.12 ± 0.05
	July 5th, 2005	1.51	3.32 ± 0.11	1.16 ± 0.06
	July 6th, 2005	1.51	3.31 ± 0.09	1.16 ± 0.05
	July 7th, 2005	1.51	3.27 ± 0.10	1.14 ± 0.05
	July 8th, 2005	1.51	3.33 ± 0.11	1.17 ± 0.06
	July 9th, 2005	1.51	3.27 ± 0.10	1.14 ± 0.05
	July 10th, 2005	1.51	3.28 ± 0.12	1.14 ± 0.06
	July 11th, 2005	1.51	3.29 ± 0.10	1.15 ± 0.05
73P–C/SW3	May 27th, 2006	0.95	3.04 ± 0.06	1.02 ± 0.03
73P–B/SW3	June 12th, 2006	0.94	3.02 ± 0.06	1.01 ± 0.03
8P/Tuttle	January 16th, 2008	1.04	3.29 ± 0.06	1.15 ± 0.03
	January 28th, 2008	1.03	3.28 ± 0.08	1.14 ± 0.04
	February 4th, 2008	1.03	3.26 ± 0.09	1.13 ± 0.05
103P/Hartley 2	October 18th, 2010	1.07	3.16 ± 0.04	1.08 ± 0.02
C/2012 S1 (ISON0	November 15th, 2013	0.60	3.28 ± 0.04	1.14 ± 0.02
C/2013 R1 (Lovejoy)	November 15th, 2013	1.07	3.26 ± 0.05	1.13 ± 0.02

Table 2.3: OPRs of NH_3, and $^{14}N/^{15}N$ ratios in CN for the comets

Comets	OPRs of NH_3	T_{spin} of NH_3 [K]	$^{14}N/^{15}N$ Ratios in CN	Orbital period [yrs]
C/1995 O1 (Hale–Bopp)	1.17 ± 0.13	28 +12/–4	143 ± 30[a]	4000
C/1999 S4 (LINEAR)	1.16 ± 0.05	28 +3/–2	150 ± 50[b]	Dynamically new
C/2001 A2 (LINEAR)	1.24 ± 0.06	25 ± 2	>60[c]	40000
153P/Ikeya–Zhang	1.14 ± 0.05	29 +4/–2	140 ± 50[d]	365
C/2000 WM_1 (LINEAR)	1.12 ± 0.02	30 ± 1	150 ± 30[e]	Dynamically new
C/2002 V1 (NEAT)	1.14 ± 0.02	29 ± 1	160 ± 35[c]	Young Long Period, 37000
C/2002 X5 (Kudo–Fujikawa)	1.13 ± 0.02	30 ± 1	130 ± 20[c]	Dynamically new
C/2002 Y1 (Juels–Holvorcem)	1.13 ± 0.03	30 ± 2	150 ± 35[c]	Old Long Period
88P/Howell	1.19 ± 0.02	27 ± 1	140 ± 20[b]	5.5
C/2001 Q4 (NEAT)	1.12 ± 0.02	30 ± 1	135 ± 20[a]	Dynamically new
C/2002 T7 (LINEAR)	1.13 ± 0.03	30 ± 2	160 ± 25[c]	Dynamically new
C/2003 K4 (LINEAR)	1.16 ± 0.04	28 +3/–2	145 ± 25[c]	Dynamically new
9P/Tempel 1	1.14 ± 0.02	29 ± 1	145 ± 25[f]	5.5
73P–B/SW3	1.01 ± 0.03	>39	210 ± 50[g]	5.4
73P–C/SW3	1.02 ± 0.03	>37	220 ± 40[g]	5.4
8P/Tuttle	1.14 ± 0.02	29 ± 1	150 ± 30[h]	13.6
103P/Hartley 2	1.08 ± 0.02	34 +3/–2	155 ± 25[i]	6.5
C/2012 S1 (ISON)	1.14 ± 0.02	29 ± 1	—	Dynamically new
C/2013 R1 (Lovejoy)	1.13 ± 0.02	30 ± 2	144 ± 37	12000

References: [a]Manfroid et al. (2005), [b]Hutsemékers et al. (2005), [c]Manfroid et al. (2009), [d]Jehin et al. (2004), [e]Arpigny et al. (2003), [f]Jehin et al. (2006), [g]Jehin et al. (2008), [h]Jehin et al. (2009a), [i]Meech et al. (2011)

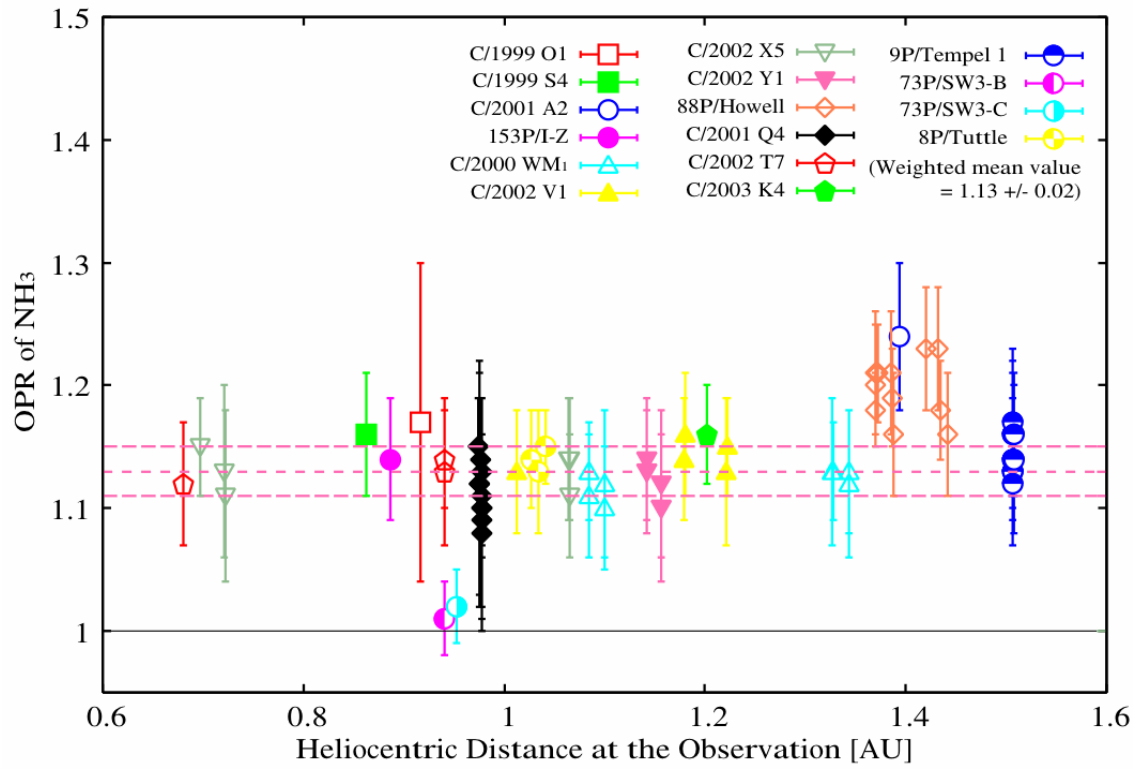

Figure 2.3: Relationship between OPRs of NH_3 and heliocentric distances at the date of the observations. The weighted mean value of OPR of cometary NH_3 in 15 comets is 1.13 ± 0.02 (pink dot and dash lines). Black bar shows the nuclear spin statistical weight ratio of ammonia (1.0). There is no correlation between the NH_3 OPRs and heliocentric distances at the observations. Therefore, OPRs may not be reflected the kinetic temperature of NH_3.

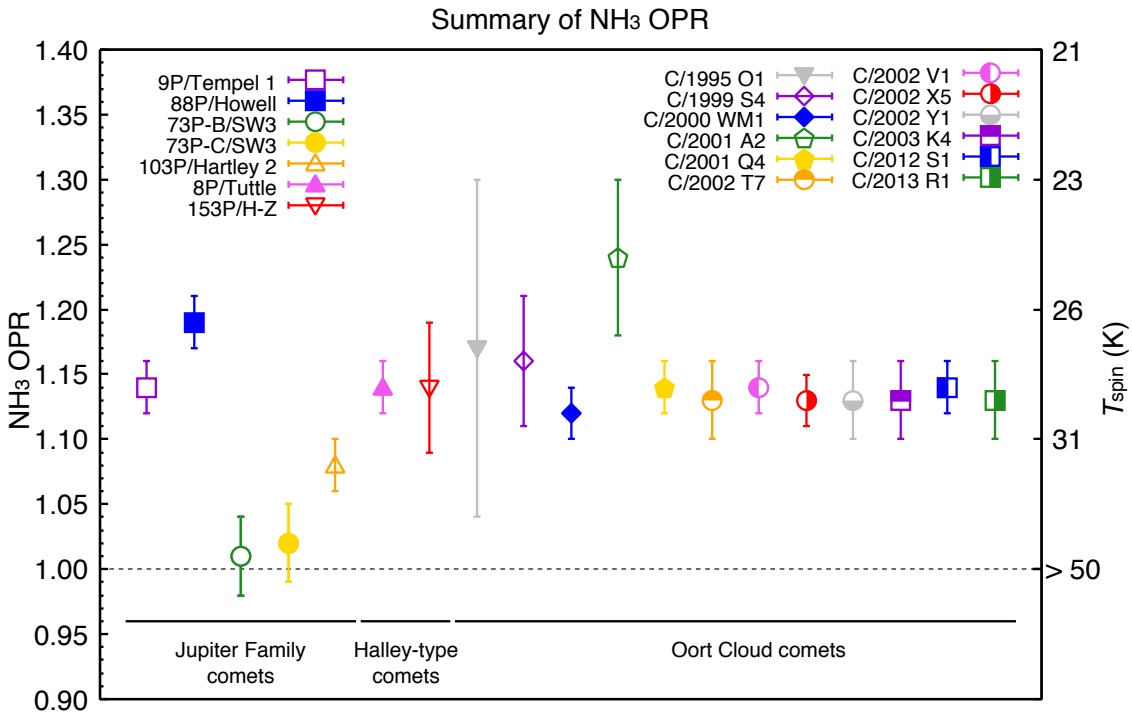

Figure 2.4: OPRs of NH_3 in comets (if multiple observations were carried out for a given comet. We show the weighted mean OPR). The dashed lines and dotted lines are the weighted mean value and ± 1 –σ levels for all measurements shown here. Both the OPRs and T_{spin} of ammonia shows a cluster between 1.1 and 1.2 and 30K for all comets in our sample except for 73P/SW3, respectively. Comet 73P/SW3 (both B– and C–fragments) shows the OPR of ammonia consistent with nuclear spin statistical weight ratio (1.0) that indicates a high temperature limit as T_{spin}.

2.5. DISCUSSIONS AND CONCLUSIONS

2.5.1 ORTHO–TO–PARA ABUNDANCE RATIO (OPR) OF COMETARY AMMONIA

Figures 2.3 and 2.4 summarize the results in this work. As clearly shown in these Figures, the OPRs of NH_3 show a cluster between 1.1 and 1.2 in our dataset. These values correspond to ~30 K as T_{spin}. Note that the fragments (–B and –C) of comet 73P/ Schwassmann–Wachmann 3 (hereafter, 73P/SW3) seem to be peculiar objects showing OPRs consistent with the high–temperature limit for NH_3 (1.0). Their error–bars are small enough to distinguish the comet 73P/SW3 from other comets. Comet 73P/SW3 is also showing a peculiar $^{15}N/^{14}N$ ratio measured in the CN radical (Jehin et al., 2008). We discuss the relationship between OPRs of NH_3 and $^{15}N/^{14}N$ ratios later.

First of all, we checked the relationship between the OPRs of NH_3 and the heliocentric distances when the comets were observed (Figure 2.3 and Table 2.2). Limbach et al. (2006) proposed that OPRs are diagnostic for the temperatures of the surface of cometary nucleus based on their theoretical studies. In this case, the OPRs should depend on the distances from the Sun at the observations since the surface temperature depends on the distance from the Sun (i.e., warmer when closer to the Sun). If we consider the blackbody approximation for the surface temperature of the nucleus, the temperature is expected to be $278/\sqrt{R_h}$ [K] at R_h [AU] from the Sun. Temperatures could vary by a factor of ~1.5 within the range of heliocentric distance from 0.7 to 1.5 AU. However, the OPRs determined in our dataset did not depend on the heliocentric distances at the observations (at least, in the range from 0.7 to 1.5 AU from the Sun) as shown in Figure 2.3. Such a trend was also found in our previous study (Kawakita et al., 2004) and also discussed by Crovisier (2006, 2007). Therefore, the OPRs probably don't reflect the temperatures of the nucleus surface.

Cacciani et al. (2009) recently calculated the nuclear spin conversion rate of NH_3 in the gas phase based on a quantum relaxation model (QRM). The conversion between ortho and para species may also be possible by proton–exchange reactions in the coma (Irvine et al., 2000). In such cases,

the nuclear spin temperatures might equilibrate with the kinetic temperatures of the gas in the coma. However, the OPRs determined in our dataset are almost constant for the comets with different gas production rates at different heliocentric distances. Since the kinetic temperature of gas in the coma depends on both the heliocentric distance (i.e., the total energy input to the comet from the Sun) and the total gas production rate (the gas in the coma would be heated up by the hot photo–dissociation products of parent molecules like water), our results imply that the OPRs are nearly constant for different kinetic temperatures of the gas in the coma. Furthermore, the OPRs of water and NH_2 were observed to be constant with distances from the nucleus in the coma for a few comets in the previous studies (Kawakita et al., 2004; Bonev et al., 2007, 2008a). It is unlikely that ortho and para species were interchanged in the coma.

The possibility that the OPRs of NH_3 equilibrated with the internal temperatures of the cometary nuclei (Mumma et al., 1993) is re–examined here. According to theoretical studies (e.g., Rosenberg & Prialnik, 2007; Prialnik et al., 2004; Podolak & Prialnik, 1996) the internal temperature at a depth of several meters or deeper is almost constant. Therefore, the OPR might equilibrate with such internal temperature for a long time. Based on Table 2.3, however, there is no clear relationship between OPRs and orbital periods, as already pointed out in the previous studies (Irvine, 2000; Kawakita et al., 2004; Crovisier, 2007). At least, it seems unlikely that all comets discussed here (their orbital periods span the range from ~5 to longer than 10^4 years) have internal temperatures near 30 K. Our results imply that the OPRs are not related to the internal temperatures of the cometary nuclei.

On the other hand, from the viewpoint of the dynamical origin of the comets, the OPR of cometary NH_3 doesn't depend on the dynamical reservoirs of comets (the Oort cloud or the Kuiper belt) as shown in Figure 2.4. Different dynamical reservoirs originated in different regions in the solar nebula (although the cometary birth places for the different reservoirs might be partly overlapped with each other, as proposed by the Nice model, see Morbidelli (2008)), and therefore, it appears that OPRs are not related to

the physical conditions in the solar nebula.

If OPRs equilibrated with the temperatures where comets formed (from 5 to 30 AU from the Sun) in the solar nebula, the nuclear spin temperatures would vary by a factor of ~2 or more based on the modeled temperature profile of the solar nebula (Boss, 2001; Hersant et al., 2001; Jang–Condell, 2008; Willacy et al., 1998) while the obtained nuclear spin temperatures are nearly constant, ~30 K. We then conclude that the OPR of NH_3 reflects an old memory before cometary formation in the solar nebula (except for comet 73P/SW3). The OPRs of NH_3 probably reflect the processes and physical conditions prevailing during the molecular formation in the pre–solar molecular cloud. Cometary ammonia (and probably also water) formed on cold grains at ~30 K in the pre–solar molecular cloud. The comet 73P/SW3 which is an exception for this scenario will be discussed in Subsection 2.5.3.

2.5.2 COMPARISON OF AMMONIA OPRs WITH OTHER PROPERTIES

The relationship between the OPRs of NH_3 and the $^{14}N/^{15}N$ ratios in CN, is the most interesting result as shown in Figure 2.5 and Table 2.3. Most comets show similar OPRs (1.1 – 1.2) and similar $^{14}N/^{15}N$ ratio (~140) except for comet 73P/SW3. Comet 73P/SW3 is clearly distinguished in the plot of the OPR of NH_3 versus the $^{14}N/^{15}N$ ratio in CN. Based on this result, there may be some link between the OPR of NH_3 and the $^{14}N/^{15}N$ ratio in CN. There may be two distinct groups of comets in the plot as shown in Figure 2.5. Bonev et al. (2008a) also pointed out the existence of two groups based on water OPRs. Such a classification is very curious for comet's taxonomy. Figure 2.5 may imply that the molecules in cometary ice formed in similar environments for most comets. Since comet 73P/SW3 shows the NH_3 OPRs of 1.0 (a high–temperature limit) and higher $^{14}N/^{15}N$ ratio in CN (lower fractionation in ^{15}N) than other comets, those facts indicate that the materials incorporated in comet 73P/SW3 formed under relatively warmer conditions than most comets.

Please note that it is hard to explain the observed $^{14}N/^{15}N$ ratios (~140) under cold temperatures (~30 K) estimated from the observed OPRs of NH_3 (1.1 – 1.2) as T_{spin}. The $^{14}N/^{15}N$ ratios in HCN (that is likely a major parent of

CN in cometary coma) in the gaseous phase were determined to be in the range 200 – 600 by radio observations of pre–protostellar cores with kinetic temperatures of 6 – 10 K (Hily–Blant et al., 2010). These values are higher than the $^{14}N/^{15}N$ ratios found in comets (~140). Such high fractionation of ^{15}N in comets is also found in interplanetary dust particles (IDPs) in our Solar system (Messenger et al., 2003). The model for ^{15}N–fractionation in nitriles could explain the discrepancy by interstellar chemistry at low temperatures proposed by Rodgers & Charnley (2008a). The authors claimed that the super–fractionation for the solid–phase isotopologues of nitriles occurs under low temperature conditions (~7 K). However, this temperature is inconsistent with nuclear spin temperatures of NH_3 in comets.

This fact may indicate that (1) physical temperatures estimated as nuclear spin temperatures are not appropriate, or (2) there might be other mechanisms to achieve the fractionation of ^{15}N in the parent molecules of CN (HCN) under temperatures at ~30 K. Regarding case (1), we usually refer to the rotational energy levels of isolated NH_3 in space. We may have to refer to the rotational energy diagram of NH_3 on the grain where the molecules formed and its OPR was fixed, as pointed out by Crovisier (2007). However, the rotational energy structure for NH_3 physisorbed on grain is expected to be not so different from the case of isolated NH_3. When we assume the isolated molecules for the calculation of T_{spin}, water and methane as well as ammonia indicate similar T_{spin} in each comet (Figure 2.6). This fact may indicate that those molecules physisorbed on cold grains at their formation.

Furthermore, the temperature of grains might not be the same as the temperature of surrounding gas in diffuse cloud environments (they might not be in thermal equilibrium). NH_3 formed on cold grain surface efficiently while HCN (as a parent of CN in cometary coma) could be formed in gas phase efficiently (Rodgers & Charnley, 2008b). Therefore, both OPRs of NH_3 and $^{14}N/^{15}N$ ratios in CN might not indicate the same temperature. Otherwise, NH_3 and HCN formed at different epoch (e.g., at different temperatures) even in the same molecular cloud or in the solar nebula. In any case, future determination of $^{14}N/^{15}N$ in NH_3 is quite essential to get more information on the relationship between OPRs and $^{14}N/^{15}N$ in cometary

materials (Charnley & Rodgers, 2008).

The D/H ratio in cometary molecules also reflects the conditions at the time of molecular formation in the early solar system. The D/H ratio is a powerful tool to investigate the formation temperature of molecules in the pre–solar molecular cloud or the solar nebula, especially under low temperature conditions. However, the number of comets in which the D/H ratios of water were determined is quite limited. Note that the D/H ratio is different for different molecular species; here we concentrate on the D/H ratio in water. The D/H ratios in water is about the same in all the comets observed so far, and the comets showing similar D/H ratios also show similar OPRs of NH_3, as shown in Figure 2.7. This result also supports the hypothesis that the OPRs of NH_3 reflect primordial information. But we clearly need more data for the D/H ratio in water to go further.

We also investigate the relationship between the mixing ratios of CO, CH_4, C_2H_2, C_2H_6, HCN, CH_3OH and NH_3 with respect to H_2O and the OPRs of NH_3 in comets (Figures 2.8, 2.9, 2.10, 2.11, 2.12, 2.13 and 2.14). Especially, the sublimation temperatures of CO and CH_4 are around 30 K and their mixing ratios may be related to the OPRs (T_{spin} ~ 30 K). The mixing ratios of 7 molecular species exhibit variety in chemistry of the comets although the OPRs of NH_3 are almost constant in our samples. There are no clear correlations in those Figures. The mixing ratios might reflect the surrounding environment where planetesimals formed or where cometary ices condensed from gas–phase in the solar nebula. Alternatively, hyper–volatiles like CO and CH_4 might sublimate from the icy grains and these icy grains accreted to cometary nuclei under warmer conditions in the solar nebula.

2.5.3 PECULIARITY OF COMET 73P/ SCHWASSMANN–WACHMANN 3 (B– AND C–FRAGMENTS)

We next consider the peculiar nature of comet 73P/SW3 in Figure 2.5. As pointed out in previous studies, comet 73P/SW3 shows not only peculiar OPRs of both H_2O and NH_3 but also peculiar chemical compositions of ice (Bonev et al., 2008a; Dello Russo et al., 2007; Jehin et al., 2008; Kobayashi et

al., 2007). The depletion in hyper–volatiles and the nuclear spin temperatures of both H_2O and NH_3 that are higher in the case of comet 73P/SW3 than in typical comets suggest that comet 73P/SW3 formed in a warmer region of the solar nebula (Jehin et al., 2008; Kobayashi et al., 2007). High $^{14}N/^{15}N$ ratio in CN also supports this hypothesis.

Several scenarios could be proposed for the peculiar OPRs in comet 73P/SW3. As a first scenario, comet 73P/SW3 might form from icy grains re–condensed in a relatively warmer region of the solar nebula. The temperatures in the solar nebula became colder as the mass–accretion rate from the surrounding envelope of the solar nebula became smaller. Icy grains falling onto the solar nebula were once evaporated by the infall–shock in the inner region (within ~30 AU, Lunine et al., 1991) and chemical reactions could occur in the gas–phase. OPRs of molecules could be modified by those reactions (e.g., proton–exchange reactions). Thus, the re–condensed icy grains from the chemically altered materials in the solar nebula may indicate the signature of higher temperatures.

As a second scenario, the warming–up by radioactive–nuclei in the interior of cometary materials may be another explanation for the observational results. Since we observed the fragments of comet 73P/SW3, fresh ices (typical of the nucleus interior) might be exposed on their surface in this case. Because of the decay of ^{26}Al (Grimm & McSween, 1993), the interior was heated up after the comet formation and both the OPR and $^{14}N/^{15}N$ ratios might have been reset in the interior while icy materials were not altered in other parts (near the surface) of the cometary nuclei. However, we could not find any mechanisms to achieve such alternations of both OPR and $^{14}N/^{15}N$ ratio. Observations of other break–up comets in the future might support this scenario.

We would like to note the difference between comets C/1999 S4 (LINEAR) and 73P/SW3. As we already discussed in subsection 2.4.2, comet C/1999 S4 (LINEAR) was depleted in organic volatiles but the T_{spin} of both H_2O and NH_3 is within the typical range as well as the $^{14}N/^{15}N$ ratio in CN. On the other hand, both the OPRs and the $^{14}N/^{15}N$ ratios are out of the typical range in the case of comet 73P/SW3 (Figure 2.5), which is also depleted in the

volatiles. This discrepancy may be explained by chemical alteration of cometary materials in the warm region of the solar nebula. Most comets are thought to consist of icy materials formed in the pre–solar molecular cloud. Some highly volatile species might evaporate partially before the icy grains were incorporated into the comet, modifying the chemical composition. In addition, the icy materials incorporated into comet 73P/SW3 might have condensed from the molecular gas in which gas–phase chemistry had changed OPRs and $^{14}N/^{15}N$ ratios.

2.5.4 SUMMARY

We present OPRs of NH_3 in 15 comets based on high–dispersion spectra of the NH_2 (0,9,0) band in the optical range. The NH_3 OPR of comets in our sample show a cluster between 1.1 and 1.2 (~30 K as T_{spin}) except for comet 73P/SW3. Both B– and C–fragments of this comet showed the ammonia OPRs consistent with the nuclear spin statistical weight ratio (1.0) indicative of the high–temperature limit. Comparisons between OPRs of NH_3 and other properties ($^{14}N/^{15}N$ ratios in CN, D/H ratios of water, and mixing ratios of volatiles) are explored.

In the plot of the OPRs of NH_3 versus $^{14}N/^{15}N$ ratios in CN, we can find that comet 73P/SW3 is clearly separated from the main group (normal). This may indicate the existence of a 2nd group as pointed out by Bonev et al. (2008a) based on the OPRs of water. Higher fractionation of ^{15}N corresponds to higher OPR (i.e., lower T_{spin}) of NH_3 in the plot. Therefore, these facts also support the hypothesis that the OPR of NH_3 is a primordial character of cometary molecules. Although the D/H ratios of water had been obtained only in a small number of comets, their values clustered around $3x10^{-4}$ and the comets showing similar D/H ratios also show similar OPRs of NH_3. This fact also supports the hypothesis that the OPR is one of the primordial properties of cometary ices. The peculiar nature of comet 73P/SW3 could be attributed to a different origin of icy materials in the solar nebula (e.g., difference in temperature, epoch, or chemical alterations).

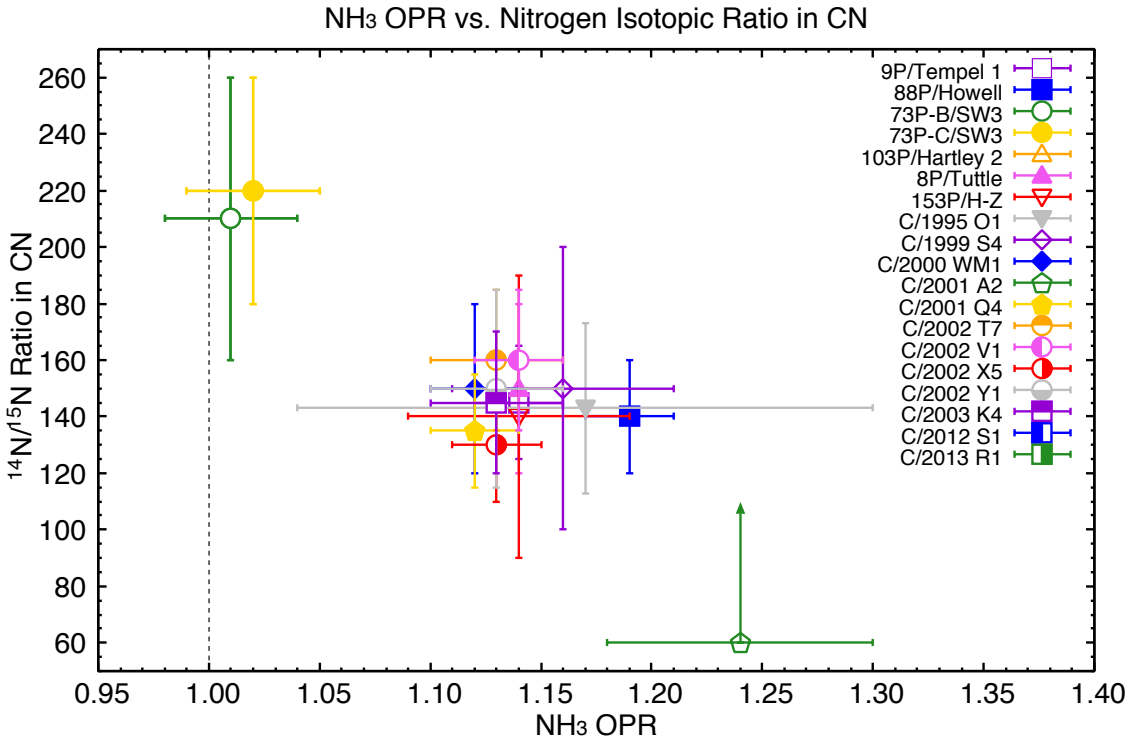

Figure 2.5: Relationship between $^{14}N/^{15}N$ ratios in CN and NH_3 OPRs. Most comets show similar OPRs (1.1 – 1.2) and similar $^{14}N/^{15}N$ ratios (~140) except for comet 73P/SW3. Comet 73P/SW3 is clearly distinguished from other comets in this plot. Based on this Figure, it is likely that both the OPR of NH_3 and the $^{14}N/^{15}N$ ratio in CN reflect the same environment at molecular formation. There may be two distinct groups of comets in this plot. This figure is based on Table 2.3. The vertical dashed line indicates the high–temperature limit of NH_3 OPR (1.0).

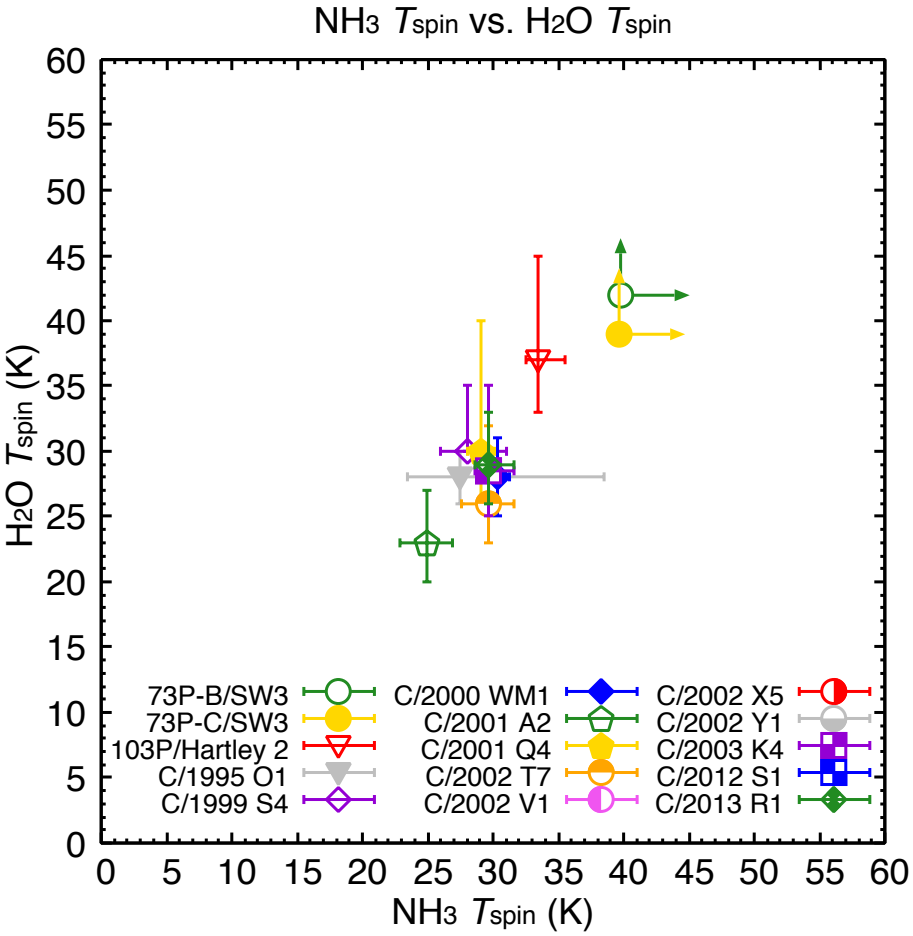

Figure 2.6: Comparison among T_{spin} of H_2O and NH_3. Water and ammonia indicate consistent T_{spin} in each comet. This fact may indicate that those molecules equilibrated with cold grains at ~30 K. They might physisorb on the cold grains at their formation (see text).

References.– C/1995 O1 (Crovisier et al., 1997), C/1999 S4 (Dello Russo et al., 2005), C/2001 A2 (Dello Russo et al., 2005), C/2000 WM_1 (Radeva et al., 2010), C/2004 Q2 (Bonev et al., 2007; Bonev et al., 2009; Kawakita & Kobayashi, 2009), C/2001 Q4 (Kawakita et al., 2006), C/2003 K4 (Woodward et al., 2007), 73P/SW3 –B and –C (Bonev et al., 2007)

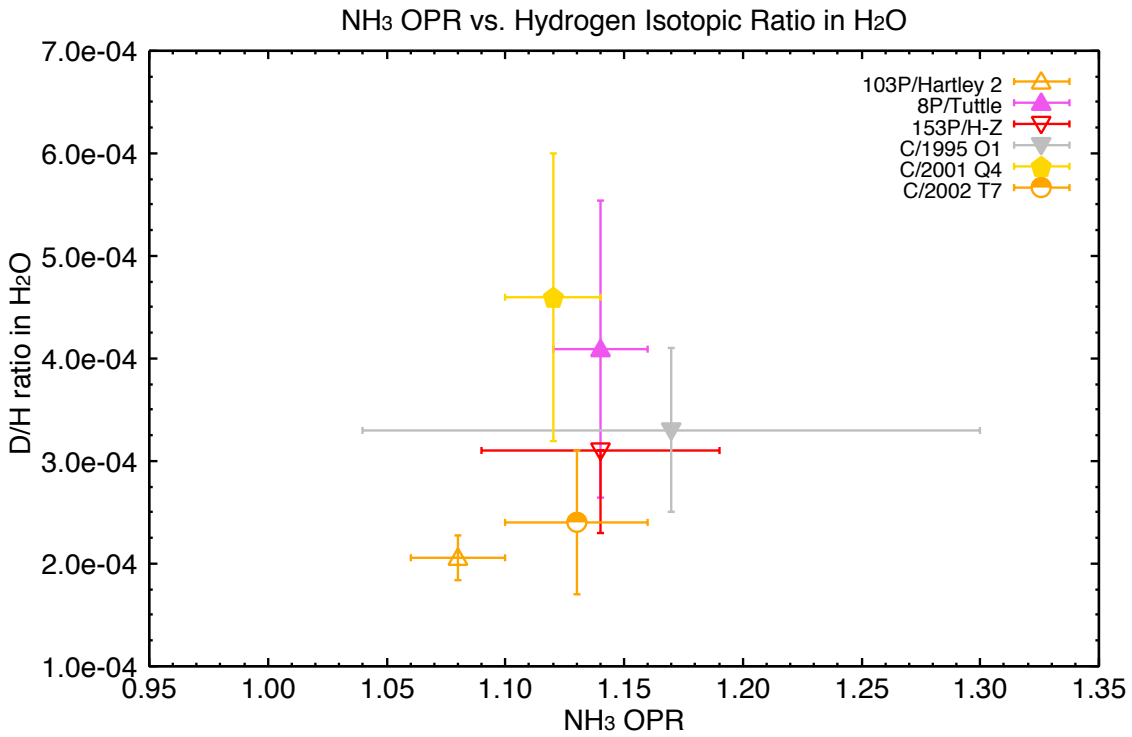

Figure 2.7: Relationship between D/H ratios in water and NH_3 OPRs. The D/H ratio in cometary molecules also reflects the conditions at the time of molecular formation in the early solar system. The D/H ratios in water is almost the same in all the comets observed so far, and the comets showing similar D/H ratios also show similar OPRs of NH_3. This result also supports the hypothesis that the OPRs of NH_3 reflect the primordial conditions in the early solar system.

References.– C/1995 O1 (Meier et al., 1998), 153P/Ikeya–Zhang (Biver et al., 2006), C/2001 Q4 (Weaver et al., 2008), C/2002 T7 (Hutsemékers et al., 2009), 8P/Tuttle (Villanueva et al., 2009)

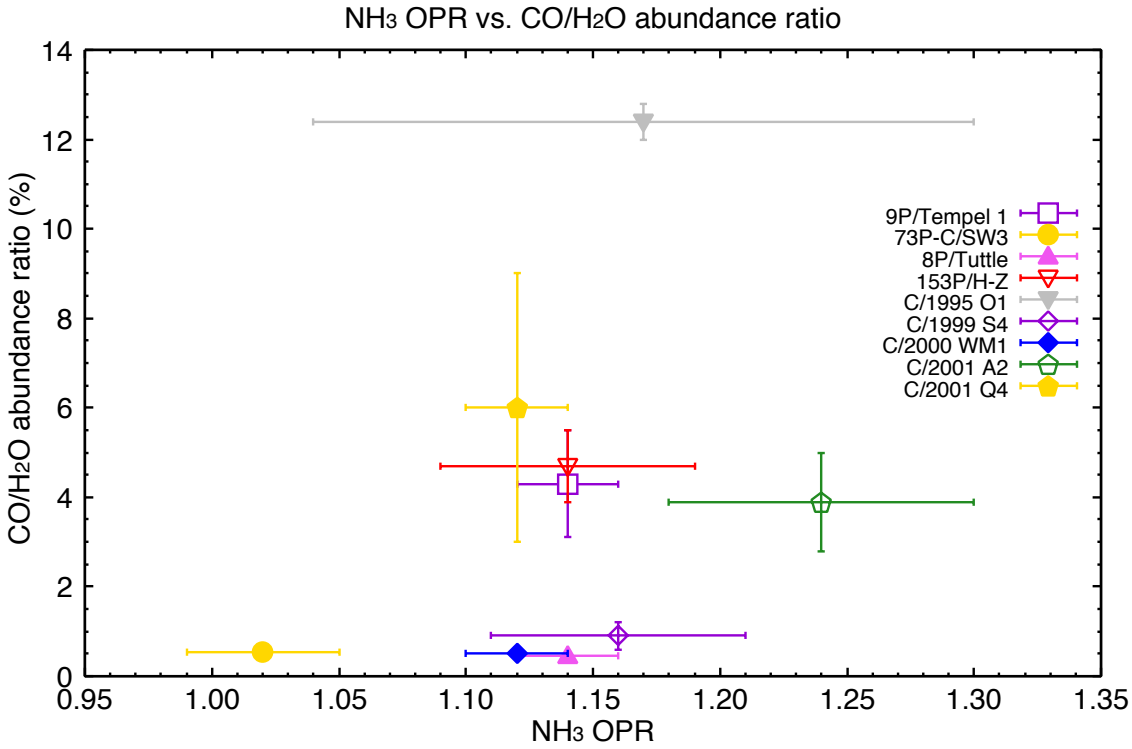

Figure 2.8: Relationship between NH_3 OPRs and CO mixing ratios (the sublimation temperature T_{subl} = 25 K in the early solar nebula: Meech & Svoren 2004). Note that T_{subl} is close to T_{spin} of NH_3 obtained for many comets (~30 K). The CO mixing ratios exhibit variety in chemistry of the comets although the OPRs of NH_3 are nearly constant in our samples. The CO mixing ratios probably reflect different environments (and /or different epochs) from that reflected by the OPR of NH_3. Otherwise, CO mixing ratio might be very sensitive to the temperature at the ice formation in the early solar nebula.

References.– C/1995 O1 (DiSanti et al., 2001), C/1999 S4 (Mumma et al., 2003), C/2001 A2 (Magee–Sauer et al., 2008), 153P/Ikeya–Zhang (Mumma et al., 2003), C/2000 WM_1 (Radeva et al., 2010), C/2001 Q4 (Combi et al., 2009), 9P/Tempel 1 (Mumma et al., 2005), 73P/SW3–C (DiSanti et al., 2007), 8P/Tuttle (Böhnhardt et al., 2008)

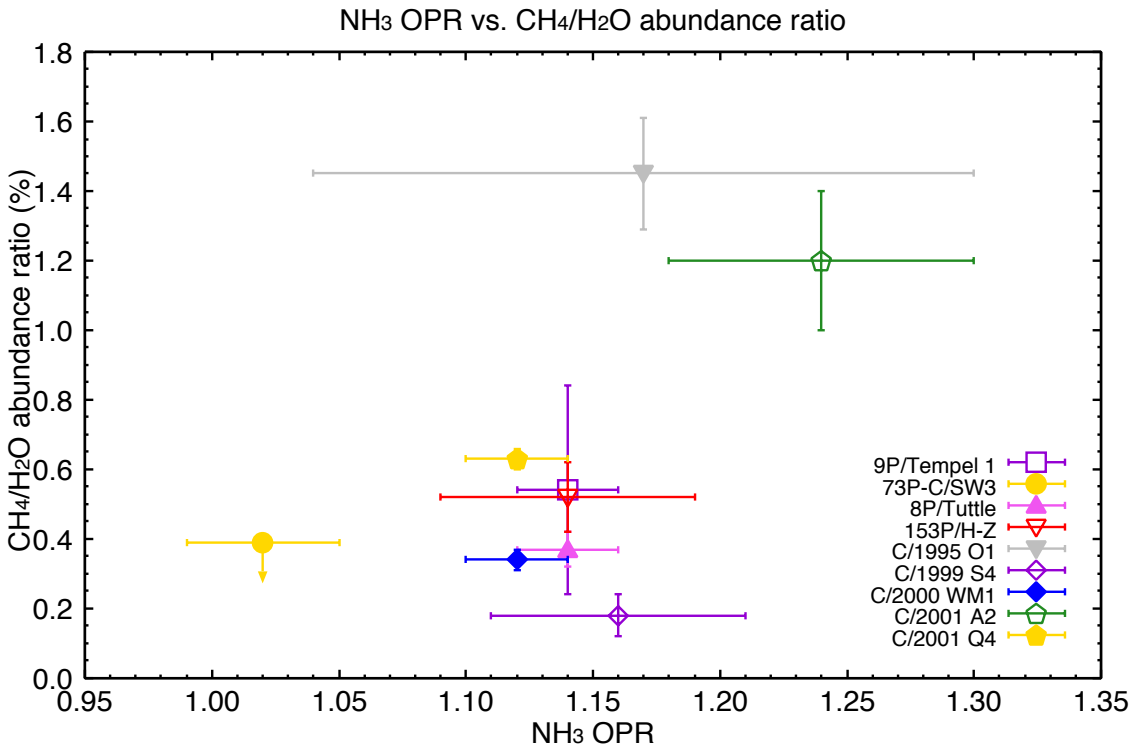

Figure 2.9: Relationship between NH_3 OPRs and CH_4 mixing ratios (T_{subl} = 31 K). The CH_4 mixing ratios also exhibit variety in chemistry of the comets although the OPRs of NH_3 are nearly constant in our samples. As in the case of CO mixing ratio, different environments might be reflected by CH4 mixing ratios and OPR of NH_3.

References.– C/1995 O1 (Mumma et al., 2003), C/1999 S4 (Mumma et al., 2005), C/2001 A2 (Magee–Sauer et al., 2008), 153P/Ikeya–Zhang (Kawakita et al., 2003), C/2000 WM_1 (Radeva et al., 2010), C/2001 Q4 (Onishi et al., 2008), 9P/Tempel 1 (Mumma et al., 2005), 73P/SW3–C (Villanueva et al., 2006), 8P/Tuttle (Böhnhardt et al., 2008; Bonev et al., 2008)

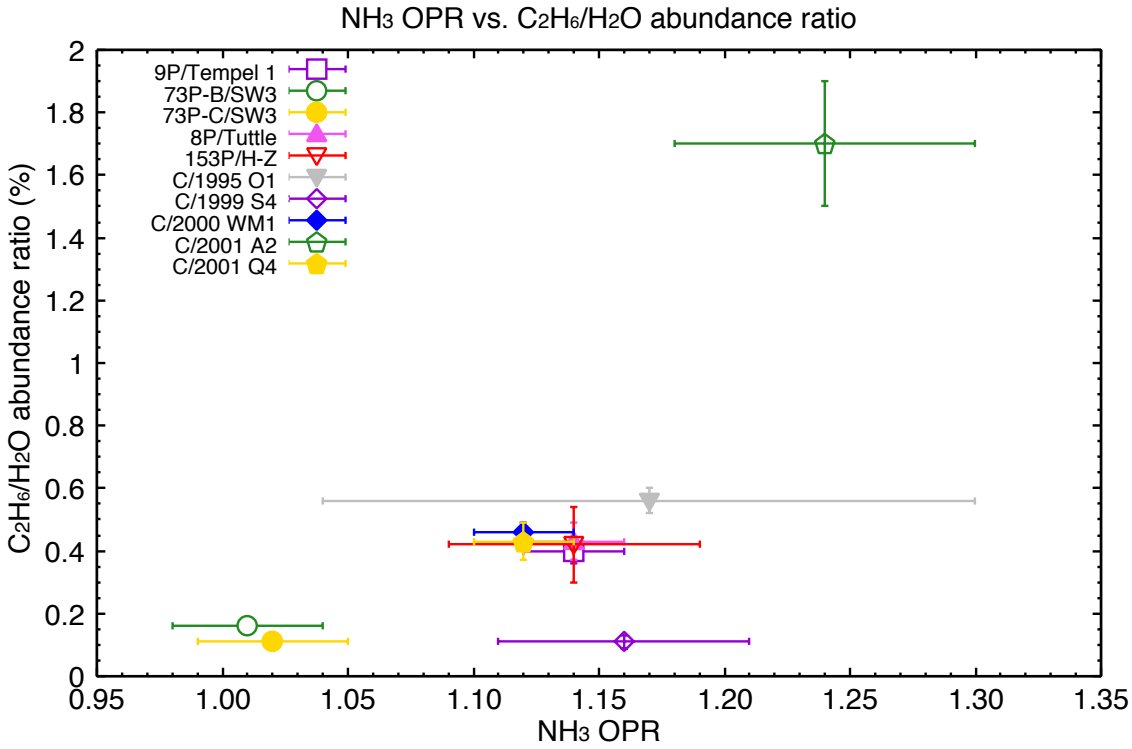

Figure 2.10: Relationship between NH_3 OPRs and C_2H_6 mixing ratios (T_{subl} = 44 K). Since he T_{subl} is higher than T_{spin} obtained for the comets (~30 K) and OPRs of NH_3 are nearly constant in our sample, little variation in mixing ratios of C_2H_6 relative to H_2O are expected if T_{spin} indicates the temperature condition at the ice formation in the early solar nebula. The C_2H_6 mixing ratios, however, also exhibit variety in chemistry of the comets although the OPRs of NH_3 are nearly constant in our samples. No clear correlation is found between them.

References.– C/1995 O1 (Dello Russo et al., 2001), C/1999 S4 (Mumma et al., 2003), C/2001 A2 (Magee–Sauer et al., 2008), 153P/Ikeya–Zhang (Kawakita et al., 2003), C/2000 WM_1 (Radeva et al., 2010), C/2001 Q4 (Onishi et al., 2008), 9P/Tempel 1 (DiSanti et al., 2007), 73P/SW3–B and –C (Dello Russo et al., 2007), 8P/Tuttle (Kobayashi et al., 2010)

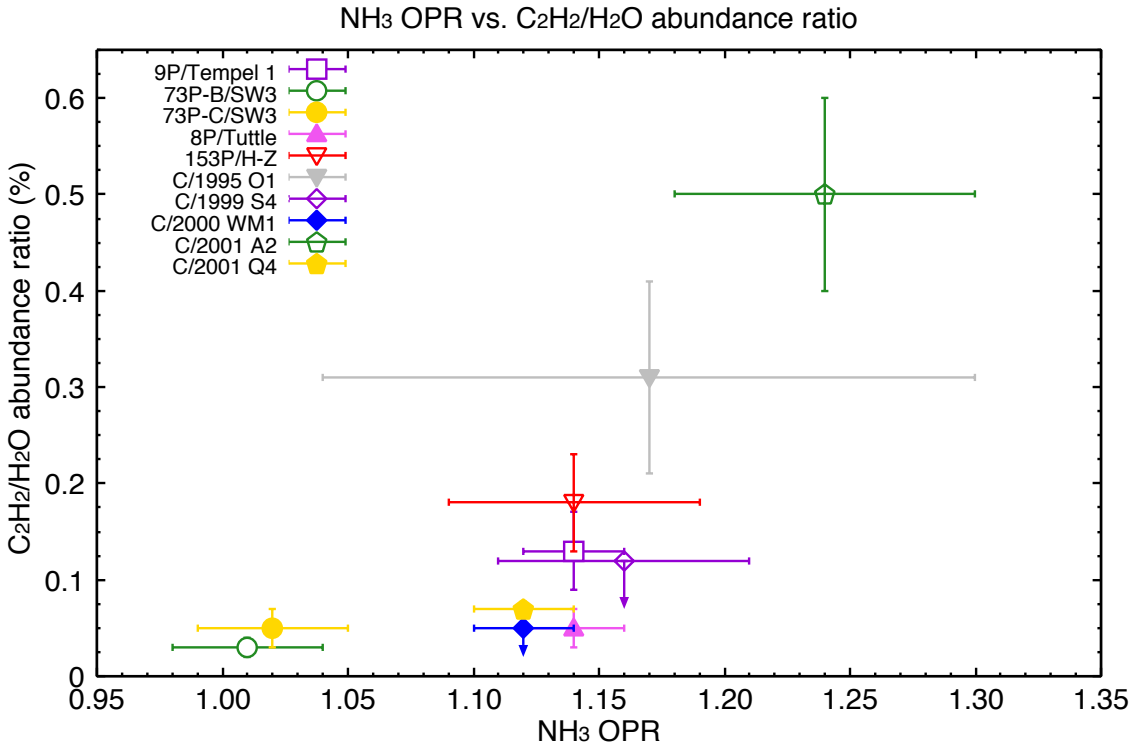

Figure 2.11: Same as Figure 2.10, but of C_2H_2 mixing ratios (T_{subl} = 57 K). References.– C/1995 O1 (Magee–Sauer et al., 2001), C/1999 S4 (Mumma et al., 2003), C/2001 A2 (Magee–Sauer et al., 2008), 153P/Ikeya–Zhang (Mumma et al., 2003), C/2000 WM_1 (Radeva et al., 2010), C/2001 Q4 (Onishi et al., 2008), 9P/Tempel 1 (Mumma et al., 2005), 73P/SW3–B and –C (Dello Russo et al., 2007), 8P/Tuttle (Kobayashi et al., 2010)

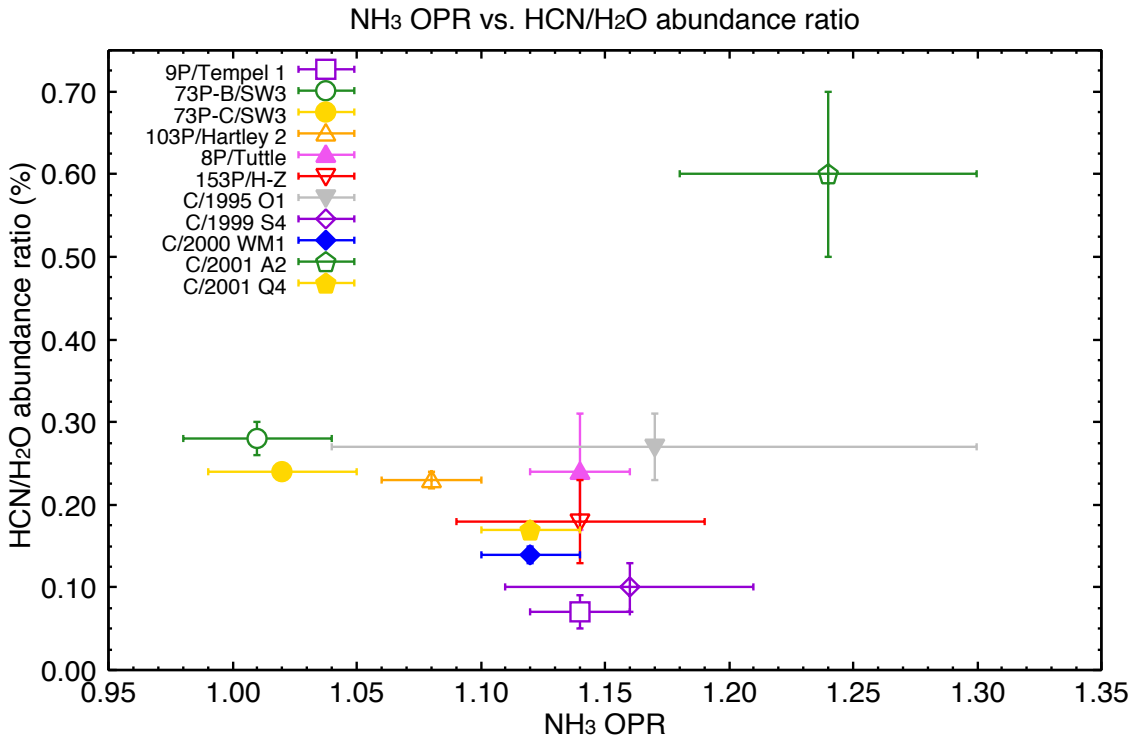

Figure 2.12: Same as Figure 2.10, but of HCN mixing ratios ($T_{\mathrm{subl}} = 95$ K). References.– C/1995 O1 (Magee–Sauer et al., 2001), C/1999 S4 (Mumma et al., 2001b), C/2001 A2 (Magee–Sauer et al., 2008), 153P/Ikeya–Zhang (Magee–Sauer et al., 2002), C/2000 WM_1 (Radeva et al., 2010), C/2001 Q4 (Onishi et al., 2008), 9P/Tempel 1 (Mumma et al., 2005), 73P/SW3–B and –C (Dello Russo et al., 2007), 8P/Tuttle (Kobayashi et al., 2010)

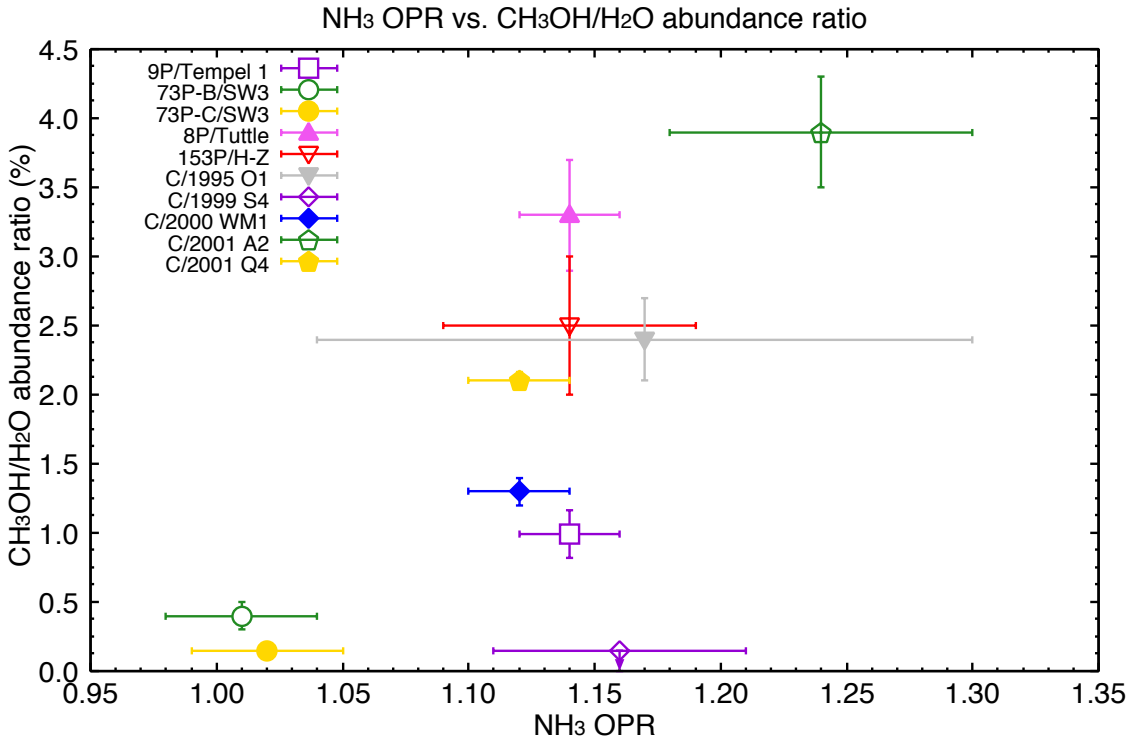

Figure 2.13: Same as Figure 2.10, but of CH_3OH mixing ratios (T_{subl} = 99 K).

References.– C/1995 O1 (Biver et al., 1999), C/1999 S4 (Mumma et al., 2003), C/2001 A2 (Magee–Sauer et al., 2008), 153P/Ikeya–Zhang (Mumma et al., 2003), C/2000 WM_1 (Radeva et al., 2010), C/2001 Q4 (Onishi et al., 2008), 9P/Tempel 1 (Mumma et al., 2005), 73P/SW3–B and –C (Dello Russo et al., 2007), 8P/Tuttle (Kobayashi et al., 2010)

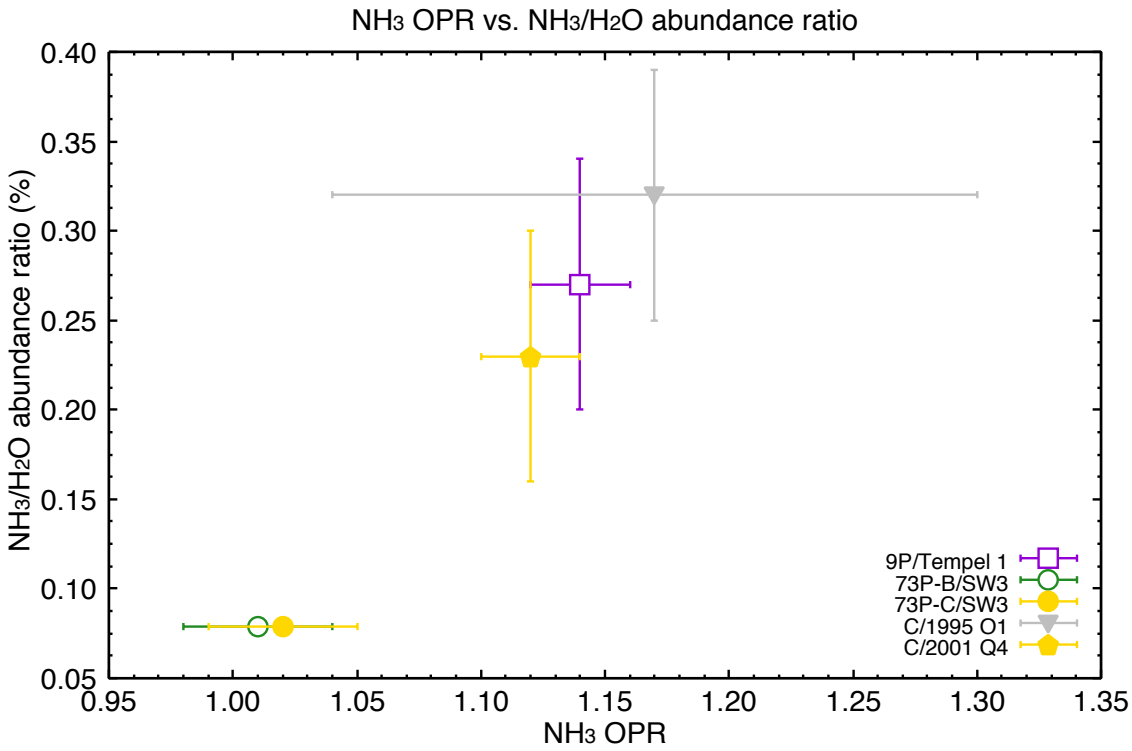

Figure 2.14: Same as Figure 2.10, but of NH_3 mixing ratios (T_{subl} = 78 K). The NH_3 mixing ratios are estimated from NH_2/H_2O ratios obtained in optical spectroscopic observations (Fink 2009) based on the photodissociation branching ratio of NH_3 to NH_2 (0.95). In this plot, there may be the correlation between OPRs of NH_3 and NH_3 mixing ratios.

3. ORTHO-TO-PARA ABUNDANCE RATIO OF WATER ION IN COMET C/2001 Q4 (NEAT): IMPLICATION FOR ORTHO-TO-PARA ABUNDANCE RATIO OF WATER

ABSTRACT

The ortho-to-para abundance ratio (OPR) of cometary molecules is considered to be one of the primordial characteristics of cometary ices, and contains information concerning their formation. Water is the most abundant species in cometary ices, and OPRs of water in comets have been determined from infrared spectroscopic observations of H_2O rovibrational transitions so far. In this paper, we present a new method to derive OPR of water in comets from the high-dispersion spectrum of the rovibronic emission of H_2O^+ in the optical wavelength region. Other molecular emission lines sometimes contaminate the rovibronic emission line of H_2O^+ but they are not affected seriously by telluric absorption compared with near-infrared observations. Since H_2O^+ ions are mainly produced from H_2O by photoionization in the coma, the OPR of H_2O^+ is considered to be equal to that of water based on the nuclear spin conservation through the reaction. We have developed a fluorescence excitation model of H_2O^+ and applied it to the spectrum of comet C/2001 Q4 (NEAT). The derived OPR of water is 2.54 +0.32 / –0.25, which corresponds to a nuclear spin temperature ($T_{\rm spin}$) of 30 +10 / –4 K. This is consistent with the previous value determined in the near-infrared for the same comet (OPR = 2.6 ± 0.3, T_{spin} = 31 +11 / –5 K).

3.1. INTRODUCTION

Comets are small icy bodies that consist of both dust and icy materials. They formed from materials that existed in the solar nebula 4.6 Gyr ago. Those materials probably formed in the presolar molecular cloud and were chemically processed in the solar nebula. Comets have conserved the information about physical and chemical conditions in the early solar system because they have spent a long time in a cold region far from the Sun (such

as the Oort Cloud or Kuiper Belt) after their formation. Thus, comets are considered to be the most pristine objects in the solar system.

Some primordial characteristics of comets have been used to investigate the physico-chemical conditions of the early solar system. Ortho-to-para abundance ratios (OPRs) of cometary molecules such as water are one of the interesting quantities considered as cosmogonic. OPRs seem to reflect the temperatures of molecular formation in the solar nebula or the pre- solar molecular cloud. However, their real meaning is still in debate (Bockelée-Morvan et al., 2009; Bonev et al., 2007, 2008, 2009; Cacciani et al., 2009; Crovisier 2006, 2007; Crovisier et al., 2008; Dello Russo et al., 2005; Jehin et al., 2008, 2009; Kawakita and Watanabe 2002; Kawakita et al., 2004, 2005, 2006, 2007; Kawakita & Kobayashi 2009; Pardanaud et al., 2007; Woodward et al., 2007, and references therein). The nuclear spin temperature ($T_{\rm spin}$, defined as the rotational excitation temperature that can reproduce a given OPR under thermal equilibrium conditions) is one possible interpretation for the OPR. The OPRs of H_2O, NH_3, and CH_4 in comets observed so far indicate T_{spin} ~30 K except for a few samples (Shinnaka et al., 2010, 2011).

The OPR of water that is the most abundant species in cometary ices has been determined from vibrational transitions in the infrared: ν_1 and ν_3 fundamental bands around 2.7μm (Mumma et al., 1987; Crovisier et al., 1997) and hot bands around 2.9 μm (e.g., Dello Russo et al., 2005; Kawakita et al., 2006; Bonev et al., 2007, 2008; Kawakita & Kobayashi 2009; Kobayashi et al., 2010) as well as the ν_2 fundamental band around 6 μm (Woodward et al., 2007; Bockelée-Morvan et al., 2009). Recent progress of near-infrared, high-dispersion spec- troscopy allows us to determine the OPR of water routinely from ground-based observatories through the hot-band emission lines. However, serious absorption by the telluric atmosphere sometimes prevents accurate determination of OPRs of water through the hot-band emission lines around 2.9 μm.

Here we present a new method to derive OPRs of water in comets from a high-dispersion, rovibronic emission spectrum of H_2O^+ in the optical. The

optical spectrum of H_2O^+ is not affected seriously by telluric absorption compared with near- infrared observations. Moreover, our new method allows us to derive OPRs of water for comets observed in the past since many high-dispersion spectra of H_2O^+ in comets have been reported. We should increase the number of samples for OPRs of water in comets.

3.2. DETERMINATION OF OPR OF WATER FROM THAT OF H_2O^+

3.2.1. PRODUCTION OF H_2O^+ IN THE COMA

Ionized water (H_2O^+) can be produced by the photoionization reaction in the coma: $H_2O + h\nu \rightarrow H_2O^+ + e^-$ (Huebner et al., 1992). Based on our chemical model in the coma (Schmidt et al., 1988; Huebner et al., 1991; Boice et al., 1995; Helbert et al., 2005; Boice & Wegmann 2007; Boice & Martinez 2010, and references therein), the contribution of other reactions to form H_2O^+ in the inner coma is not significant compared with the photoionization of water. These include charge exchange of water with other water-group ions (OH^+, O^+), CO_2^+, CO^+, and protons (see below). Our previous coma models (Boice & Martinez 2010) show that these reactions contribute less than ~20% to the formation of H_2O^+ at 1000–10,000 km from the nucleus (where the number density of H_2O^+ ions is the highest in cometary coma and most significantly contributes to the observed flux). The main chemical reactions related to H_2O^+ at 1000–10,000 km from the nucleus are shown in Figure 3.1. Possible reactions to form H_2O^+, their reaction rates and OPRs of H_2O^+ are as follows (Wegmann et al., 1999):

1. Photoionization ($H_2O + h\nu \rightarrow H_2O^+ + e$): the reaction rate due to photoionization at 1 AU from the Sun is 0.334×10^{-6} s^{-1} . The resultant OPR of H_2O^+ is the same as the OPR of water in this case based on the nuclear spin selection rules (Oka, 2004; Quack, 1977).
2. Charge exchange ionization with an ion ($H_2O + X^+ \rightarrow H_2O^+ + X$; X designates a reaction partner with H_2O): The charge exchange ionizations with a water-group ion (OH^+, H^+ or O^+) are considered as the most important since these ions can be produced from abundant

water in coma. Its reaction rate can be represented as $qv_i n_i$ [s^{-1}]; that is proportional to the velocity (v_i) and the number density of the ions (n_i). The cross section q depends on the energy of the ions. The reaction rates are usually smaller than the photoionization rate in the coma. Charge exchange reactions with other ions (CO_2^+ or CO^+) are not negligible compared with water-group ions but are still less than photoionization.

Regarding the OPR of H_2O^+, results depend on the partners of charge exchange reaction of water. Since ^{12}C and ^{16}O atoms do not have any nuclear spins (i.e., I=0), the OPRs of H_2O^+ formed by the charge exchange ionization reactions with CO_2^+, O^+, and CO^+ are the same as the OPR of water. In the case of charge exchange reaction with H^+ or OH^+, the OPR of H_2O^+ is considered equal to the OPR of water if H^+ or OH^+ could remove an electron from H_2O without exchanging protons between H_2O and H^+ or OH^+. For the simplicity we take this assumption. On the other hand, if we assume "complete scrambling of protons" (which means that three protons are indistinguishable from one another in the intermediate complex state, e.g., $H_2O + H^+ \rightarrow (H_3O^+)^* \rightarrow H_2O^+ + H$) during the reaction as an extreme case, the OPR of H_2O^+ is not the same as but slightly higher than the OPR of water. However, such complete scrambling of protons is not assumed in some studies about interstellar chemistry (Park et al., 2006; Morisawa et al., 2006). We will discuss about the influence caused by the complete scrambling of protons in the reaction later (in Section 4).

3. Electron impact ionization ($H_2O + e \rightarrow H_2O^+ + 2e$): The reaction rate for electron impact ionization ($H_2O + e \rightarrow H_2O^+ + 2e$) represented as kn_e is proportional to the density of the electrons (n_e). The rate coefficient k is calculated from the electron temperature T_e by the Arrhenius formula; $k = a(T_e/300)^b \exp(-c/T_e)$. The endothermic process consumes a certain energy e. The coefficients of a, b, c, and e are 1.58×10^{-9} s^{-1}, 0.5, 1.45×10^5 K, and -12.6 eV, respectively. If we consider the conditions for a comet with $Q(H_2O) = 10^{29}$ molecules s^{-1},

the resultant reaction rate for electron impact ionization can be negligible compared with the photoionization rate of H_2O. This is consistent with the findings of Bhardwaj (2003) for low to moderate production rate comets. Only for comets with Q greater than about 10^{30} molecules s^{-1} are electron impact reactions of significance in the formation of the water ion. The OPR of H_2O^+ formed by the electron impact ionization reaction is considered as the same as that of water based on the nuclear spin selection rules.

Therefore, we can consider that the OPR of H_2O^+ is the same as that of water in cometary coma even though the different processes listed above can contribute to the H_2O^+ formation in the coma. The determination of the OPR of H_2O^+ from optical high-dispersion spectra is a key task to obtain the OPR of water. However, a line-by-line fluorescence excitation model of cometary H_2O^+ in the optical (useful to derive OPR of H_2O^+) has never been proposed although the band g-factors of relevant vibronic transition were reported by Lutz (1987).

3.2.2. THE LINE-BY-LINE FLUORESCENCE EXCITATION MODEL OF H_2O^+ IN COMETS

We developed a line-by-line fluorescence excitation model of H_2O^+ in comets to derive the OPRs of H_2O^+ from their high-dispersion spectra in the optical. In the model, we take the followings into account;

1. the rovibronic transitions between $\tilde{A}$ (0,v_2',0) and $\tilde{X}$ (0,0,0) where v_2' = 6—17,
2. the pure rotational transition in $\tilde{X}$ (0,0,0) to concern radiative cooling in the ground state,
3. the fine structure of energy levels, i.e., split to F_1 and F_2 levels, and
4. the Swings effect (which is caused by the Doppler shift of the solar spectrum due to a cometary motion relative to the Sun) by using the high-dispersion spectrum of the Sun.

The fluorescence equilibrium condition is assumed for H_2O^+. The wavelengths of the rovibronic transitions and term values of the fine structure of the energy levels were taken from tables in Lew (1976), Huet et al. (1997), and Wu et al. (2003). The permanent electric dipole moment of the vibronic ground state is calculated as 2.370 Debye for H_2O^+ by Wu et al. (2004). Note that Wu et al. (2004) mistakenly listed the dipole moment in atomic units as Gerin et al. (2010) pointed out. The molecular constants reported by Lew (1976) and vibronic transition moments calculated by Wu et al. (2004) are also used to evaluate transition probabilities for the rovibronic transitions. The 385 levels and 2208 transitions are included in our model calculation. The high-dispersion solar spectrum by Kurucz (2005) is used in the optical wavelength region. In the far-infrared region (from 200 um to 1 mm) responsible for the pure rotational transitions, we used the values reported by Thekaekara (1974). Temporal variation of the solar spectrum with solar activity is not considered here since the variation is less than 1% in the optical region (Learn 2001).

The population distribution of H_2O^+ is determined by solving equations assuming fluorescence equilibrium. For the *i*-th energy level in the excited electronic state, the condition of detailed balance (i.e., a balance between outgoing and incoming rates for the level) becomes

$$n_i \sum_j \left(A_{ij} + B_{ij}\rho(\lambda_{ij}) \right) = \sum_j \left(n_j B_{ji}\rho(\lambda_{ij}) \right)$$

where n_i is the population in the *i*-th energy level and r is the energy density of the solar radiation at a given heliocentric distance. The l_{ij} is the wavelength corresponding to the transition between the *i*-th and the *j*-th energy levels (the *j*-th energy levels are in the ground state) while A_{ij} and B_{ij} are Einstein *A* and *B* coefficients between the *i*-th and the *j*-th energy levels, respectively. The optically thin condition in the coma is assumed to calculate the strength of the emission line. Therefore, the emission line strength is proportional to $g_{ij} = n_i A_{ij}$ (i.e., the line *g*-factor). The OPR of H_2O^+ is a free parameter in the model.

3.3. OBASERVATIONAL MATERIALS AND DATA ANALYSIS

In order to demonstrate our new method to determine OPR of water in comets from the optical spectrum of H_2O^+, we apply our fluorescence excitation model of H_2O^+ to the high-dispersion spectrum of comet C/2001 Q4 (NEAT) observed by the High Dispersion Spectrograph (HDS; Noguchi et al., 1998) mounted on the Subaru Telescope atop Mauna Kea, Hawaii (Kawakita et al., 2006). We could recognize H_2O^+ emission lines in the spectra.

As we discussed in the previous section, we can estimate the OPR of water from the OPR of H_2O^+ that can be determined by comparing the observed spectrum with the modeled spectrum.

Although the H_2O^+ ions have rovibronic transitions in the optical region (the $\tilde{A} - \tilde{X}$ system) caused by the solar fluorescence excitation mechanism, the emission line intensities of H_2O^+ in the optical are usually weaker than those of NH_2 and C_2 (Figure 3.2) in the inner coma. We chose the H_2O^+ (0,10,0) band to measure the emission lines of H_2O^+ and to determine the OPR of H_2O^+ since this band is the strongest band in the optical region for comets around 1AU from the Sun (based on our calculation) and there is no serious contamination of H_2O^+ by other species (Figure 3.3). Furthermore, the telluric absorption lines do not significantly affect this wavelength region (Figure 3.2). We detected the H_2O^+ emission lines belonging to the (0,11,0), (0,10,0), and (0,9,0) vibronic bands for comet C/2001 Q4 (NEAT) in the optical wavelength region (Figure 3.3). However, not only H_2O^+ bands but also C_2 Swan bands, NH_2 vibronic bands, and many emission lines of other species are present in the spectra. The H_2O^+ (0,10,0) band is the strongest H_2O^+ band in optical wavelength region and this band is almost free from the contamination by other molecular emission lines in the longer wavelength part of (0,10,0) band although this band is strongly contaminated by the C_2 Swan band in its shorter wavelength part (Figures 3.2 and 3.3 (B)). Therefore, we use the longer wavelength region of the (0,10,0) band of H_2O^+ to determine the OPR of H_2O^+. On the other hand, emission lines in other bands of H_2O^+ are hard to measure accurately because of contamination by other strong emission lines and/or severe telluric absorption lines. We need higher spectral resolving power to distinguish them. Figure 3.3

demonstrates that our fluorescence excitation model of H_2O^+ in comets reproduces the observed spectrum. However, these emission lines are thought to be contaminated significantly by other molecular lines.

Detailed information about the data reduction is described in Shinnaka et al. (2010) and Kawakita et al. (2006). We used the high-dispersion solar spectrum convolved with telluric transmittance curve at the solar continuum subtraction for the comet. Telluric transmittance is considered for the measured flux in order to get the flux value at the top of the telluric atmosphere. Thus, the OPR of H_2O^+ is finally obtained by comparing the observation with the calculations based on the χ^2-fitting technique. Table 3.1 list the measurements of H_2O^+ used here. We use both the pure and blended lines of ortho- and para-H_2O^+ to determine the H_2O^+ OPR. The best-fit OPR is 2.54 ± 0.22 (error corresponds to $\pm 1\sigma$ level).

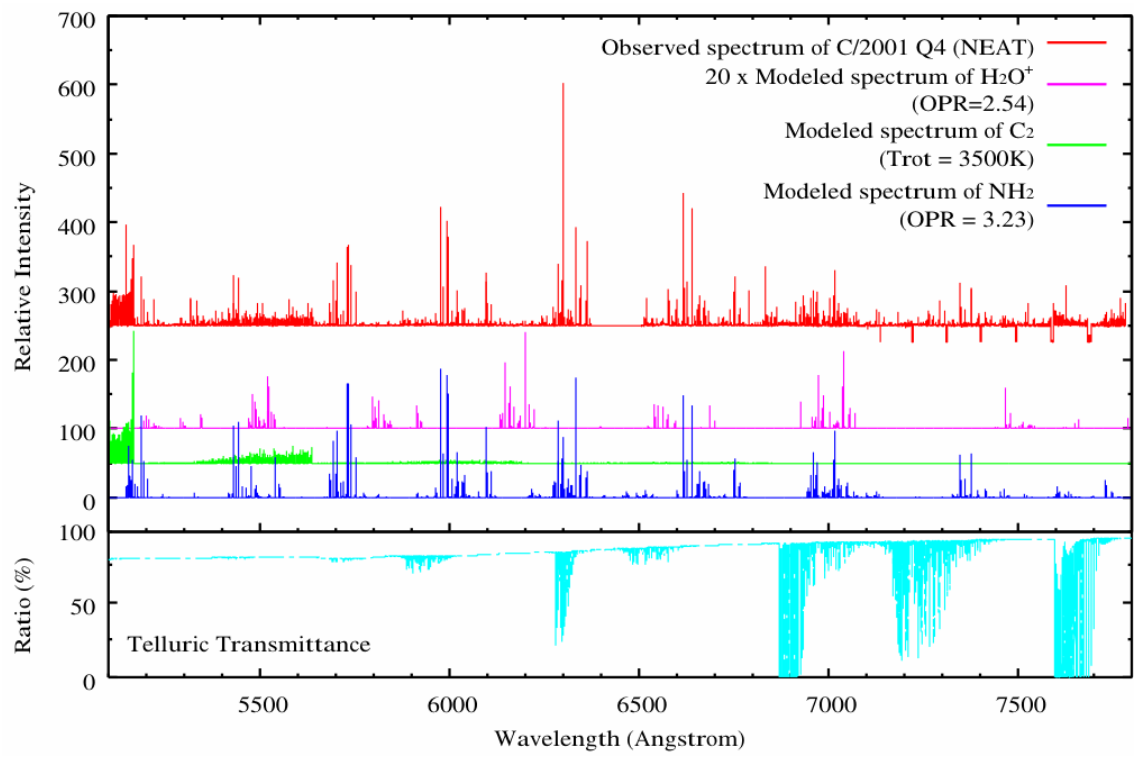

Figure 3.2: Cometary spectra in the optical wavelength region. The top (red) spectrum is the observed spectrum of comet C/2001 Q4 (NEAT). The second (pink), third (green) and fourth (blue) spectra are the modeled spectra of H_2O^+ (× 20), C_2 and NH_2, respectively. The bottom (sky blue) spectrum is the absorption by the telluric atmosphere. Although the band intensity of H_2O^+ is much weaker than other species (like a NH_2, C_2 and so on.) in optical wavelength region, we can obtain the OPR of water from the H_2O^+ (0,10,0) band because there is both no serious contamination of H_2O^+ by other species and no severe telluric absorption in this region.

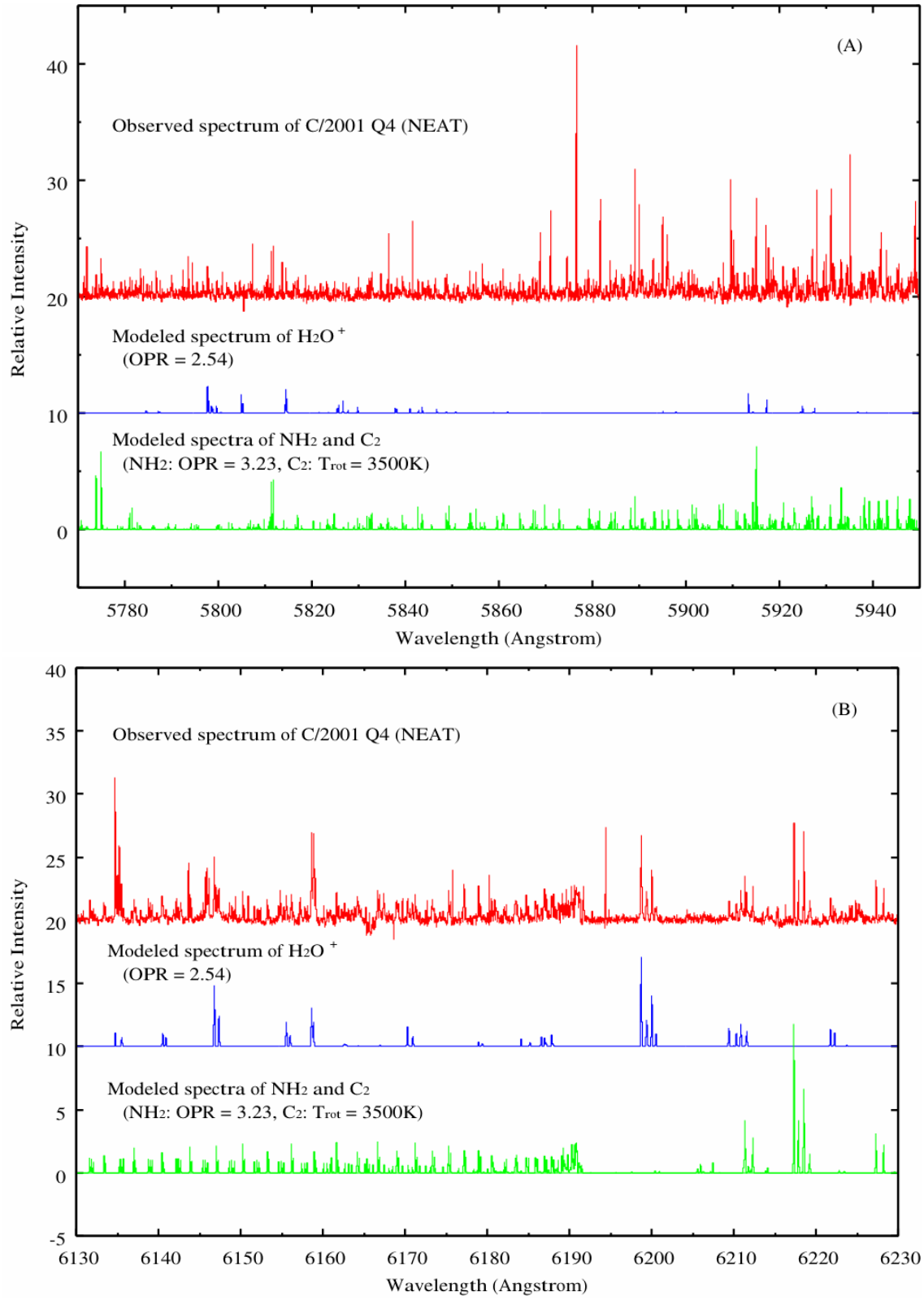
(A)
Observed spectrum of C/2001 Q4 (NEAT)
Modeled spectrum of H2O+
(OPR = 2.54)
Modeled spectra of NH2 and C2
(NH2: OPR = 3.23, C2: Trot = 3500K)
Relative Intensity
Wavelength (Angstrom)
(B)
Observed spectrum of C/2001 Q4 (NEAT)
Modeled spectrum of H2O+
(OPR = 2.54)
Modeled spectra of NH2 and C2
(NH2: OPR = 3.23, C2: Trot = 3500K)
Relative Intensity
Wavelength (Angstrom)

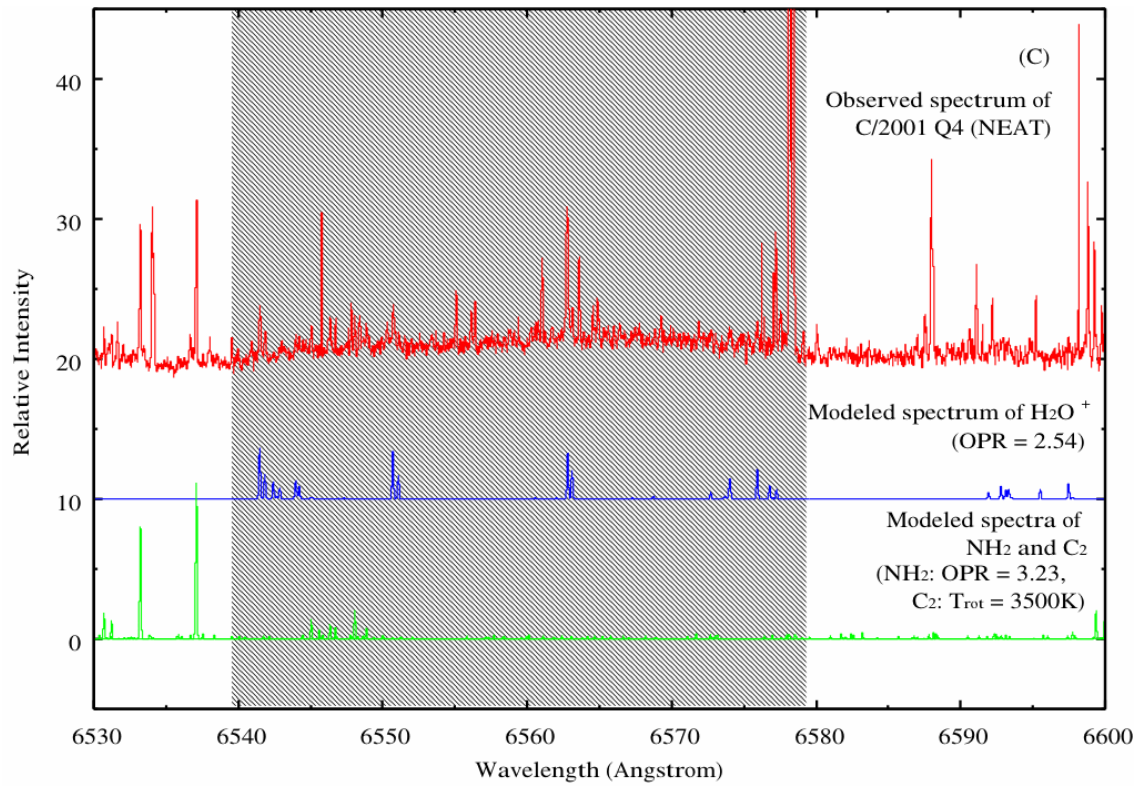

Figure 3. 3: (A) Not only H_2O^+ (0,11,0) band but also C_2 Swan band ($\Delta v = -2$), NH_2 (0,10,0) and (0,9,0) bands as well as many unidentified lines are present in this wavelength region. It is impossible to remove the contamination of H_2O^+ by unidentified lines. Therefore, we do not use this band to determine the OPR of H_2O^+. (B) This panel shows the H_2O^+ (0,10,0) band. In this wavelength region, not only H_2O^+ band but also C_2 Swan band ($\Delta v = -2$) and NH_2 (0,8,0) are present. Although the H_2O^+ emission lines were strongly contaminated by the C_2 Swan band at shorter wavelength region of this band, the longer wavelength part is almost free from those contaminations. Therefore, we use this region to determine the OPR of H_2O^+. (C) Not only H_2O^+ (0,9,0) band but also NH_2 (0,7,0) band and many other molecular lines (including unidentified lines) are there in this region. In this wavelength region, flux-calibration and continuum-subtraction were not perfect because of deep and wide absorption of H-alpha in the solar spectrum at ~6560 Å (shown as grey region in the panel). In addition to this issue, H_2O^+ lines are so weak that we do not use this band to determine the OPR of H_2O^+.

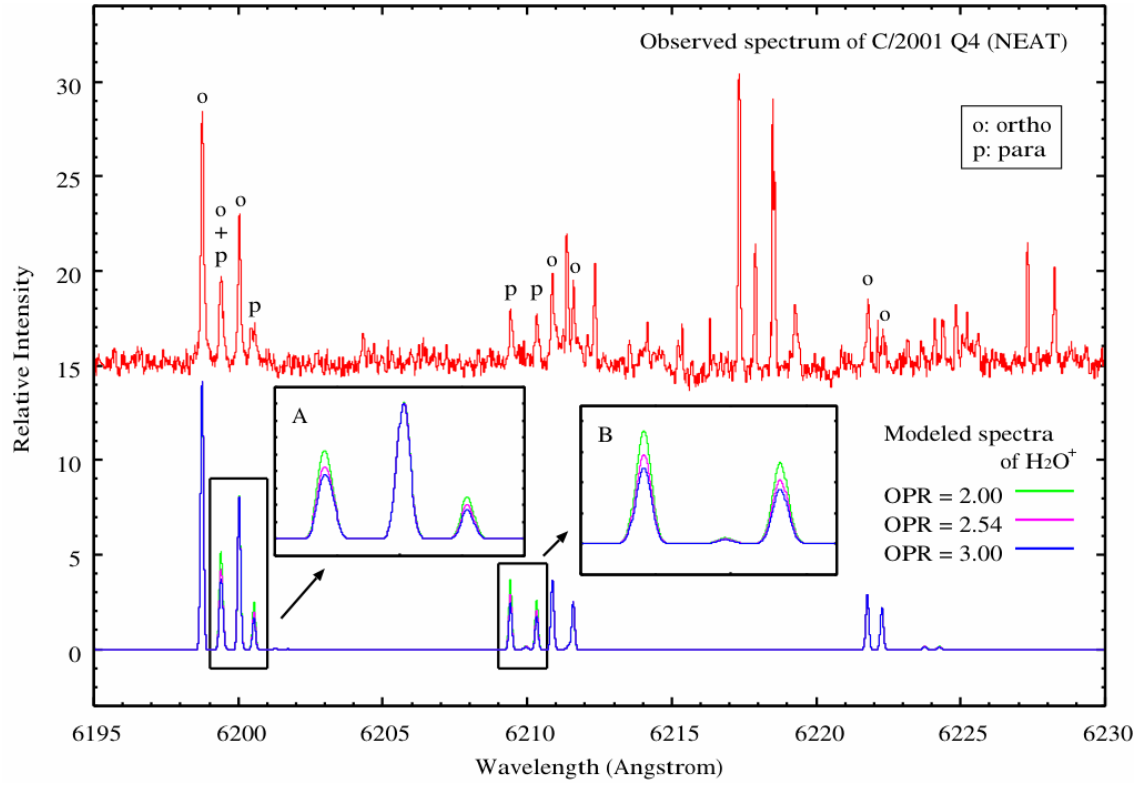

Figure 3.4: Comparison between the observed (upper) and modeled spectra (lower) of the H_2O^+ (0,10,0) band. For the modeled spectra we use OPR = 2.00, 2.54 (best-fit), and 3.00 (high-temperature limit). The ortho- and para-H_2O^+ lines are labeled in these spectra. The para-H_2O^+ lines are sensitive to determine the OPR of H_2O^+ (see insets A and B). This figure shows that our emission models of H_2O^+ reproduced the observed spectrum well. The obtained OPR of H_2O^+ in comet C/NEAT is 2.54 ± 0.22.

Table 3.1: Measured line flux of the H_2O^+ (0,10,0) band.

Wavelength [Å]	Line assignment ($N'_{Ka'Kc'} - N''_{Ka''Kc''}$)*	Ortho/Para	Relative intensity**
6198.75	1_{10}–2_{20} F1	Ortho	12.39 ± 0.31
6199.41	1_{10}–2_{20} F1–2 1_{11}–2_{21} F2	Ortho + Para	5.73 ± 2.58
6200.03	1_{10}–2_{20} F2	Ortho	6.84 ± 0.30
6200.54	1_{11}–2_{21} F2	Para	1.91 ± 0.49
6209.42	2_{11}–3_{21} F1	Para	2.08 ± 0.38
6210.33	2_{11}–3_{21} F2	Para	2.60 ± 0.39
6210.87	2_{12}–3_{22} F1	Ortho	4.56 ± 0.35
6211.59	2_{12}–3_{22} F2	Ortho	3.33 ± 0.30
6221.77	3_{12}–4_{22} F1	Ortho	3.21 ± 0.37
6222.28	3_{12}–4_{22} F2	Ortho	1.53 ± 0.37

* All lines belong to the H_2O^+ $\tilde{A}$ (0,10,0) — $\tilde{X}$ (0,0,0) band. N denotes the quantum number of the total angular momentum of H_2O^+ without electron spin while K_a and K_c are the quantum numbers representing the angular momentum along a- and c-axes of asymmetric top. F1 and F2 indicate $J = N + \frac{1}{2}$ and $J = N - \frac{1}{2}$, respectively. F1–2 denotes a transition from the F1 to F2 states.

** At the top of the atmosphere, in arbitrary units.

3. 4. RESULTS AND DISCUSSIONS

Figure 3.4 shows the comparison between the observed and modeled spectra of H_2O^+ in the case of C/2001 Q4 (NEAT). The OPR of H_2O^+ is obtained as 2.54 ± 0.22 by the least χ^2-fitting. As we discussed in Section 2, the OPR of water is considered to be the same as the OPR of H_2O^+. Therefore, the T_{spin} of water is derived to be 30 +6 / –4 K in this work.

The OPR of water in comet C/2001 Q4 (NEAT) had already been reported in our previous study by the near-infrared spectroscopic observations of water (Kawakita et al., 2006). The OPRs of water determined through the hot-band emission lines of water in 2.9 μm region was 2.6 ± 0.3 and this value is consistent with the OPR of water based determined from H_2O^+ in this work. This excellent agreement supports the soundness of our new method to derive the OPR of water from H_2O^+ for comets.

Finally, we should consider the charge exchange ionization reaction of water with H^+ or OH^+, again (see Section 2). If we assume complete scrambling of protons during the reaction, the OPR of H_2O^+ is slightly higher than that of water. By applying the nuclear spin selection rule to the reactions we obtain the following relation (Oka, 2004):

$$\mathrm{OPR}(H_2O^+) = \frac{4 \times \mathrm{OPR}(H_2O)}{\mathrm{OPR}(H_2O) + 3} + 1.$$

In this case, the obtained OPR of H_2O^+ is higher than that of water (where $0 \le \mathrm{OPR}(H_2O) \le 3$). If we assume a typical OPR of water in comet (~2.5), the resultant OPR of H_2O^+ is larger by about 10% than that of water. The larger contribution to the H_2O^+ production by these charge exchange ionization reactions will lead to higher OPR of water (closer to but not larger than 3.0). Obtained OPR in this work (2.54 ± 0.22) is consistent with a previous study (2.6 ± 0.3) by Kawakita et al. (2006). This result may indicate that the complete scrambling of protons during the charge exchange ionization reaction with H^+ or OH^+ can be neglected to estimate the OPR of water from that of H_2O^+. The electron of H_2O could be removed by collision with H^+ or OH^+ without the exchange of protons between H_2O and H^+ or OH^+. Otherwise, the charge exchange ionization reaction by H^+ or OH^+ could not play an important role for the ionization of H_2O in the coma (the

photo-ionization of H_2O may be much more important). These ionization reactions by H^+ and OH^+ contribute less than ~20% to the formation of H_2O^+ in cometary coma based on our previous coma models (Boice & Martinez, 2010). As a result, the OPR of H_2O^+ would be different from the OPR of H_2O by less than ~5% for OPRs of H_2O from 2.0 to 3.0 (smaller differences for OPRs of H_2O closer to 3.0) although the charge exchange ionization reaction of H_2O with H^+ and OH^+ occurred with the complete scrambling of protons.

The OPR of water in Comet C/2001 Q4 (NEAT) can be also compared with the other observations. As already discussed in our previous study (Kawakita et al., 2006), the T_{spin} of H_2O, NH_3 and CH_4 were all consistent in comet C/2001 Q4 (NEAT) (see Table 3.2). Even though the real meanings of the OPR and T_{spin} are still in debate, this consistency supports the hypothesis that all of these molecules formed (or equilibrated) with the same temperature conditions, probably on cold dust grains.

In any event, our new method will allow us to measure the OPR of water in the optical for many comets in the future and also will allow us to determine the OPR of water in the comets already observed, increasing the number of samples for the OPRs of water in comets.

Table 3.2: Comparison by T_{spin} of 3 species.

Molecules	T_{spin} (K)	Reference
H_2O	30 +6 / –4	Shinnaka et al. (2012) (from H_2O^+)
	31 +11 / –5	Kawakita et al. (2006) (from H_2O hot-band)
NH_3	30 ± 1	Shinnaka et al. (2010)
CH_4	33 +2 / –1	Kawakita et al. (2005)

Table 3.3: Summary of T_{spin} of water estimated from that of H_2O^+ comets.

Comets	OPR	T_{spin} (K)
C/2001 Q4 (NEAT)	2.6 ± 0.3	30 +6 / –4
103P/Hartley 2	2.14 +0.76 / –0.46	34 +19 / –4
C/2002 T7 (LINEAR)	2.31 ± 0.30	26 +6 / –3
C/2013 R1 (Lovejoy)	2.45 ± 0.20	29 +4 / –3

4. $^{14}NH_2/^{15}NH_2$ RATIO IN COMETS C/2012 S1 (ISON) OBSERVED DURING ITS OUTBURST IN 2013 NOVEMBER

ABSTRACT

We performed high–dispersion optical spectroscopic observations of comet C/2012 S1 (ISON) using the High Dispersion Spectrograph (R = 72,000) at the Subaru Telescope on UT 2013 November 15.6, during an outburst that started on UT 2013 November 14. Due to the high gas–production rate of NH_2 during the outburst, we successfully detected weak emission lines of $^{15}NH_2$ and many strong emission lines of $^{14}NH_2$ in the optical wavelength region from 5500 to 8200 Å. The ratio of $^{15}NH_2/^{15}NH_2$ is derived to be 139 ± 38 in comet C/2012 S1 (ISON). This ratio is close to that recently revealed based on the averaged spectrum of 12 comets, ~130. This is also comparable to the typical cometary isotopic ratio of CN ($^{12}C^{14}N/^{12}C^{15}N$, observed in optical) and HCN ($H^{12}C^{14}N/ H^{12}C^{15}N$, observed in radio), ~150. However, these ratios are much smaller than the protosolar value, $^{14}N/^{15}N$ = 441 ± 5. Because NH_2 is considered to be a photodissociation product of NH_3 in cometary coma, our result implies the occurrence of ^{15}N–fractionation of NH_3 in the solar nebula or in the presolar molecular cloud.

4.1. INTRODUCTION

Isotope ratios of cometary molecules are diagnostic tools to investigate the physicochemical evolution in the presolar molecular cloud and solar nebula. Deuterium–to–hydrogen (D/H) ratios in cometary water show water D–fractionation during the early stages of solar system formation (Lis et al., 2013; Mumma & Charnley, 2011) and are indicative of low temperature conditions. Combined with D/H ratios in water and hydrogen cyanide in comet C/1995 O1 (Hale–Bopp), temperatures where the D–fractionation occurred have been estimated to be ~30 K based on chemical reaction network models (Mumma & Charnley, 2011 and references therein). In contrast to the D/H ratio, the $^{14}N/^{15}N$ ratio in comets is not well understood.

The $C^{14}N/C^{15}N$ ratio was obtained in many comets through optical high–dispersion spectroscopy (Manfroid et al., 2009). In the case of HCN (which photodissociates into CN through solar UV radiation in the cometary coma), the $HC^{14}N/HC^{15}N$ ratio was obtained in comets C/1995 O1 (Hale–Bopp) and 17P/Holmes (Bockelée–Morvan et al., 2008). These ratios are consistent with ~150 for those comets and are significantly smaller than the protosolar value, 441 ± 5 (Marty et al., 2011). The ^{15}N–fractionation in cometary molecules is an unsolved issue in comet science at present and the key parameter for understanding ^{15}N–fractionation in comets is considered to be the $^{14}N/^{15}N$ ratio in cometary ammonia (Mumma & Charnley, 2011).

Rousselot et al. (2014) recently derived the $^{14}NH_2/^{15}NH_2$ ratio in comets for the first time. They experimentally determined accurate line positions of $^{15}NH_2$ and successfully detected seven emission lines in a single combined spectrum of 12 comets with the best signal–to–noise ratios (S/Ns). Because ammonia is considered to be the sole parent of NH_2 in the coma (Kawakita & Mumma, 2011; Kawakita & Watanabe, 1998), the $^{14}NH_2/^{15}NH_2$ ratio of ~130 obtained by Rousselot et al. (2014) is considered to be close to the $^{14}N/^{15}N$ ratio in cometary ammonia. However, the diversity in the $^{14}NH_2/^{15}NH_2$ ratio has never been investigated due to the lack of high S/N observations for an individual comet.

In this Section, we report the $^{14}N/^{15}N$ ratio in comet C/2012 S1 (ISON) (hereafter ISON). This is the first report on the clear detection of $^{15}NH_2$ lines in a spectrum of a single comet. Comet ISON was on its near–parabolic orbit (with 111the perihelion distance of 0.0124 AU) and it is considered to have originated in the Oort Cloud. Although this comet was expected to be spectacularly bright near its perihelion passage, it disintegrated at perihelion (Battams, 2013; Knight, 2013; Nakano, 2013). Fortunately, we observed the comet before perihelion passage at 0.6 AU from the Sun during an outburst in the middle of 2013 November (Combi et al., 2013).

4.2. OBSERVATIONS AND DATA REDUCTION

On UT 2013 November 15.6, high–dispersion optical spectroscopic observations of comet ISON were conducted with the High Dispersion Spectrograph (HDS; Noguchi et al., 2002) mounted at the Nasmyth focus of the Subaru Telescope on top of Mauna Kea, Hawaii. Its heliocentric and geocentric distances were 0.601 AU and 0.898 AU, respectively. We put the optical center of the comet on the slit and integrated the comet for 1,200 s. The obtained spectrum covers the wavelength region from 5500 to 8300 Å with $R = (\lambda/\Delta\lambda) = 72{,}000$ for the slit size of 0″.5 by 9″.0 on the sky. A multitude of gas emission lines of molecules and atoms (such as CN, C_2, NH_2, H_2O^+, Na D–lines, and [OI] forbidden lines at 5577, 6300, and 6364 Å) were detected in our spectrum.

Data reduction was accomplished using standard IRAF software routines distributed by NOAO. Details for the reduction and calibration of the data obtained by the Subaru Telescope with the HDS are described at the Subaru Telescope's home page.4 We used the spectra of a Th–Ar lamp for wavelength calibration and also observed spectrophotometric standard stars (HR 718, HR 1544, and HR 3454) for sensitivity correction.

Once we obtained the calibrated one–dimensional spectrum of the comet, we subtracted the continuum component (which was the sunlight reflected by the cometary dust grains in the coma) from the calibrated spectrum. For this continuum subtraction, we modeled the reflected sunlight as the product between the high–dispersion solar spectrum (Kurucz 2005) and the reflectivity spectrum of cometary dust grains. We used a quadratic function to approximate the reflectivity spectrum. The modeled spectrum of reflected sunlight was convolved with both the telluric transmittance spectrum calculated by the LBLRTM code (Clough & Iacono, 1995) and the instrumental profile approximated by the Gaussian function. Finally, we fitted the modeled continuum spectrum to the observed cometary spectrum within the wavelength windows where there are no significant emission lines from the comet (Figure 4.1).

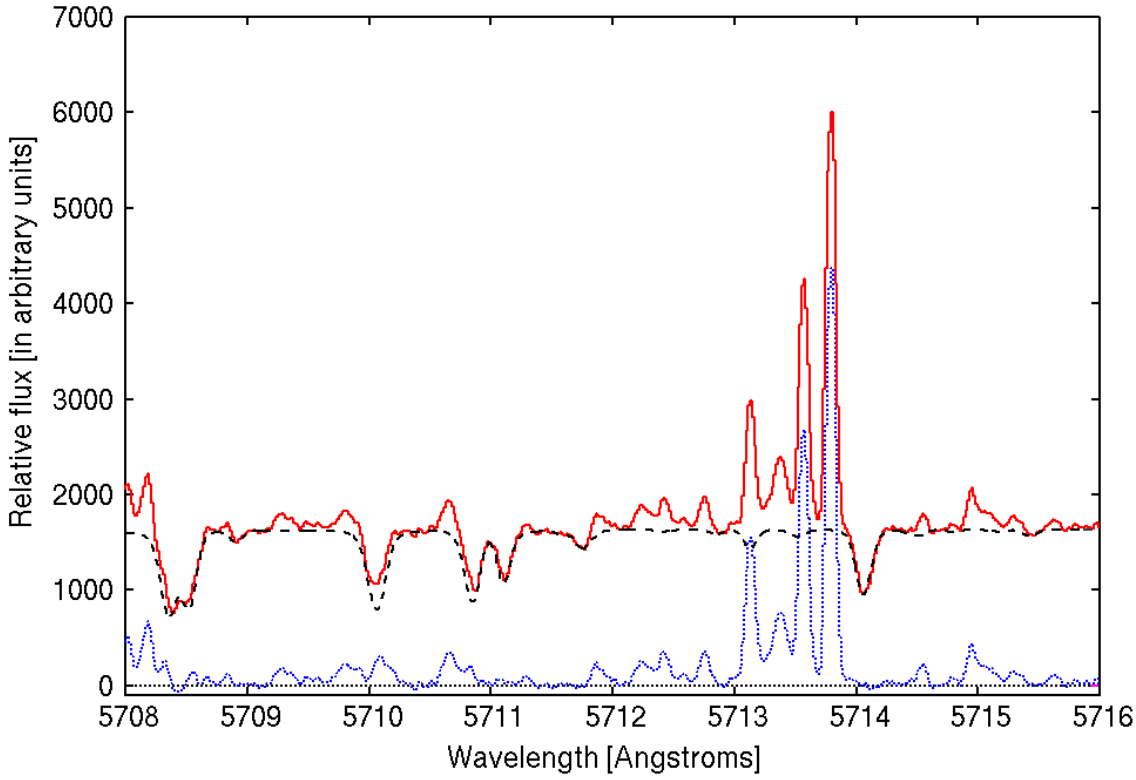

Figure 4.1. Example of continuum subtraction for the calibrated spectrum. The solid line shows the observed spectrum, the dashed line shows the modeled continuum, and the dotted line shows the residual (cometary and telluric emission lines).

Table 1. Emission Lines of $^{15}NH_2$ Measured in Our Spectrum

Transition in $\tilde{A}-\tilde{X}$ (0, 10, 0) band	$^{15}NH_2$		$^{14}NH_2$	
	Wavelength (Å)	Relative flux	Wavelength (Å)	Relative flux
1_{11}–1_{01} (F_2–F_2)	5710.94	3.3 ± 0.7	5700.75	507.6 ± 0.8
1_{11}–1_{01} (F_1–F_1)	5711.29	8.3 ± 0.7	5701.00	1006 ± 0.8
1_{10}–2_{02} (F_2–F_2)	5723.83	4.1 ± 0.8	5713.79	415.3 ± 0.8
3_{12}–4_{22} (F_1–F_1) 3_{12}–4_{22} (F_2–F_2)	5763.02	12.4 ± 1.0	5752.78	2874 ± 1.0

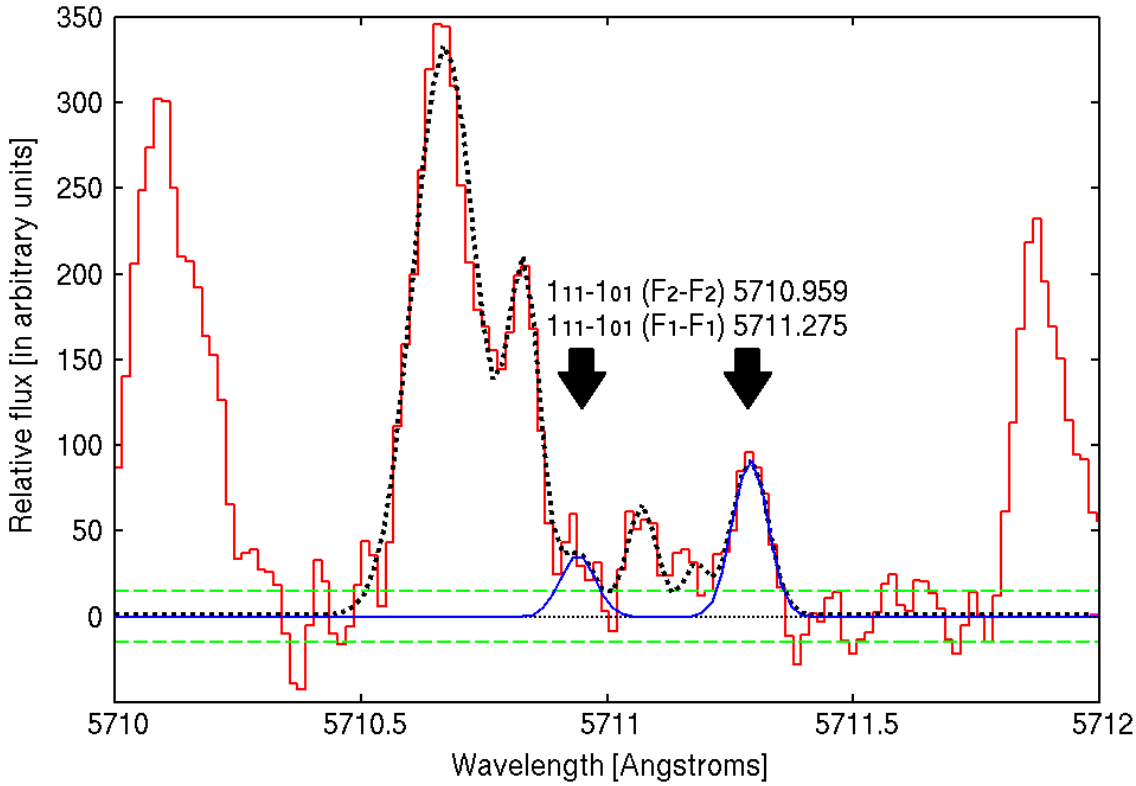
Relative flux [in arbitrary units]
350
300
250
200
150
100
50
0
5710
5710.5
5711
5711.5
5712
Wavelength [Angstroms]
1₁₁-1₀₁ (F₂-F₂) 5710.959
1₁₁-1₀₁ (F₁-F₁) 5711.275

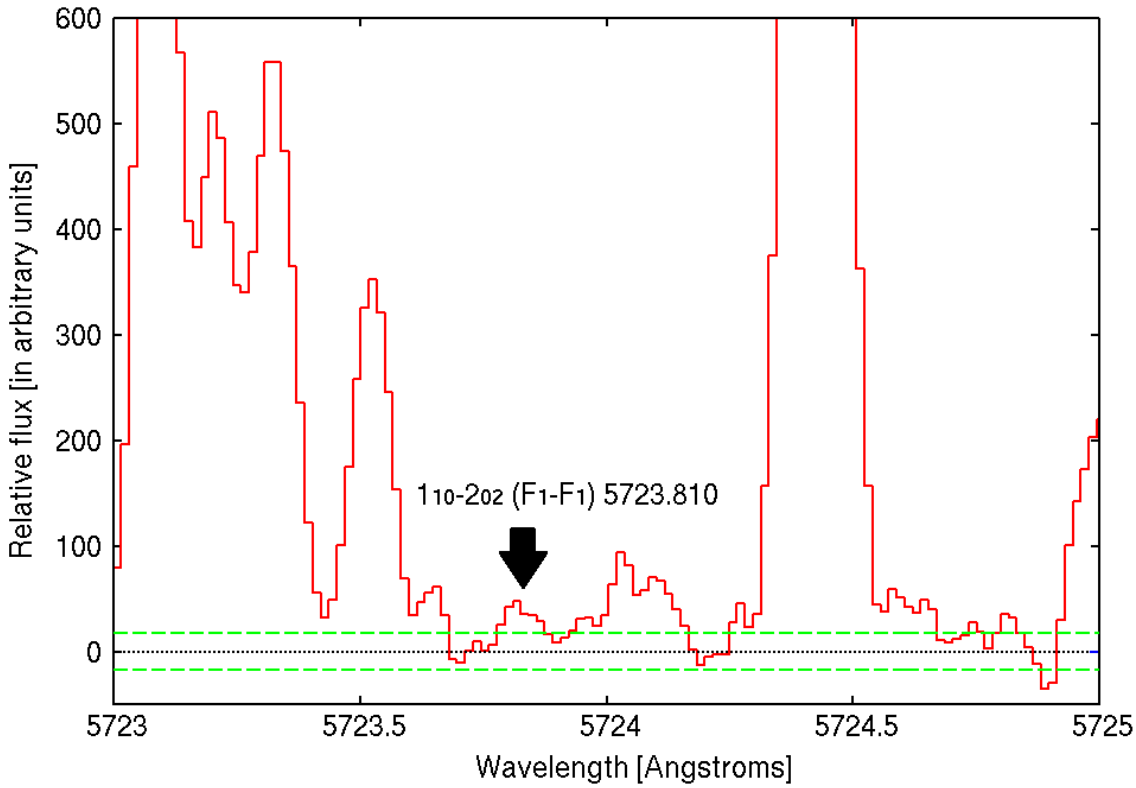
Relative flux [in arbitrary units]
600
500
400
300
200
100
0
5723
5723.5
5724
5724.5
5725
Wavelength [Angstroms]
1₁₀-2₀₂ (F₁-F₁) 5723.810

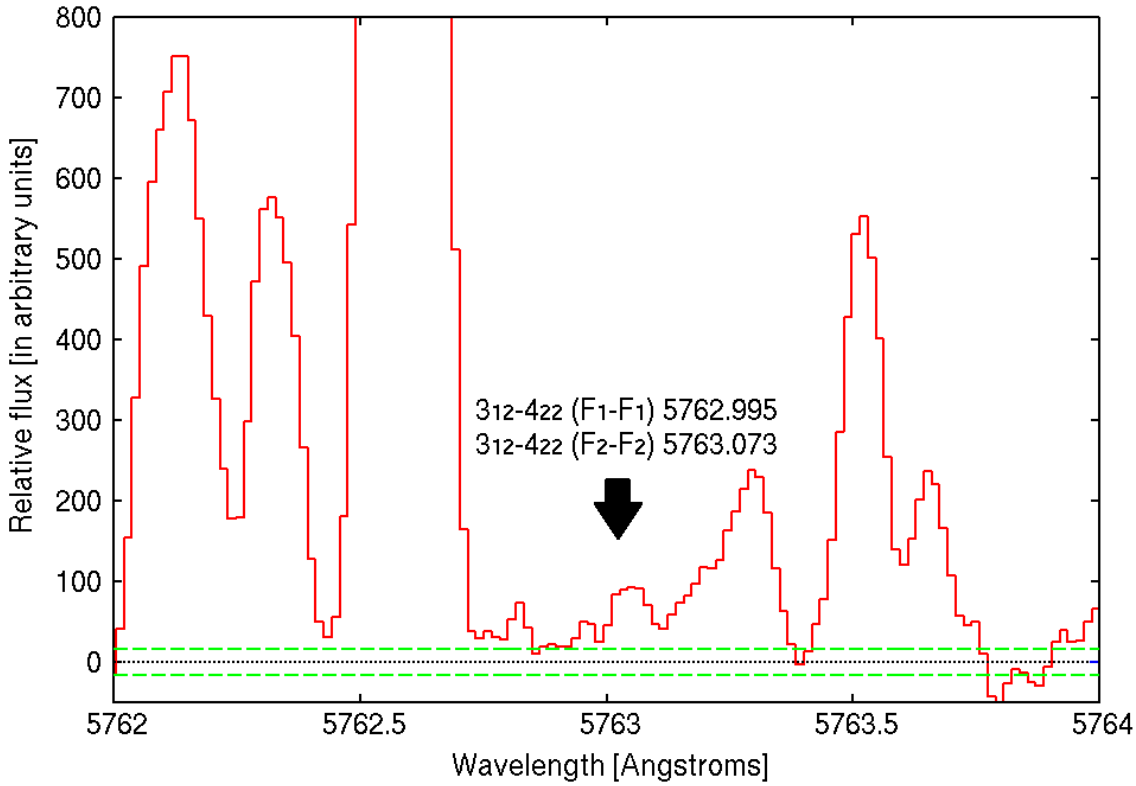

Figure 4.2. Three panels show the $^{15}NH_2$ emission lines detected in our spectrum. The dashed lines indicate the ±1σ error levels. In the top panel, the thick dotted line indicates the result of ad hoc fitting for unidentified components around 5711 Å. All $^{15}NH_2$ emission lines shown above are for the (0, 10, 0) band. The labeled wavelengths for $^{15}NH_2$ are taken from Table 2 of Rousselot et al. (2014).

4.3. RESULTS AND DISCUSSIONS

Figure 4.2 shows the spectra for the emission lines of the $^{15}NH_2$ (0, 10, 0) band. We searched for the lines listed in Table 2 of Rousselot et al. (2014). For the measurements of the 1_{11}–1_{01} (F2–F2) and (F1–F1) line fluxes of $^{15}NH_2$ we used an ad hoc fitting routine for unidentified lines close to the $^{15}NH_2$ lines of Rousselot et al. (2014) as shown in Figure 4.2. We fixed the FWHM of the $^{15}NH_2$ line as 0.085 Å (determined from the high S/N emission line of $^{14}NH_2$, 1_{11} –1_{01}) in each transition. Table 1 shows the measurements for the emission lines. The difference in wavelength between our measurements and those listed in Table 2 of Rousselot et al. (2014) is smaller than 0.02 Å and 0.01 Å for the $^{15}NH_2$ and $^{14}NH_2$ lines, respectively.

In order to estimate the $^{15}N/^{15}N$ ratio in ammonia, Rousselot et al. (2014) assumed (1) a similar photodissociation efficiency for $^{14}NH_3$ and $^{15}NH_3$ to produce $^{14}NH_2$ and $^{15}NH_2$, respectively, and (2) similar transition probabilities for both $^{14}NH_2$ and $^{15}NH_2$. Based on these assumptions, the intensity ratio between the $^{14}NH_2$ and $^{15}NH_2$ emission lines (with the same line assignment) is equal to the $^{14}NH_2/^{15}NH_2$ ratio and also close to the $^{15}N/^{15}N$ ratio in ammonia. We estimate the uncertainty of the $^{14}NH_2/^{15}NH_2$ ratio in the comet considering random errors in the flux measurements of NH_2 and systematic errors as follows: (1) the difference in photodissociation rates from ammonia to NH_2 between ammonia isotopologues, (2) the difference in transition probabilities (Einstein A and $B \times \rho_{SUN}$) for the transitions with the same line assignment (rovibronic quanta) for the isotopologues, and (3) the uncertainty in measured flux caused by the continuum subtraction. The uncertainty of (1) is probably about 10% (Suto & Lee, 1983; Liang et al., 2007) or less while we consider the uncertainties for (2) and (3) to total about ~25% (individual mean ratios listed in Table 2 of Rousselot et al. (2014) are scattered ~25% around the weighted mean, ~130). Thus, we estimate the $^{14}NH_2/^{15}NH_2$ ratio to be 139 ± 38 for comet ISON.

The obtained ratio of $^{14}NH_2/^{15}NH_2$ for comet ISON is consistent with the result determined by Rousselot et al. (2014) based on the averaged spectrum for 12 comets. Comet ISON seems to be typical from the viewpoint of the

$^{14}NH_2/^{15}NH_2$ ratio. The observed $^{14}NH_2/^{15}NH_2$ ratio is considered close to the $^{14}N/^{15}N$ ratio of ammonia in cometary ices. Rousselot et al. (2014) proposed the hypothesis that there were two distinct nitrogen reservoirs in the solar nebula: (1) primordial N_2 gas with $^{14}N/^{15}N \sim 441$ (protosolar value) and (2) less volatile molecules (probably in solids) such as NH_3 and HCN enriched in ^{15}N, which were incorporated into comets. Our result supports this hypothesis.

On the other hand, Hily–Blant et al. (2013a, 2013b) proposed the hypothesis that there are two distinct reservoirs for nitrogen with different $^{14}N/^{15}N$ ratios: the molecules carrying the nitrile–functional group and the molecules carrying the amine–functional group. They considered that the former family (e.g., HCN) derives from atomic nitrogen while the latter (e.g., NH_3) are formed from N+, which is the product of N_2 dissociative ionization. Indeed, amines and nitriles have been separated in the gas–phase chemical reaction network as proposed by Hily–Blant et al. (2013a). This might explain the observations for some dense cloud cores, in which the nitrile–bearing molecules like HCN are enriched in ^{15}N (~150) even though the amine–bearing molecules like NH_3 are not (~300), as summarized in Table 2. However, recent observations in comets have revealed the high ^{15}N–fractionation in cometary ammonia (~140) comparable to that for HCN in comets (~150), as reported by Rousselot et al. (2014) and this study. Thus, the hypothesis proposed by Hily–Blant et al. (2013a, 2013b) does not seem to be appropriate for cometary ices.

The differences in processing time and epoch between the cometary and interstellar molecules might cause the different $^{14}N/^{15}N$ ratios of ammonia (but similar for HCN) between these two sources. The $^{14}N/^{15}N$ ratio varies with time in a molecular cloud, and different molecular species show different $^{14}N/^{15}N$ ratios as demonstrated by Rodgers & Charnley (2008). In their models, the ^{15}N–fractionation occurred for NH_3 in a relatively later stage than HCN (after $\sim 10^5$ yr for NH_3). However, more sophisticated treatment for the model requires accurate rate coefficients for key reactions (Rodgers & Charnley, 2008). The observational constraints for the nitrogen

isotopic ratios in cometary molecules will improve the models of chemical evolution from the presolar molecular cloud to the early solar system.

The alternative explanation for the comparable $^{14}N/^{15}N$ ratios of ammonia and HCN in cometary ices is based on grain–surface chemistry. Note that the $^{14}N/^{15}N$ ratios of NH_3 and HCN in comets are for the molecules in cometary ices (solid) while the observations of dense molecular cloud cores revealed the $^{14}N/^{15}N$ ratio of the molecules in gas. As listed in Table 2, ammonia in the gas phase shows a mild enrichment in ^{15}N ($^{14}N/^{15}N \sim 300$) while HCN in the gas phase shows larger enrichment in ^{15}N ($^{14}N/^{15}N \sim 150$) than ammonia. Here the key species to understand the chemical pathways to ammonia is N_2H^+, which is an intermediate product for the chemical reaction network from N_2 to NH_3 in gas–phase chemistry. The gas–phase N_2H^+ is not enriched in ^{15}N compared to HCN in dense molecular cloud cores, $^{14}N/^{15}N \sim 400$ or higher (Table 2). Ammonia produced by gas–phase chemistry from N_2 might not be enriched in ^{15}N. However, an alternative process to produce ammonia is grain–surface chemistry.

Successive hydrogenation reactions of atomic nitrogen with atomic hydrogen on cold grains can also produce ammonia under low temperature conditions (Hiraoka et al., 1995). Most of the ammonia formed on cold grains may remain solid if the temperatures are cold enough, and some fraction of ammonia may desorb by thermal or non–thermal processes (e.g., photosputtering) into the gas phase. The point of this hypothesis is ammonia can be formed from atomic nitrogen (not from the primordial molecular nitrogen that has a $^{14}N/^{15}N$ ratio of protosolar value). Since HCN can also be formed by gas–phase chemistry from atomic nitrogen, ammonia formed by the grain surface chemistry (from atomic nitrogen) may have $^{14}N/^{15}N$ ratios comparable to HCN. Atomic nitrogen in the gas phase might be enriched in ^{15}N through the photodissociation of N_2 and ^{15}NN by the interstellar UV radiation field (i.e., the self–shielding effects for N_2 and ^{15}NN are different). Since ^{15}NN can be dissociated much further into the cloud, the atomic nitrogen may be fractionated in ^{15}N for the deeper region of the molecular cloud.

Finally, we discuss about the possibility of ^{15}N–fractionation of cometary volatiles in the coma because the nitrogen isotopic ratios of volatiles not reflect the past information if nitrogen exchange reactions in nucleus or coma were happen easily. NH_3 and HCN might be contributed those reactions because these volatiles are abundant nitrogen–bearing molecules in cometary volatiles. In the ice of nucleus, the ^{15}N–fractionation was hard to occur because the abundances of nitrogen–bearing molecules were less than several percentages (> 80 % was water in ice) and molecules could not move freely in the ice. In general, in gas–phase chemistry, the exchange of nitrogen of a nitrogen–bearing polyatomic molecule was difficult since nitrogen usually bonded with other atoms strongly in contrast with hydrogen. Moreover, collision rate between nitrogen–bearing molecules in the coma were small because both the abundances of these molecules is less than several percent relative to water. Other candidate for the nitrogen exchange is the nitrogen molecule (N_2) because the N_2 greatly contributes to ^{15}N–fractionation of NH_3 and HCN through the gas–phase chemical reactions in a dense molecular cloud (Wirström et al., 2012, Rodgers & Charnley, 2008). However, there is no report to clear detection of the nitrogen molecules in comet (Cochran & Cochran, 2000). N_2 might not be captured to the cometary nucleus. Other possibility is the reactions with nitrogen–bearing molecules released from collapse of cometary dusts in coma. However, there is no repot what molecules were released from dusts in the coma. If the production of N–bearing molecules and the nitrogen exchange reactions in coma occurred, the nitrogen isotopic ratios of cometary volatiles change depending on the distance from the nucleus surface. There is no report on the heliocentric and nucleocentric distances dependence on the nitrogen isotopic ratio in cometary volatiles. The spatial resolved determination of the nitrogen isotopic ratios is essentially important to investigate this possibility. Therefore, it is considered that the nitrogen isotope exchange in cometary ice and coma was hard to occur and it is likely that the nitrogen isotopic ratios of cometary volatiles reflect the interstellar environment.

Future measurements of $^{14}NH_2/^{15}NH_2$ in individual comets (especially, we would like to obtain the Jupiter–family comets because these is no sample) are essential to reveal the diversity of the ^{15}N–fractionation in cometary ammonia as in the case of HCN (which shows small variations for different comets). Since ^{14}N and ^{15}N atoms are not easily exchangeable, unlike protons that easily exchange with ice after the molecular formation (Hily–Blant et al., 2013a), $^{14}N/^{15}N$ ratios might be chemically unaltered in the cometary the solar nebula. It is likely that the $^{14}N/^{15}N$ ratio in cometary ammonia also shows small variations for comets that formed at different conditions in the solar nebula. Thus, the $^{14}N/^{15}N$ ratios in comets may be more pristine than D/H ratios of cometary molecules and more useful in probing the physicochemical conditions in the presolar molecular cloud.

Table 4.2. Isotopic Ratios of Nitrogen in the Interstellar Medium

Probe	Source	X–^{14}N/X–^{15}N	References
NH_3	Barnard 1	300 +55 / –40	(1)
NH_2D	Barnard 1	230 +105 / –55	(1)
HCN	L1521E	~150	(2)
HCN	L183	140 – 250	(3)
HCN	L1544	140 – 360	(3)
HCN	Barnard 1	165 +30 / –25	(1)
N_2H^+	L1544	446 ± 71	(4)
N_2H^+	Barnard 1	400 +100 / –65 for $N^{15}NH^+$ > 600 for $^{15}NNH^+$	(1)
CN	L1498	476 ± 70	(5)
CN	L1544	510 ± 70	(5)

References. (1) Daniel et al. (2013); (2) Ikeda et al. (2002); (3) Hily–Blant et al. (2013a); (4) Bizzocchi et al. (2010); (5) Hily–Blant et al. (2013b)

5. GENERAL DISCUSSIONS

This section discusses the origin of cometary volatiles based on the discussions in the previous sections and on recent related studies. We first summarize the results of the previous sections, in which we obtained the OPRs of cometary volatiles (ammonia and water) and the nitrogen isotopic ratios in cometary ammonia.

The OPRs of cometary ammonia were very similar (~1.13) and corresponded to a nuclear spin temperature of ~30 K (see Section 2). The OPRs of cometary water were also clustered and consistent with the nuclear spin temperature of ammonia (see Section 3). Therefore, the OPRs of cometary volatiles might reflect the temperature of the molecular cloud that sourced the solar system. Given the fact that cometary ammonia and water yielded similar nuclear spin temperatures, the temperature of the molecular cloud was probably around 30 K (Sections 2 and 3; see also Bonev et al., 2007; Mumma et al., 1987; and references therein). If the OPRs of cometary volatiles reflect the temperature of the solar nebula, the nuclear spin temperatures should exhibit greater diversity than observed, because the temperature in the solar nebula within the cometary formation region is widely variable (10 K to ~150 K; see Hersant et al., 2001).

On the other hand, the ^{15}N-fractionation in cometary volatiles (HCN, CN, and ammonia) was determined as $^{14}N/^{15}N$~150. According to theoretical models, this ratio is possible only under low-temperature conditions (around 10 K) (Wirström et al., 2012; Rodgers & Charnley, 2008). Present models of ^{15}N-fractionation in the molecular cloud are based on isotopic exchange during chemical reactions and the selective photodissociation of volatiles (especially of molecular nitrogen, N_2). Therefore, if the volatiles actually formed at ~30 K, the nitrogen isotopic ratios observed in the comets demand alternative fractionation mechanisms in the molecular cloud or the solar nebula. Moreover, the average nitrogen isotopic ratio in individual young stellar objects (YSOs) is observationally correlated with the temperature of their outer envelopes at the projected beam radius (Wampfler et al., 2014). The YSOs with similar nitrogen isotopic ratios to that of the cometary

volatiles have temperatures of 15 K or lower (Wampfler et al., 2014).

Thus, the temperatures estimated from OPRs of water and ammonia (~30 K) contradict those estimated from the nitrogen isotopic ratios in cometary volatiles (~10 K). The estimated OPRs and $^{14}N/^{15}N$ of ammonia yielded different temperatures for the same molecular species. Indeed, the nitrogen isotopic ratio might better reflect the molecular formation environment than the OPR, because it is determined by the chemical reactions at the molecular formation stage. Once incorporated into cometary nuclei, these ratios are not readily modified, as discussed in Section 4. On the other hand, the OPR might equilibrate with the surrounding temperatures by undetermined processes after the volatiles have formed. Therefore, the OPRs of volatiles might not reflect their molecular formation environment.

There are several possible scenarios for the OPRs of ammonia and water, depending on the timescale of the ortho–para conversion. Here, we consider the three scenarios listed below:

(1) the timescale of the ortho–para conversion is very long (>10^9 years),

(2) the timescale is long but shorter than 10^9 years,

(3) the timescale is very short (within several seconds).

Note that the intrinsic OPR of cometary ammonia might be changed by chemical reactions between NH_3 and water-group ions (e.g., H_3O^+ and H_2O^+) in the cometary coma. Once NH_4^+ is formed by proton transfer between the NH_3 and a water-group ion, it reverts to NH_3 by recombining with the liberated electron (i.e., $NH_3 + H_3O^+ \rightarrow NH_4^+ + H_2O$ and $NH_4^+ + e^- \rightarrow NH_3$). Since the coma gas is chiefly water (>80%), with lower proton affinity than NH_3, this refresh cycle of NH_3 could reset the OPR of NH_3. If so, the resultant OPR of NH_3 would depend on the OPRs of H_3O^+ and other species, themselves dependent on the OPR of H_2O. Although the ammonia OPR indicated a temperature of <~15 K in the molecular cloud, the refresh mechanism might shift the nuclear spin temperature inferred from the OPR of ammonia in the coma to T_{spin} = 20–45 K. Therefore, untangling the real meaning of the OPR of cometary water is especially important.

In Scenario (1), the OPRs of both ammonia and water reflect the molecular formation environment of the volatiles and indicate warm

formation conditions in the molecular cloud. If the timescale largely differed between H_2O and NH_3 formation, both volatiles would undoubtedly yield different temperatures, because their temperature environments would vary according to the stage and evolutionary age of the solar system. Another possibility is that cometary water constitutes an arbitrary ratio of materials formed at ~15 K in the molecular cloud and at >50 K in the solar nebula. Scenario (1) is dismissed for ammonia because the nitrogen isotopic ratio in ammonia is probably long-term stable, and the temperature derived from the OPR (~30 K) differs from that of the nitrogen isotopic ratio (<~15 K). Meanwhile, the OPR of water should exhibit large diversity, because it depends on the formation position of icy planetesimals in the solar nebula and the mixture ratio of water formed in the molecular cloud and in the solar nebula.

In Scenario (2), the OPRs of both ammonia and water equilibrate with the interiors of the cometary nuclei, reflecting the temperatures of those nuclear interiors. Assuming that the temperature of the nucleus is determined by the solar radiation ($278/\sqrt{R_h}$, where R_h denotes the heliocentric distance of the comet) and the cosmic microwave background (~2.7 K), the interior temperature of the nucleus should range from ~2.7 K (outer position of the Oort cloud) to ~40 K (inner region of the Kuiper belt). However, the obtained OPRs of the cometary water and ammonia yielded similar temperature regions with small variations. Therefore, Scenario (2) is also dismissed.

In Scenario (3), the water OPR would be determined immediately after its sublimation from the cometary nucleus and would therefore be equilibrated with the sublimation temperature (~150 K). In this case, the water OPR would correspond to the high-temperature limit (3.0) just after sublimation from the nucleus. Since the observed water OPRs yield temperatures below the high-temperature limit, if this scenario is correct, ortho–para conversion processes must be occurring in the coma. Namely, in Scenario (3), the OPRs of cometary water reflect the coma environment. In the next subsection, we discuss whether ortho–para conversion in the coma is consistent with recent laboratory and theoretical studies.

5.1. SUMMARY OF RECENT LABORATORY EXPERIMENTS AND THEORETICAL STUDIES

Laboratory experiments are important for interpreting the observed OPRs of cometary volatiles. Recently, some important laboratory experiments on the grain surface chemistry and theoretical studies related to H_2O molecules have been reported. Here we briefly summarize the results of these studies.

By combining temperature-programmed desorption and resonance-enhanced multi-photon ionization (REMPI), Hama et al. (2011) investigated the nuclear spin conversion in solid phase. They sublimated amorphous water ice (Amorphous Solid Water: ASW) formed on a cold substrate (~8 K) in a vacuum chamber and thereby measured the OPR of water in the gas phase. The surface temperature of ASW (~8 K) was unrelated to the measured nuclear spin temperature of H_2O (>50 K). The nuclear spin temperature of gaseous H_2O molecules desorbed from ASW may not reflect the surface temperature of ASW under laboratory conditions for two reasons: either nuclear spin conversion is inefficient in/on water ice at 8 K or nuclear spin conversion occurs on/in water ice but immediately reequilibrates the OPR of H_2O during thermal desorption. As these laboratory results are inconsistent with the observed OPRs from cometary volatiles (in gas phase), Hama et al. (2011) proposed that both ortho–para conversion in the coma and the desorption temperature of volatiles from cometary ice are relevant. Namely, OPRs equilibrated under the sublimation condition might reach the high-temperature limit (3.0) immediately following sublimation from ice, regardless of their values in the ices of the cometary nuclear interior.

The next of important laboratory experiments was conducted by Sliter et al. (2011). Adopting the matrix deposition method, they identified fast nuclear spin conversion in water clusters and ices. They isolated a single para-H_2O molecule in a solid argon matrix at 4 K and subsequently heated the copper IR cell containing a solid sample to $T = 250$ K. The intensities of ortho- and para-H_2O molecules were measured from their ro-vibrational transitions observed by Fourier transform infrared spectroscopy (FTIR).

Measurements were conducted in the regions of the three rotational modes (v_1, v_2, and v_3) of H_2O. The nuclear spin relaxation is mediated by spin–spin interactions. In the water dimers, the nuclear spin relaxation was determined as within 100 μs by model calculations. This result indicates that ortho–para conversion is feasible in the coma (even in the gas phase) if water clusters and ices formed therein.

One of the most important laboratory experiments concerns the nuclear spin symmetry conversion and relaxation in gas-phase water (Tanner et al., 2011, 2013). Tanner and colleagues measured the OPRs in H_2O using cavity ring-down spectroscopy. In H_2O supersonically expanded with argon gas, the ortho lines (2_{21}–1_{10} and 3_{21}–2_{12}) and the para line (2_{20}–1_{11}) were consistent with temperatures of 20–30 K (before the expansion, the water temperature was ~300 K). At the lowest relative water concentration in the H_2O/Ar gas mixture (0.3%; gas pressure below 1.6 kPa), the OPR appeared to remain at its statistical weight value (3.0). On the other hand, at the highest relative water concentration (1.6%; gas pressure above 1.8 kPa), the measured OPRs were consistent with the nuclear spin temperatures under low-temperature thermal equilibrium conditions, to within several hundred μs. Tanner et al. suggested that reactive exchange occurs during collisions with water clusters, or that intermolecular interconversion occurs within an intermediate cluster with a high density of states or accidental degeneracy. Their result can be explained by two sequential mechanisms. First, larger water clusters could form by runaway growth of small clusters when the water density exceeds some threshold density (possibly when the relative proportion of monomer water molecules $n(H_2O_{monomers})/n(H_2O_{total})$ reaches ~0.5). In this expression, $n(H_2O_{monomers})$ and $n(H_2O_{total})$ indicate the number densities of the water monomers and total water structures (monomers and clusters), respectively. The second mechanism is fast ortho–para conversion in the water clusters.

The final important report is a theoretical study of ortho–para conversion based on the spontaneous transitions of water ions (H_2O^+) (Tanaka et al., 2013). These authors theoretically calculated the spontaneous emission lifetimes of H_2O^+ ions transiting between the ortho- and para-levels. The electron spin–nuclear interaction term mixes the ortho- and para-levels into

a “forbidden” ortho- to para-transition ($|\Delta I| = 1$). The mixing term is four orders of magnitude higher for H_2O^+ than for its neutral counterpart H_2O, in which the magnetic field interacts with the proton spins by molecular rotation rather than with free electrons. Although the spontaneous emission lifetime of the vibronic transitions of water ions has not been calculated, spontaneous emissions of H_2O^+ from the coma are probably hard to detect because the lifetime between the ortho- and para-levels is very long; consequently, the H_2O^+ emission lines should be very weak. Hydrogen exchange reactions of H_2O in the coma ($H_2O + H_2O^+ \rightarrow H_2O + H_2O^+$, $H_2O + H_3O^+ \rightarrow H_2O + H_3O^+$…) might contribute to cometary ortho–para conversion because they involve water ions, which exist in the coma and ion tail (where they comprise ~3% of the water content).

Finally, we compare the temperatures inferred from the water OPRs and the D/H ratios in water. We focus on the water D/H ratio as a primordial property of cometary volatiles. Recently, cometary water ice has been hypothesized to include the water formed in both the molecular cloud and the solar nebula (Cleeves et al., 2014; Furuya et al., 2013). Therefore, by determining the D/H ratio in cometary water, we could estimate the mixing ratio of the water sourced from these two bodies. If the deuterated water formed in the solar nebula can be assumed negligible (Cleeves et al., 2014), the water fraction f_X in a solar system body X (where X denotes a comet, asteroid, or planet) and interstellar materials (ISM) can be estimated by the following formula (Cleeves et al., 2014):

$$f_{\mathrm{ISM}} = \frac{\mathrm{D/H_X} - \mathrm{D/H_{sun}}}{\mathrm{D/H_{ISM}} - \mathrm{D/H_{sun}}},$$

where D/H_X refers to the D/H ratio of the water in a solar system body X, $D/H_{Sun} = 2 \times 10^{-5}$ (Yan et al., 2011) and $D/H_{ISM} = (2.95–9.50) \times 10^{-4}$ (Lowe & Thorneley, 1984). According to this analysis, the interstellar water content of comets should exceed 14%. Next, we estimate the expected OPR of cometary water, assuming molecular cloud and solar nebula temperatures of ~15 K and >50 K, respectively. Thus, the OPRs of the water formed in the interstellar matter and in the solar nebula are estimated as 0.4 and 3.0, respectively (corresponding to nuclear spin temperatures of 15 K and >50 K,

respectively). If we accept the mixing ratios inferred from the observed D/H ratios, the expected OPR of water in the coma is below 1.57, inconsistent with the observed OPRs in comets. Therefore, the temperature of the molecular cloud either differs from ~15 K, or the OPR of the cometary water reflects a temperature environment other than that of the molecular cloud. This result rejects Scenario (1) which posits long timescales of the ortho–para conversion in water.

Chemical reactions play an important role in forming water dimers in the inner coma, as first pointed out by Murad & Bochsler (1987) and further demonstrated by Korth et al. (1989) and Marconi et al. (1989). However, in a theoretical study, the estimated fraction of water dimers (relative to all water) was below 10^{-5} everywhere in the coma (Crifo & Slanina, 1991). The same calculation can yield large water clusters in the coma (up to 260 molecules/cluster). Moreover, water dimers comprise less than 6% of the water production rate in comet C/1995 O1 (Hale–Bopp), according to radio observations by the MPIfR 100 m telescope, the NRAO 12 m telescope, and the IRAM 30 m telescope (Scherer et al., 1998). However, the error in these observations (~6%) is larger than the abundance ratios of most species (relative to water). Because of the low S/N ratio and low spatial resolution of existing observational equipment, water dimers and clusters have not been clearly detected in comets. According to our calculated number density of water dimers in the coma, water clusters larger than dimers might form in regions of abundant water dimers (relative to H_2O monomers).

5.2. ORTHO–PARA CONVERSION OF WATER IN THE COMETARY COMA BY CHEMICAL REACTIONS WITH WATER CLUSTERS

From recent observational, experimental, and theoretical studies, we propose a scenario for ortho–para conversion in cometary comas.

1. The OPR of immediately sublimated cometary water (in gas phase) was 3.0, different from the water OPRs observed in cometary ices. It appears that prior to sublimation from the cometary nucleus, cometary water takes an arbitrary OPR value, which is lost at the

moment of sublimation.

2. Relaxation of OPRs of water with the surrounding temperature occurs by interaction of water molecules with water clusters formed in the inner coma. Finally, the OPR of water equilibrates with that of water clusters in the expanding gas flow. The gas temperature initially drops under the adiabatic expansion and later increases by photodissociative heating (mainly contributed by photodissociation of water to OH). On the other hand, the water clusters in the cometary coma sublimed at ~30 K because their evaporation rate follows the unimolecular dissociation theory (UDT) which predicts that (k_{UDT}) rapidly increases around 30 K (see Figure 5.1 of Bormer et al., 2013). The UDT evaporation rate is expressed as follows:

$$k_{\mathrm{UDT}} = n^{2/3}\omega_{\mathrm{H2O}}\exp\left(\frac{H_v}{kT_c}\right),$$

where n and ω_{H2O} denote the cluster size and the vibrational frequency of a water molecule within the cluster, respectively (the latter was proposed as 2.68×10^{12} /s by Oka & Hara, 2007). H_{v} is the latent heat of vaporization of a water cluster (equal to 1.46, 2.17, 1.619, 1.44, 2.13, and 2.02×10^{-20} J for n = 2, 3, 4, 6, 8, and 10, respectively), and k and T_{c} are the Boltzmann constant and cluster temperature (K), respectively. Fast ortho–para conversion can occur in the cometary coma under the following conditions; a high proportion of water molecules in the clusters (>~0.5 of total H_2O) and temperatures below ~35 K. Water dimers, assumed as the major cluster components, are considered to form by three-body collisional reactions among the waters and by ion–molecular reactions between H_3O^+ and water. The number density of the water dimers (cluster size of n = 2) can be calculated by the following system of equations:

$$\begin{aligned} k_{\mathrm{UDT}}(2)N[(\mathrm{H_2O})_2] = {} & q_{\mathrm{H2O-H2O}}\sigma_{\mathrm{H2O-H2O}}v_{\mathrm{thermal,H2O}}d_{\mathrm{H2O}}l_{\mathrm{H2O}}N[\mathrm{H_2O}]^2 \\ & + k_{\mathrm{Langevin}}q_{\mathrm{H2O-H3O+}}N[\mathrm{H_3O^+}]N[\mathrm{H_2O}] \end{aligned}, \quad \text{(A)}$$

$$N[(H_2O)_{total}] = \frac{Q[H_2O]}{4\pi r_{nc} v_{exp.,H2O}} \exp\left(-\frac{t}{\tau_{H2O}}\right) = N[H_2O] + 2N[(H_2O)_2], \quad (B)$$

where N $[(H_2O)_2]$, N $[H_2O]$, N $[H_3O^+]$, and N $[H_2O_{total}]$ denote the number densities of water dimers ((H_2O_2)), H_2O monomers, H_3O^+ ions, and total H_2O (= N $[(H_2O)_2]$ + $N[H_2O]$), respectively. Note that the total H_2O number density excludes N $[H_3O^+]$, because the absolute number density of H_3O^+ is much smaller than that of H_2O. In equation (A), the parameter $q_{H2O\text{-}H2O}$ is the formation rate of water dimers by collisional reactions with the reaction intermediate $(H_2O)_2$* and H_2O monomers ($0 < q_{H2O\text{-}H2O} < 1$),$\sigma_{H2O\text{-}H2O}$ is the collisional crosssection between waters [/m^2], $v_{thermal,H2O}$ denotes the mean velocity of water in thermodynamic equilibrium [m/s], d_{H2O} is the geometric radius of the water monomer [m], l_{H2O} is the mean free path of water in thermodynamic equilibrium [m], $k_{Langevin}$ is the Langevin rate coefficient, corresponding to the reaction rate of the ion–molecular chemistry [m^3/s], and $q_{H2O–H3O+}$ denotes the formation rate of water dimers by reactions between H_3O^+ ions and free electrons ($0 < q_{H2O\text{-}H3O+} < 1$). In equation (B), the parameter Q $[H_2O]$ denotes the water production rate [/s], r_{nc} is the nucleocentric distance [m], $v_{exp.,H2O}$ is the expansion velocity of water [m/s], $\tau$is the lifetime of water [s] (determined as 4.5×10^4 s by Huebner et al., 1992), and $t = r / v_{exp.,H2O}$ is the time elapsed since water sublimed from the surface of the cometary nucleus [s].

In general, the region of ortho–para conversion in the coma is limited to the region of the contained water clusters. Its extent depends on the temperature distribution in the coma (and on other factors such as water production rate and heliocentric distance).

3. Ortho–para conversion requires the presence of water clusters (once the gas temperature in the expanding coma has increased to above ~35 K by the solar radiations). The OPR observed in the cometary water reflects the temperature range over which water clusters are destroyed. Namely, the observed OPRs of cometary water reflect the

evaporation temperature of the water clusters in the inner coma (~30 K), not the sublimation temperature of water in the cometary nucleus (~150 K). If no region of the cometary coma is below ~30 K (i.e., no ortho–para conversion occurs in the coma), the OPR of cometary water should be 3.0 (the high-temperature limit).

Figure 5.2 presents the calculated spatial distributions of water dimers, assuming a water production rate of 1.0×10^{30} /s and a heliocentric distance of 1.0 AU. Also plotted are the spatial distributions of H_3O^+ in 1P/Halley, obtained from the radial variations of the number density measured by the Giotto spacecraft (Ip, 1989). The calculation is detailed in Appendix C.

Figure 5.2 shows that ortho–para conversion can occur within a limited area (30–100 km from the nucleus) where the relative proportion of monomer water is below ~50 %. The OPRs of cometary water may also reflect the sublimation and/or dissociation temperature of water dimers to monomers in the coma. The second of these is feasible because the relaxation time of water is very short (within several micro seconds; Sliter et al., 2011; Tanner et al., 2013). Within the conversion area, $(H_2O)_2$ formed at a rate exceeding 4×10^{16} /s/m^3, implying a coma temperature below 28 K.

Larger clusters (n >3) facilitate the ortho–para conversion of water because the hyperfine interactions of ortho–para mixing are more easily accomplished in large clusters than in dimers. The total crosssections of large clusters are much larger than those of water dimers. However, ionic water clusters can collide more easily than neutral clusters.

Unless all of the water in the coma can undergo ortho–para conversion, the observed OPRs of water are contributed by water that is equilibrated with the sublimation temperature of cometary nuclear water (OPR = 3.0; the high-temperature limit) and by water that is converted in the coma (OPR = 2.2, corresponding to T_{spin} = 25 K). If these waters are mixed in the coma, the observed OPRs of water should widely vary.

In this study, the number density of water dimer in the coma is calculated in a steady state condition. However, the number density of water dimer in the actual coma might become smaller than our calculation because

the realistic expanding coma might not be in a steady state condition. Therefore, to check the temporal evolution of the number density of water cluster in the coma, we require very highly spatially resolved observations of water dimer at infrared wavelengths from space, monitoring observations of H_2O OPR during a outburst of comets with a short time-dependent, and development of time integration calculation of number density of water clusters in the coma.

We assume that ammonia undergoes similarly fast ortho–para conversion by sublimation from the nucleus. Immediately after sublimation from the cometary nucleus, we expect that the ammonia OPR is balanced with the sublimation temperature of cometary ices at ~150 K (the sublimation temperature of water, which comprises most of the cometary nucleus). The observed OPRs of ammonia were shifted from their equilibrium value of 1.0, indicating that ortho–para relaxation occurs in the coma under low-temperature conditions. Although ammonia clusters ($(NH_3)_n$) could conceivably form in the coma, ammonia–ammonia collisions are much rarer than H_2O–H_2O collisions because the abundance ratio of ammonia is only ~1% that of water. Therefore, we suggest that ammonia collides and chemically reacts with both water-group species (e.g., H_3O^+ and H_2O^+) and water clusters (e.g., $(H_2O)_n$; n is integers more than 2). These collisions and reactions might enable ortho–para conversion of ammonia.

Thus, because the OPR of water is probably relaxed in the coma based on our simple calculation of number density water dimer in the coma, OPRs of cometary volatiles are not suitable as the physics parameter to obtain information before the cometary nuclei formed.

5.3. PECULIAR COMET: 73P/ SCHWASSMANN–WACHMANN 3

Finally, we discuss the anomalous properties of the peculiar comet named 73P/Schwassmann–Wachmann 3 (hereafter 73P/SW3). Not only are the OPRs of its cometary ammonia and water consistent with the high-temperature limit values (being equal to 3.0 and 1.0, respectively) but also is the nitrogen isotopic ratio in its cometary CN ($^{14}N/^{15}N$ ~ 220; see

Section 2). The temperature in the coma of Comet 73P/SW3 is everywhere above 30 K, because the comet is disintegrated into many small nuclei rather than containing a single large nucleus (that is, the sources are distributed throughout the coma). Consequently, unlike other comets whose intact cometary nuclei are cooled below 30 K, Comet 73P/SW3 contains multiple small nuclei that have remained relatively warm. Other features of this comet include (1) poor abundances of organic molecules (Kobayashi et al., 2007), (2) typical abundances of crystalline silicates in the cometary dust grains (Harker et al., 2011), and (3) low ^{15}N-fractionation in CN (Manfroid et al., 2009). These features were revealed in observational studies. From our own and previous studies of Comet 73P/SW3, we infer that the formation region of the cometary nucleus was similar to other comets, although numerous ices recondensed from the gas-phase had been formed in relatively warmer regions. Such peculiar comets might form in the subnebulae of giant planets, such as Jupiter. Alternatively, Comet 73P/SW3 might be an extrasolar comet. However, the orbital evolution of an object from hyperbolic to elliptical is energetically unfavorable because orbital evolution necessarily loses potential energy of the object. The orbit of an object should evolve to the Kuiper belt or the Oort cloud when an object passes over the inner solar system captured by the solar system

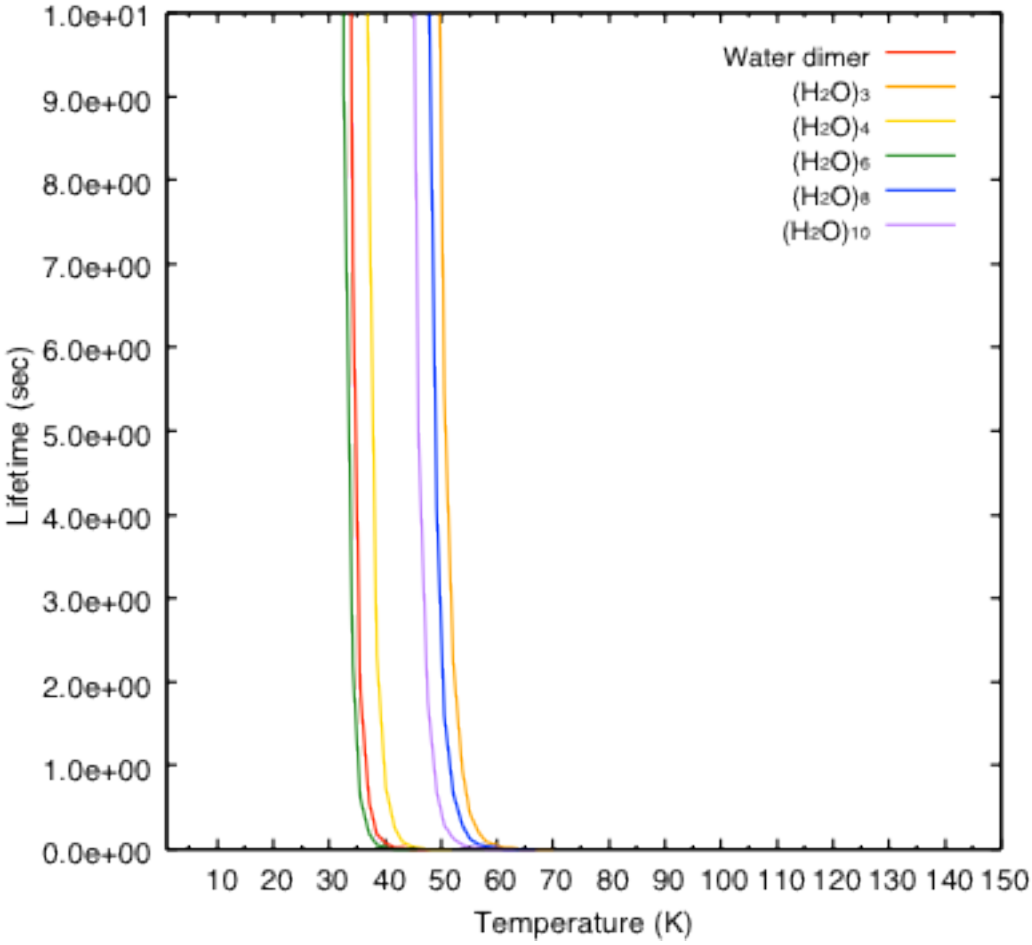

Figure 5.1 Lifetimes of water clusters (τ_{WC} (n); n = 2, 3, 4, 6, 8, and 10) calculated from the UDT evaporation rate formula: k_{UDT} (τ_{WC} (n) = 1/k_{UDT} (n)). The lifetime rapidly increases below ~40 K at some cluster sizes (n = 2, 4, 6) and below 55 K at others (n = 3, 8, 10).

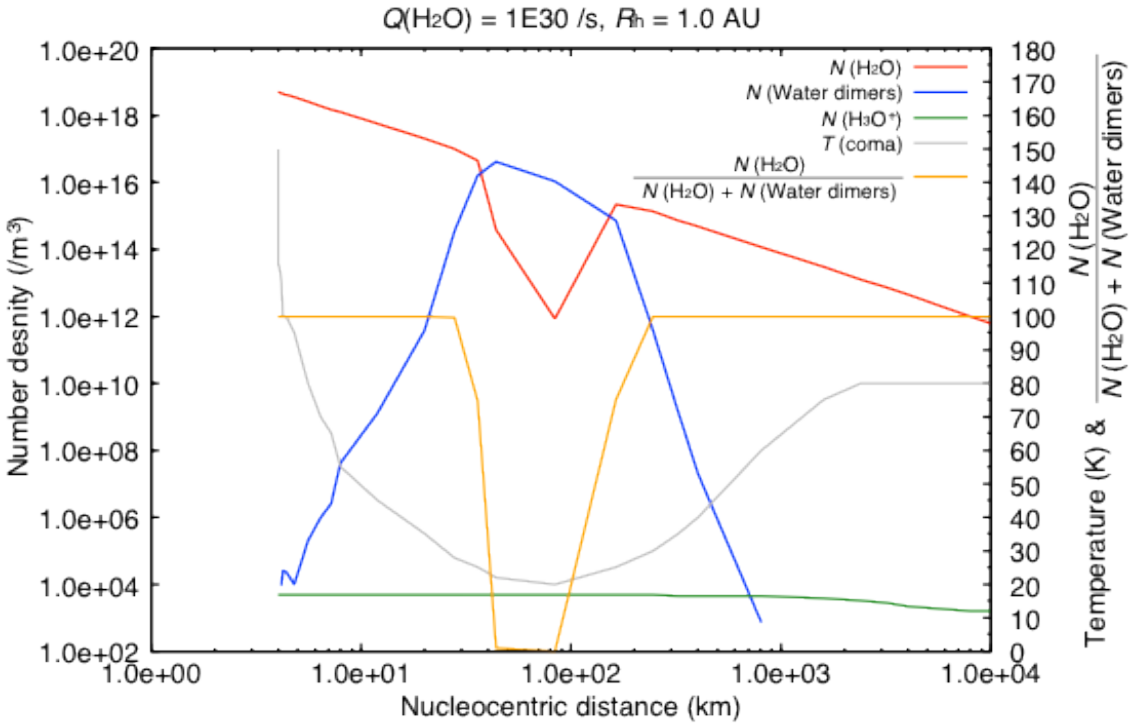

Figure 5.2 Spatial distribution of water dimers in the coma. The water production rate is 1×10^{30} /s and the heliocentric distance is 1.0 AU. Water dimers are formed by three-body H_2O collisions (formation rate = 10^{-3}) and by recombination of $(H_2O)_2^+$ and electrons (recombination rate = 10^{-3}). Red, blue, green, gray, and orange lines denote the number densities of water monomers [/m^3] (left axis), water dimers [/m^3] (left axis), and H_3O^+ ions [/m^3] (left axis), the gas temperature in the coma [K] (right axis), and the relative proportion of monomer water [%] (right axis), respectively. Ortho–para conversion can occur within a small area (30–100 km from the nucleus). The OPRs of cometary water may reflect the sublimation and/or dissociation temperatures of water dimers in the coma.

6. CONCLUSIONS AND FUTURE DIRECTIONS

Ortho–para conversion of cometary water can occur by chemical reactions with water clusters in a limited region of the coma. Within this region, the relative proportion of monomer water is below ~0.5 and the surrounding gas temperature is lower than ~30 K (both parameters are considered to control ortho–para conversion in the coma). The observed nuclear spin temperatures of cometary water (~30 K) reflect the evaporation temperature of the water clusters in the coma. To confirm our hypothesis that water clusters of reasonable amount are formed in a steady state coma, we require (1) very highly spatially resolved observations of water dimer at infrared wavelengths from space, (2) monitoring observations of H_2O OPR during a outburst of comets with a short time interval, and (3) development of a time-dependent model of number density of water clusters in the coma.

The nitrogen isotopic ratios in cometary volatiles, such as ammonia, HCN, and CN may retain their memory of molecular formation, being consistent with formation at low temperatures (~10 K). Because the nitrogen isotopic ratios of cometary volatiles (at least those of CN) are largely consistent, they apparently reflect the temperature of the molecular cloud that sourced the solar system, which was probably around 10 K. On the other hand, ammonia, NCN, and CN might have undergone ^{15}N-fractionation slowly by chemical reactions with ^{15}N fractionated nitrogen molecules ($^{14}N^{15}N$ and $^{15}N^{15}N$) in the solar nebula or the interior of the nucleus. Therefore, we hope to determine the nitrogen isotopic ratios of cometary nitrogen molecules. To this end, we must first detect the nitrogen molecules in comets, which have not been reported to date.

Cometary water comprise water formed in the interstellar environment (very low-temperature conditions of ~10 K) and in the solar nebular (warmer temperatures of >30 K) because the D/H enrichments of cometary water cannot be explain only by chemical reactions in the solar nebula (Cleeves et al., 2014). The disk parameters (such as turbulent viscosity coefficient and mass accretion rate) that can explain the observed D/H ratio in cometary water can be obtained by comparing the observational results with results of

a disk model for the solar nebula. To confirm the validity of these disk parameters, we need to check the soundness of the disk model (i.e., we should confirm whether other physical parameters can be explained by the same disk parameters).

One of a key volatile is CH_3D to measure the D/H ratio in methane (CH_4). This value will give us strong constraints for chemical evolution models in the solar nebular and in the presolar molecular cloud. A key point is the difference of the sublimation temperatures between methane (~30 K) and water (~150 K). Methane can be in solid-phase in the presolar molecular cloud at 10 K. Methane ice formed in the interstellar space does not sublimate under higher temperature environments, i.e., higher than the sublimation temperature of methane and lower than that of water, (e.g., in the solar nebula) because these methane molecules are trapped in water ice that is dominated volatile in interstellar ices in general. Only in limited areas of the solar nebula (further than 13 AU from the Sun, based on a temperature distribution of the normal solar nebula model, Hersant et al., 2001), methane can exist in solid-phase. Then, the D/H ratio observed in cometary methane is probably influenced by the radial and vertical mixing in the solar nebula.

However, in current theoretical deuteration model of methane in the solar nebula (Aikawa & Herbst, 1999), the mixing in the solar nebula has never been considered. To reproduce not only the D/H ratio in water but also that of methane, an inflexible constraint to the disk parameters is required.

Finally, quantitative evaluation of the effect of the mixing in the solar nebula on cometary physical parameters is essentially important to clarify an interpretation of the cometary physical parameters (such as OPRs of water and ammonia, isotopic ratios in volatiles, mixing ratios relative to water in each volatile). To clarify the effect of the mixing in the solar nebular to cometary physical parameters, we should reveal a statistical relationship between a crystalline-to-amorphous ratio (CAR) of cometary silicate grain and the physical parameters because the CARs of the silicate grain probably reflect the strength of radial mixing in the solar nebula.

ACKNOWLEDGEMENT

I would like to thank my supervisor Professor Hideyo Kawakita, Director of Koyama Astronomical Observatory, at Kyoto Sangyo University. He supported me and gave me many advices and fruitful comments on this dissertation. He also gave me the special opportunity to present my study at the international conference in 2008, and it was my turning point.

I am also grateful to Dr. Hitomi Kobayashi (Estrista), Dr. Daniel C. Boice (Scientific Studies and Consulting), Dr. Yuji Ikeda (Photocoding), Dr. Michael J. Mumma (NASA Goddard Space Flight Center), Dr. Emanuël Jehin, Dr. Alice Decock, Cyriel Opitom (Université de Liège), and many other colleagues who I met at some conferences for their fruitful comments on my studies and many advices to me.

The observational data used in my dissertation were taken at the Subaru Telescope, VLT (Very Large Telescope), TNG (Telescopio Nazionale Galileo), Xinglong 2.16 m Telescope and the 1.3-m Araki Telescope. Many staffs operate those observatories and I appreciate their great help to my observations.

The author would like to thank Enago (www.enago.jp) for the English language review.

Finally, I would like to express my appreciation to my family and friends for their continuous encouragement and support.

REFERENCES

Aikawa, Y., & Herbst, E., 1999, ApJ, 526, 314

Adande, G. R., & Ziurys, L. M., 2012, ApJ, 744, 194

A'Hearn, M. F., Belton, M. J. S., Delamere, W. A., Feaga, L. M., Hampton, D., et al., 2011, Science, 332, 1396

A'Hearn, M. F., Millis, R. L., Schleicher, D. G., Osip, D. J., & Birch, P. V., 2005, Icarus, 118, 223

Alexander, C. M. O'D., Fogel, M., Yabuta, H., & Cody, G. D., 2007, Geochim. Cosmochim. Acta, 71, 4380

Altwegg, K., Balsiger, H., Bar–Nun, A., Berthelier, J. J., Beiler, A., et al. 2015, Science, 347, 1261952

Altwegg, K., 1996. PhD thesis, Habilitationsschrift University of Bern

Anders, E., & Grevesse, N., 1989, Geochem. Cosmochim. Acta, 53, 197

Arpigny, C., Jehin, E., Manfroid, J., Hutsemékers, D., Schulz, R., et al., 2003, Science, 301, 1522

Arpigny, C., Schulz, R., Manfroid, J., Ilyin, I., Stüwe, J. A., Zucconi, J. –M., 2000, Bull. Amer. Astron. Soc., 32, 1074

Balsiger, H., Altwegg, K., & Geiss, J., 1995, J. Geophys. Res., 100, 5827

Battams, K., 2013, CBET, 3731

Bhardwaj, A., 2003, Geophysical Research Letters, 30, 2244

Bird, M. K., Huchtmeier, W. K., Gensheimer, P., Wilson, T. L., Janardhan, P., & Lemme, C., 1997, A&A, 325, 5

Biver, N., Bockelée–Movan, D., Crovisier, J., Lecacheux, A., Lis, D. C., et al., 2008, LPICo, 1405, 8149

Biver, N., Bockelée–Morvan, D., Crovisier, J., Lis, D. C., Moreno, et al., 2006, A&A, 449, 1255

Biver, N., Bockelée–Morvan, D., Colom, P., Crovisier, J., Germain, B., et al., 1999, EM&P, 78, 5

Bizzocchi, L.,Caselli, P., & Dore, L., 2010, A&A, 510, L5

Bockelée–Morvan, D., Biver, N., Swinyard, B., de Val–Borro, M., Hartogh, P., et al. 2012, A&A, 544, L15

Bockelée–Morvan, D., Woodward, C. E., Kelley, M. S., & Wooden, D. H.,

2009, ApJ, 696, 1075

Bockelée–Morvan, D., Biver, N., Jehin, E., et al. 2008, ApJL, 679, L49

Bockelée–Morvan, D., Dello Russo, N., Jehin, E., Manfroid, J., Smette, A., et al., 2008, LPICo, 1405, 8190

Bockelée–Morvan, D., Biver, N., Moreno, R., Colom, P., Crovisier, J., et al., 2001, Science, 292, 1339

Bockelée–Morvan, D., Lis, D. C., Wink, J. E., Despois, D., Crovisier, J., et al., 2000, A&A, 353, 1101

Bockelée–Morvan, D., & Crovisier, J., 1987, ESASP, 278, 2358

Bockelée–Morvan, D., Crovisier, J., Baudry, A., Despois, D., Perault, M., et al., 1984, A&A, 141, 411

Böhnhardt, H., Mumma, M. J., Villanueva, G. L., DiSanti, M. A., Bonev, B. et al., 2008, ApJ, 683, L71

Boice, D. C. & Martinez S. E., 2010, LPICo, 1533, 2733

Boice, D. C. & Wegmann, R., 2007, Adv. Space Res. **39**, 407

Boice, D. C., Benkhoff, J. & Gladstone, G. R., 1995, Earth, Moon, and Planets **71**, 235

Bonev, B. P., Villanueva, G. L., Paganini, L., DiSanti, M. A., Gibb, E. L., et al., 2013, Icarus, 222, 740

Bonev, B. P., Mumma, M. J., Gibb, E. L., DiSanti, M. A., Villanueva, G. L., et al., 2009, ApJ, 699, 1563

Bonev, B. P., Mumma, M. J., Kawakita, H., Kobayashi, H., & Villanueva, G. L., 2008a, Icarus, 196, 241

Bonev, B. P., Mumma, M. J., Radeva, Y. L., DiSanti, M. A., Gibb, E. L., & Villanueva, G. L., 2008b, ApJ, 680, L61

Bonev, B. P., Mumma, M. J., Villanueva, G. L., DiSanti, M. A., Ellis, R. S., et al., 2007, ApJ, 661, L97

Boss, A. P., 2001, ApJ, 563, 367

Busemann, H., Young, A. F., O'D. Alexander, C. M., Hopper, P., Mukhopadhyay, S., & Nittler, L. R., 2006, Science, 312, 727

Cacciani, P., Cosléou, J., Khelkhal, M., Tudorie, M., Pizzaromo, C., & Pracna, P., 2009, Physical Review, 80, 42507

Capria, M. T., Cremonese, G., Boattini, A., de Sanctis, M. C., D'Abramo, G.,

& Buzzoni, A., 2002, ESASP, 500, 693

Charnley, S. B. & Rodgers, S. D., 2008, in Origin and early evolution of comet nuclei, pp. 59–73

Cleeves, L. I., Bergin, E. A., Alexander, C. M. O'D., Du. F., Graninger, D., öberg, K. I., Harries, T. J., 2014, Science, 345, 1590

Clough, S. A., & Iacono, M. J., 1995, J. Geophys. Res., 100, 519

Combi, M. R., Bertaux, J. –L., Quemerais, E., Maekinen, J. T. T. & Ferron, S., 2013, CBET, 9266

Cochran, L., & Cochran, W. D., 2000, Icarus, 146, 583

Combi, M. R., Mäkinen, J. T. T., Bertaux, J. –L., Lee, Y., & Quémerais, E., 2009, ApJ, 137, 4734

Combi, M. R., Harris, W. A., & Smyth, W. H., 2004, in Comet II, ed. M. C. Festou, H. U. Keller, & H. A. Weaver (Tucson: Univ. Arizona Press), 523

Crifo, J. F. & Slanina, Z., 1991, ApJ, 383, 351

Crovisier, J., Biver, N., Bockelée–Morvan, D., Boissier, J., & Colom, P., 2008, SF2A, 401,

Crovisier, J., Bockelée–Morvan, D., Colom, P., Biver, N., Despois, D., et al., 2004. Astron. Astrophys., 418, 1141

Crovisier, J., 2007, Astrophysics, 0703785

Crovisier, J., 2006, Faraday Discussions, 133, 375

Crovisier, J., Leech, K., Bockelée–Morvan, D., Brooke, T. Y., Hanner, M. S., et al., 1997, Science, 275, 1904

Daniel, F., Gérin, M., Roueff, E., et al., 2013, A&A, 560, A3

Dekker, H. D'Odorico, S., Kaufer, A., Delabre, B., & Kotzlowski, H., 2000, SPIE, 4008, 534

Dello Russo, N., Vervack, R. J., Weaver, H. A., Biver. N., Bockelée–Morvan, D., et al., 2007, Nature, 448, 172

Dello Russo, N., Mumma, M. J., DiSanti, M. A., Magee–Sauer, K., Gibb, E. L., et al., 2006, Icarus, 184, 255

Dello Russo, N., Bonev, B. P., DiSanti, M. A., Mumma, M. J., Gibb, E. L., et al., 2005, ApJ, 621, 537

Dello Russo, N., Mumma, M. J., DiSanti, M. A., Magee–Sauer, K., & Novak, R., 2001, Icarus, 153, 162

DiSanti, M. A., Villanueva, G. L., Bonev, B. P., Magee–Sauer, K., Lyke, J. E., & Mumma, M. J., 2007, Icarus, 187, 240

DiSanti, M. A., Dello Russo, N., Magee–Sauer, K., Gibb, E. L., Reuter, D. C., & Mumma, M. J., 2001, Asteroids, Comets, Meteors (ESA SP–500, ESTEC; Noordwijk: ESA), 571

Eberhardt, P., Meier, R., Krankowsky, D., & Hodges, R. R., 1994, A&A, 288, 315

Feldman, P. D., Cochran, A. L., & Combi, M. R., 2004, in Comet II, ed. M. C. Festou, H. U. Keller, & H. A. Weaver (Tucson: Univ. Arizona Press), 425

Floss, C., Stadermann, F. J., Bradley, J. P., Dai, Z. R., Bajt, S., et al., 2006. Geochim. Cosmochim. Acta, 70, 2371

Gerin, M., De Luca, M., Black, J., et al., 2010. A&A, 518, L110

Gratton, R. G., Bonanno, G., Bruno, P., Calí, A., Claudi, R. U., et al., 2001, Experimental Astron., 23, 107

Fink, U., 2009, Icarus, 201, 311

Gibb, E. L., DiSanti, M. A., Magee–Sauer, K., Dello Russo, N., Bonev, B. P., & Mumma, M. J., 2007, Icarus, 188, 224

Grimm, R.E., & McSween, H.Y., 1993, Science, 259, 653

Hama, T., Watanabe, N., & Charnley, S. B., 2011, SApJ, 738, 15

Harker, D. E., Woodward, C. E., Kelley, M. S., Sitko, M. L., Wooden, D. H., et al., 2011, ApJ, 141, 26

Hartogh, P., Lis, D. C., Bockelée–Morvan, D., de Val–Borro, M., Biver, N., et al., 2011, Nature, 478, 218

Helbert, J., Rauer, H., Boice, D. & Huebner, W., 2005, A&A, 442, 1107

Hersant, F., Gautier, D., & Hure, J. –M., 2001, ApJ, 554, 391

Hily–Blant, P., Bonal, L., Faure, A., & Quirico, E., 2013a, Icarus, 223, 582

Hily–Blant, P., Pineau des Forêts, G., Faure, A., Le Gal, R., & Padovani, M., 2013b, A&A, 557, A65

Hily–Blant, P., Walmsley, M., Pineau D. F., & G., Flower, D., 2010, A&A, 513, 41

Hiraoka, K., Yamashita, A., Yachi, Y., Aruga, K., & Sato, T., 1995, ApJ, 443, 363

Huebner, W. F., Keady, J. J., & Lyon, S. P., 1992, Ap&SS, 195, 1

Huebner, W.F., Boice, D.C., Schmidt, H.U. & Wegmann, R., 1991, in Comets in the Post-Halley Era, (R. Newburn, Jr., M. Neugebauer, and J. Rahe, eds.), pp. 907

Huet, T. R., Bachir, I. H., Destombes, J. L., & Vervloet, M., 1997, J. Chem. Phys., 107, 5645

Hutsemékers, D., Manfroid, J., Jehin, E., & Arpigny, C., 2009, Icarus, 204, 346

Hutsemékers, D., Manfroid, J., Jehin, E., Zucconi, J. –M., Arpigny, C., 2008, A&A, 490, 31

Hutsemékers, D., Manfroid, J., Jehin, E., Arpigny, C., Cochran, A., et al., 2005, A&A, 440, L21

Ikeda, M., Hirota, T., & Yamamoto, S., 2002, ApJ, 575, 250

Ip, W. –H., 1989, ApJ, 343, 964

Irvine, W. M., Schloerb, F. P., Crovisier, J., Fegley, B., Jr., Mumma, M. J., 2000, in Protostars and Planets IV (Book Tucson: University of Arizona Press; eds Mannings, V., Boss, A.P., Russell, S. S.), pp. 1159

Jang–Condell, H., 2008, ApJ, 679, 797

Jehin, E., Manfroid, J., Hutsemékers, D., Arpigny, C., & Zucconi, J. –M., 2009a, EM&P, 105, 167

Jehin, E., Bockelée–Morvan, D., Dello Russo, N., Manfroid, J., Hutsemékers, D., et al., 2009b, EM&P, 105, 343

Jehin, E., Manfroid, J., Kawakita, H., Hutsemékers, D., Weiler, M., et al., 2008, LPICo, 1405, 8319

Jehin, E.; Manfroid, J. Hutsemékers, D., Cochran, A. L., Arpigny, C., et al., 2006, ApJ, 641, L145

Jehin, E., Manfroid, J., Cochran, A. L., Arpigny, C., Zucconi, J. –M., et al., 2004, ApJ, 613, L161

Jehin, E., Boehnhardt, H., Sekanina, Z., Bonfils, X., Schütz, O., et al., 2002, EM&P, 90, 147

Jensen, P., Kraemer, W. P., & Bunker, P. R., 2003, Molecular Physics, 101, 613

Jewitt, D., Matthews, H. E., Owen, T., & Meier, R., 1997, Science, 278, 90

Justtanont, K., Yamanura, I., de Jong, T., & Waters, L. B. F. M., 1997,

Ap&SS, 251, 25
Kawakita. H., & Mumma, M. J., 2011, ApJ, 727, 91
Kawakita, H., & Kobayashi, H., 2009, ApJ, 693, 388
Kawakita, H., Jehin, E., Manfroid, J., & Hutsemékers, D., 2007, Icarus, 187, 272
Kawakita, H., Dello Russo, N., Furusho, R., Fuse, T., Watanabe, J., et al., 2006, ApJ, 643, 1337
Kawakita, H., Watanabe, J., Furusho, R., Fuse, T., & Boice, D. C., 2005, 623, L49
Kawakita, H., Watanabe, J., Furusho, R., Fuse, T., Capria, M. T., et al., 2004, ApJ, 601, 1152
Kawakita, H., Watanabe, J., Kinoshita, D., Ishiguro, M., & Nakamura, R., 2003, ApJ, 590, 57
Kawakita, H., & Watanabe, J., 2002, ApJ, 572, 177
Kawakita, H., Watanabe, J., Ando, H., Aoki, W., Fuse, T., et al., 2001, Science, 294, 1089
Kawakita, H., Ayani, K., & Kawabata, T., 2000, PASJ, 52, 925
Kawakita, H., & Kobayashi, H., 2009, ApJ, 693, 388
Kawakita, H., & Watanabe, J., 1998, ApJ, 495, 946
Knight, M., 2013, CBET, 3731
Kobayashi, H., Bockelée–Morvan, D., Kawakita, H., Dello Russo, N., Jehin, E., et al., 2010, A&A, 509, 80
Kobayashi, H., Kawakita, H., Mumma, M. J., Bonev, B. P., Watanabe, J., & Fuse, T., 2007, ApJ, 668, 75
Korth, A., Marconi, M. L., Mendis, D. A., Krueger, F. R., Richter, A. K., et al., 1989, Nature, 337, 53
Kurucz, R. L., 2005, Mem. Soc. Astron, Ital. Suppl., 8, 189
Lew, H., 1976, Can. J. Phys., 54, 2028
Learn, J., 2001, Geophysical Research Letters, 27, 2425
Liang, M. –C., Cheng, B. –M,. Lu, H. –C, et al., 2007, ApJL, 657, L117
Limbach, H., Buntkowsky, G., Matthes, J., Gründemann, S., Pery, T., et al., ,
Lis, D. C., Biver, N., Bockelée–Morvan, D., Hartogh, P., Bergin, E. A., et al., 2013, ApJL, 774, L3

Lovell, A. J., Kallivayalil, N., Schloerb, F. P., Combi, B. R., Hansen, C., & Gembosi, T. I., 2004, ApJ, 613, 615

Lowe, D. J., & Thorneley, R. N. F., 1984, Biochem. J., 224, 895

Lunine, J. I., Engel, S., Rizk, B., & Horanyi, M., 2001, Icarus, 94, 333

Lutz, B. L., 1987, ApJ, 315, L147

Magee–Sauer, K., Mumma, M. J., DiSanti, M. A., Dello Russo, N., Gibb, E. L., et al., 2008, Icarus, 194, 347

Magee–Sauer, K., Mumma, M. J., DiSanti, M. A., Dello Russo, N., Gibb, E. L., & Bonev, B. P. 2008, Icarus, 194, 347

Magee–Sauer, K., Mumma, M. J., DiSanti, M. A., & Dello Russo, N. 2002, J. Geophys. Res., 107, 5096

Magee–Sauer, K., Mumma, M. J., DiSanti, M. A., & Dello Russo, N. 2001, DPS meeting, #33, #20.09

Manfroid, J., Jehin, E., Hutsemékers, D., Cochran, A., Zucconi, J. –M., et al., 2009, A&A, 503, 613

Manfroid, J., Jehin, E., Hutsemékers, D., Cochran, A., Zucconi, J. –M., et al., 2005, A&A, 432, 5

Marconi, M. L., Korth, A., Mendis, D.A., Lin, R. P., Mitchell, D. L., et al., 1989, ApJ, 343, L77

Marty, B., Chaussidon, M., Wiens, R. C., Jurewicz, A. J. G., & Burnett, D. S., 2011, Science, 332, 1533

Meech, K. J., & Svoren, J., 2004, in Comet II, ed. M. C. Festou, H. U. Keller, & H. A. Weaver (Tucson: Univ. Arizona Press), 317

Meier R., Owen, T. C., Matthews, H. E., Jewitt, D. C., Bockelée–Morvan, D., et al., 1998a, Science, 279, 842

Meier R., Owen, T. C., Jewitt, D. C., Matthews, H. E., Senay, M., et al., 1998b, Science, 279, 1707

Meier R., Wellnitz, D., Kim, S. J., & A'Hearn, M. F., 1998c, Icarus, 136, 268

Messenger, S., Stadermann, F. J., Floss, C., Nittler, L. R., & Mukhopadhyay, S., 2003, Space Science Reviews, 106, 155

Milam, S. N., Savage, C., Brewster, M. A., Ziurys, L. M., & Wycoff, S., 2005, ApJ, 634, 1126

Millar, T. J., Bennett, A., & Herbst, E., 1989, ApJ, 340, 906

Morbidelli, A., 2008, in Trans–Neptunian Objects and Comets (Saas–Fee Advanced Course 35. Swiss Society for Astrophysics and Astronomy), pp. 79–164

Morisawa, Y., Fushitani, M., Kato, Y., Hoshina, H., Simizu, Z., et al., 2006, ApJ, 642, 954

Mousis, O., Gautier, D., & Coustenis, A., 2002, Icarus, 159, 156

Mumma, M, J., & Charnley, S, B., 2011, ARA&A, 49, 471

Mumma, M. J., DiSanti, M. A., Magee–Sauer, K., et al., 2005, Science, 310, 270

Mumma, M. J., DiSanti, M. A., Dello Russo, N., Magee–Sauer, K., Gibb, E., & Novak, R., 2003, Adv. Space Res., 31, 2563

Mumma, M. J., Dello Russo, N., DiSanti, M. A., Magee–Sauer, K., Novak, R. E., et al., 2001a, Science, 292, 1334

Mumma, M. J., McLean, I. S., DiSanti, M. A., Larkin, J. E., Dello Russo, N., et al., 2001b, ApJ, 546, 1183

Mumma, M. J., Weissman, Paul R., & Stern, S. A., 1993, in Protostars and Planets III, pp. 1177–1252

Mumma, M. J., Weaver, H. A., & Larson, H. P., 1987, A&A, 187, 419

Murad, E., & Bochsler, P., 1987, Nature, 326, 366

Nakano, S., 2013, CBET, 3731

Noguchi, K., Aoki, W., Kawanomoto, S, et al., 2002, PASJ, 689, 1448

Noguchi, T., Ando, H., Izumiura, H., Kawanomoto, S., Tanaka, W., & Aoki, W., 1998, Proc. SPIE, 3355, 354

Oka, T., 2004, J. Mol. Spec., 228, 635

Onishi, R., Shinnaka, Y., Kobayashi, H., Kawakita, H., 2008, DPS meeting, #40, # 16.09

Pardanaud, C., Crovisier, J., Bockelée–Morvan, D., & Biver, N., 2007, Molecules in Space & Laboratory, Paris

Park, I. H., Wakelam, V., & Herbst, E., 2006, A&A, 449, 631

Podolak, M. & Prialnik, D., 1996, P&SS, 44, 655

Prialnik. D., Festiy, M. C., Keller, H. U. & Weaver, H. A., 2004, in Comets II, University of Arizona Press, Tucson, pp.359–387

Quack, M., 1977, Mol. Phys., 34, 477

Radeva, Y. L., Mumma, M. J., Bonev, B. P., DiSanti, M. A., Villanueva, G. L., et al., 2010, Icarus, 206, 764

Rodgers, S. D., & Charnley, S. B., 2008a, ApJ, 689, 1448

Rodgers, S. D., & Charnley, S. B., 2008b, MNRAS, 385, 48

Rodgers, S. D., & Charnley, S. B., 2002, MNRAS, 330, 660

Rosenberg, E. D. & Prialnik, D., 2007, New Astronomy, 12, 523

Rousselot, P., Pirali, O., P., Jehin, E., Vervloet, M., Hutsemékers, D., et al., 2014, ApJL, 780, L17

Schere, M., Havenith, M., Mauersberger, R., & Wilson, T. L., 1998, A&A, 335–1070

Schleicher, D. G., & Bair, A. N., 2008, LPICo, 1405, 8174

Schmidt, H.U., Wegmann, R., Huebner W.F. & Boice, D.C., 1988, Comp. Phys. Comm. 49, 17

Shinnaka, Y., Kawakita, H., Kobayashi, H., et al., 2011, ApJL, 782, L16

Shinnaka, Y., Kawakita, H., Kobayashi, H., Boice, D. C., & Martinez, S. E., 2012, ApJ, 749, 101

Shinnaka, Y., Kawakita, H., Kobayashi, H., Emmanuël, J., Jean, M., et al., 2011, ApJ, 729, 81

Shinnaka, Y., Kawakita, H., Kobayashi, H., & Kanda, Y., 2010, PASJ, 62, 263

Suto, M., & Lee, L. C., 1983, JCP, 78, 4515

Tajitsu, A., Aoki, W., Kawanomoto, S., & Narita, N., 2010, Publ. Natl. Astron. Obs. Japan, 13, 1

Tanner, C. V., Quack, M., & Schmidiger, D., 2013, J. Chem. Phys. A, 117, 10105

Tanner, C. V., Quack, M., & Schmidiger, D., 2011, Faraday Discuss., 150, 118

Thekaekara, M. P., 1974, Apl. Opt., 13, 51

Uy, D., Cordonnier, M., & Oka, T., 1997, Phys. Rev. Lett., 78, 3844

Villanueva, G. L., Mumma, M. J., Bonev, B. P., DiSanti, M. A., Gibb, E. L., et al., 2009, ApJ, 690, L5

Villanueva, G. L., Bonev, B. P., Mumma, M. J., Magee–Sauer, K., DiSanti, M. A., et al., 2006, ApJ, 650, 87

Wampfler, S. F., Jorgensen, J. K., Bizzarro, M., & Bisschop, S. E., 2014, astro–ph, 1408.0285v1

Waters, L. B. F., Molster, F. J., de Jong, T., Beintema, D. A., Waelkens, C. et al., 1999, A&A, 315, L361

Weaver, H. A., A'Hearn, M. F., Arpigny, C., Combi, M. R., Feldman, P. D., et al., 2009, Conference on Asteroids, Comets, Meteors 2008 held July 14–18, 2008, in Baltimore, Maryland. LPI Contribution No. 1405, paper id. 8216

Weaver, H. A., Sekanina, Z., Toth, I., Delahodde, C. E., Hainaut, O. R., et al., 2001, Science, 292, 1329

Wegmann, R., Jockers, K., & Benev, T., 1999, P&SS, 47, 745

Willacy, K., Klahr, H. H., Millar, T. J., & Henning, Th., 1998, A&A, 338, 995

Wilson, T. L., & Rood, R., 1994, ARA&A, 32, 191

Wirström, E, S., Charnley, S. B., Cordiner, M. A., & Milam, S. N., 2012, ApJ, 757, L11

Woodward, C. E., Kelley, M. S., Bockelée–Morvan, D., & Gehrz, R. D., 2007, ApJ, 671, 1065

Wu, S., Chen, Y., Yang, X., Guo, Y., Liu, Y., Li, Y., Buenker, R. J., & Jensen, P., 2004, J. Mol. Spec., 225, 96

Wu, S., Yang, X., Guo, Y., Zhuang, H., Liu, Y., & Chen, Y., 2003, J. Mol. Spec., 219, 258

Yan, L., Dapper, C. D., George, S. J., Wang, H., Mitra, D., et al., 2011, Eur. J. Inorg. Chem., 2011, 2064

Zecca, A., Karwasz, P., & Brusa, R. S., 1992, Phys. Rev. A, 45, 2777

Zhang, G., & Li, H. –B., 2001, Chin. J. Astron. Astrophys., 1, 555

APPENDIXES

APPENDIX A: DATA REDUCTION OF HDS

In this Appendix, I describe the data reduction procedures and calibration of the observational data obtained by the Subaru Telescope with the HDS. This material is based on the Subaru Telescope's homepage (*). Below is a brief summary of each item.

(*) http://www.naoj.org/Observing/Instruments/HDS/hdsql-e.html

A.1. OVERSCAN

The HDS has two CCDs (RED and BLUE) and readout was carried out at two points for each CCD. Independent bias frames are not subtracted; instead, the "over scan region" at the center of the frame is averaged, and the average count is then subtracted from the object frames. This correction is handled by the "overscan" task prepared in the HDS. The overscan task calculates the average ADU in the scan regions in each frame and subtracts this value from the entire image. This process is very similar to bias subtraction. At the same time, it changes the counts in the frame from ADU to electron numbers through a conversion factor (number of electrons = 1.7 × ADU).

A.2. BIAS AND/OR DARK SUBTRACTIONS

This step subtracts the Bias, Dark, or both from the object frames and is followed by another step that masks bad pixels. The BIAS does not need to be subtracted from the target frames. The dark counts are automatically scaled referring to the exposure times of the dark and target frames.

A.3. MASKING BAD PIXELS

Some bad columns exist in each CCD of HDS. These bad columns corrupt the scientific data, and the affected regions must be corrected.

A.4. LINEARITY CORRECTION OF HDS'S CCDs

Significant nonlinearity was found in the CCDs of HDS at higher electron

numbers (>10000 e-; Tajitsu et al., 2010). This nonlinearity is corrected by the "hdslinear" task.

A.5. COSMIC-RAY REJECTION

During long-term exposure, counts originating from cosmic rays are collected. The effect of cosmic rays is rejected by the "wacosm11" task which applies a median filter to the object frame at first out-stand pixels, then, replace counts of these pixels with extrapolated values. The important parameter of this task is the baseline count "cr_base". This should be similar to the peak count of the object frame. Smaller value is better to find cosmic-ray hits. But it is afraid that smaller value can lead misunderstanding real count as cosmic ray hits.

A.6. SCATTERED LIGHT SUBTRACTION

I obtained a curved surface by interpolating the gaps between traced orders and subtracting the fitted result from all frames. This step uses the "apscatter" task.

A.7. FLAT FIELDING

Flat fielding simultaneously corrects for nonuniformities of the transmittance and reflectance of the optical elements, the varying pixel-to-pixel sensitivities of the CCDs, and the fringe patterns appearing on the detector.

To correct for these effects, I constructed a flat fielding frame from instrumental flat images.

A.8. APERTURE EXTRACTION

I extracted 11–32 spectral images from each CCD at different grating settings, using "aptrace" and "apall" tasks includes the IRAF software.

A.9. WAVELENGTH CALIBRATION

I calibrated only the wavelength of the HDS (not the spatial direction) because the spatial direction on the CCD is parallel to the lines of the CCD.

The wavelength accuracy of the final spectra is better than ±0.01 Å in all wavelength regions.

A.10. SENSITIVITY CALIBRATION

I calibrated the flux using a standard star taken in a very close area of the sky. This method conserves the flux information of the target. In HDS, the blaze function of the echelle orders might be relatively unstable and sensitive to the telescope position and/or focus offsets. Therefore, as calibrators, I used both spectrophotometric standard stars and some normal Early type star (earlier than A-type stars) and a spectrum-type and the magnitude are well-known objects as normal stars.

Flux calibration of object frames needs a three-step process. First, the flux of the standard stars is measured using the "standard" task. Second, a sensitivity function is created by the "sensfunc" task. Finally, the intensity is calibrated from electron number to flux using the "calibrate" task.

A.11. MAKING A COMBINED SPECTRUM

I combined all orders of the target using the "scombine" task.

APPENDIX B: DATA ANALYSIS OF HIGH-DISPERSION OPTICAL SPECTRA IN COMET

In this Appendix, I explain the data analysis of high-dispersion spectra (after calibration). Calibrated spectra taken by ground-based telescopes include the cometary gas (emissions of volatiles) and dust (reflected sunlight by the cometary dust particle in the coma) components, the absorptions by the telluric atmosphere, and the incident light to the instrument, which is blurred thorough the optical pass of the instrument (called the instrumental profile). As I am studying cometary volatiles, I am interested in the gas component. Therefore, I remove the continuum components (the sunlight reflected by the cometary dust particles and absorption lines introduced by the telluric atmosphere) from the calibrated comet spectra. These unwanted continuum components are removed by the following steps.

B.1. CONTINUUM SUBTRACTION

For continuum subtraction from the cometary spectra, I modeled the reflected sunlight between the high-dispersion solar spectrum (Kurucz, 2005) and the color spectrum of cometary dust grains at different wavelengths. The modeled spectrum of reflected sunlight was convolved with both the telluric transmittance spectrum calculated by the Line-By-Line Radiative Transfer Model (LBLRTM; Clough & Iacono, 1995) and the instrumental profile approximated by a Gaussian function, using the "gauss" task of IRAF software (see Figure B.2).

B.1.1. SYNTHESIZED SPECTRUM OF SUN

As the solar spectrum, I employed the high resolution Kitt Peak Irradiance Atlas from 300 to 1000 nm with the telluric lines removed (Figure B.1; Kurucz, 2005). High-resolution solar spectra (S/N ratio=10^4; resolving power=10^6) were taken by J. Brault and L. Testerman at the Kitt Peak Observatory. Wavelength coverage is 300 to 1000 nm. Although the flux spectrum from 300 to 1300 nm has been already published as the Solar Flux

Atlas (Kurucz et al., 1984), it includes broad O_3 and O_2 dimer (or $[O_2]_2$) features, and telluric absorptions have been removed. Therefore, the spectrum of the telluric absorptions was computed using HITRAN (Rothman et al., 2005) and other line data for H_2O, O_2, and CO_2. The line parameters were adjusted to approximately match the observed spectra (Kurucz, 2005).

For the solar spectrum, I shifted to the cometary center wavelengths (or to any other wavelength of the gas emission) corresponding to the relative velocity between the comet and the Sun and approximated the instrumental profile by the Gaussian function using the "gauss" task of IRAF software.

B.1.2. SYNTHESIZED SPECTRUM OF TELLURIC ABSORPTION

The LBLRTM code is an accurate line-by-line model that calculates the spectral transmittance and radiance with efficiency and high flexibility. Detailed information is provided on the Web page of Atmospheric and Environmental Research (*1). I calculated an arbitrary spectrum by specifying arbitrary observational and atmospheric conditions (such as the observatory location, zenith angle of the observation, temperature, pressure, and humidity at the Earth's surface) in arbitrary wavelength regions.

For the telluric absorption spectrum, I also shifted to the cometary center wavelengths corresponding to the relative velocity between the comet and the Earth. The instrumental profile is again approximated by the Gaussian function using the "gauss" task of IRAF software.

*1: http://rtweb.aer.com/lblrtm.html

B.1.3. ESTIMATION OF THE COLOR SPECTRUM OF DUST GRAINS

The color spectrum of cometary dust grains was estimated from the divided spectrum (the calibrated spectrum divided by the convolved spectrum of the solar and telluric lines spectra) using the "background" task of IRAF software.

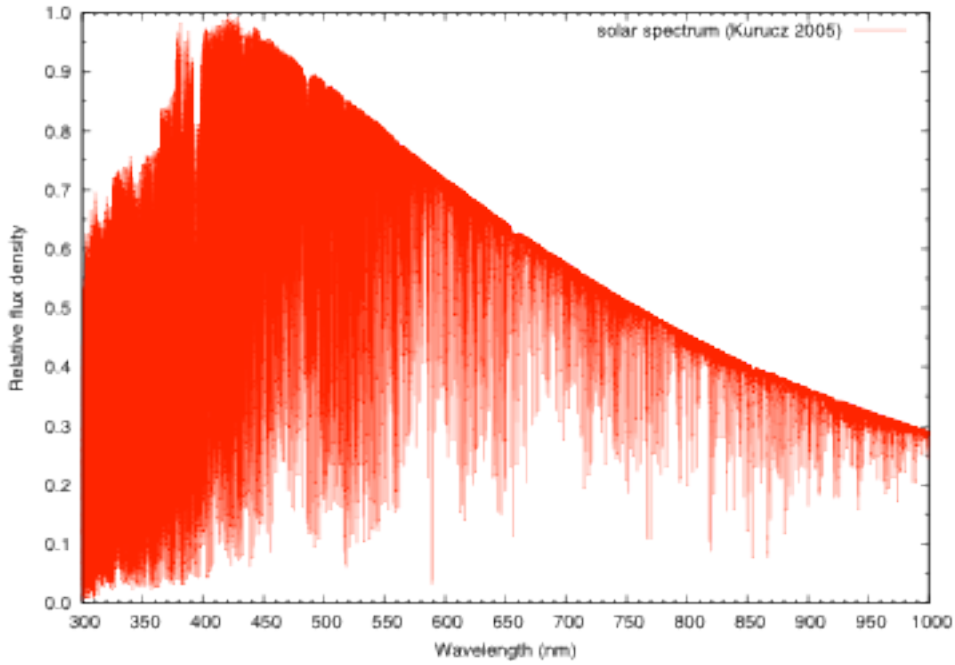

Figure B.1 A high-resolution Kitt Peak Irradiance Atlas from 300 to 1000 nm with the telluric lines removed (Kurucz, 2005).

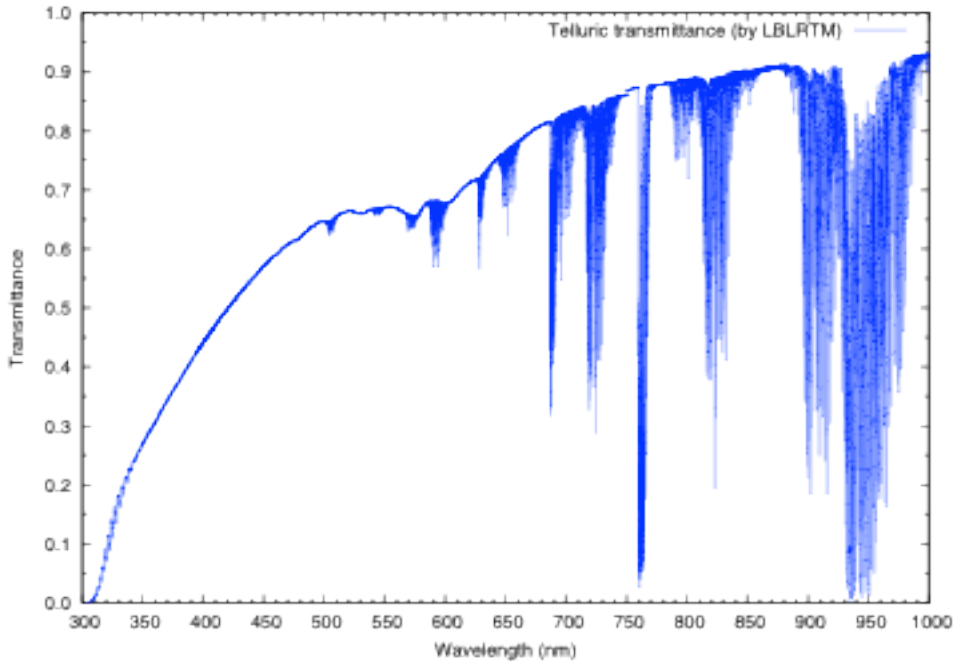

Figure B.2 Synthesized spectrum of the telluric transmittance of comet C/2012 S1 (ISON), calculated by the LBLERTM code.

APPENDIX C: CALCULATION OF NUMBER DENSITY DISTRIBUTION OF WATER DIMERS IN THE COMA

In this Appendix, I explain the method for calculating the number density of water dimers in the coma at each nucleocentric radius. The calculation proceeds through the following steps. The formation processes of water dimers in the coma are neutral–neutral three-body reactions of water and ion–molecule reactions with H_3O^+, and the dissociation process is thermal evaporation under thermal equilibrium conditions. Formation process should release the excess energy of the formation reaction of water dimers because the bonding energy of water cluster is weak.

C.1. FORMATION PROCESSES OF WATER DIMERS

As mentioned above, water dimers form by (1) neutral–neutral three-body reactions of water and (2) ion–molecule reactions with H_3O^+.

First, the number of water dimers [/s/m^3] produced by the neutral–neutral three-body reactions of water is calculated by the following formula. This formula is based on three-body collisions between molecules of the same type (in this case, H_2O molecules).

$$N[(H_2O)_2] = q_{H2O-H2O}\sigma_{H2O-H2O}v_{thermal,H2O}\frac{d_{H2O}}{l_{H2O}}N[H_2O]^2 \quad , (C.1)$$

where

$N[(H_2O)_2]$ is the production number of $(H_2O)_2$ dimers [/s/m^3],

$N[H_2O]$ is the number density of water [/m^3],

$q_{H2O–H2O}$ is the rate of water dimers formed by collisional reactions with the reaction intermediate $(H_2O)_2$* and H_2O monomers ($0 < q_{H2O\text{-}H2O} < 1$),

$\sigma_{H2O–H2O}$ is the collisional crosssection between waters ($\pi d_{H2O}^2 = \pi(1 \times 10^{-10})^2$ [/m^2]),

$v_{thermal,H2O}$ is the mean velocity of water in thermodynamic equilibrium [m/s],

d_{H2O} is the geometric radius of a water monomer [m], and

l_{H2O} is the mean free path of water under the thermodynamic

equilibrium condition [m].

The mean velocity of water monomer is calculated under the thermal equilibrium condition:

$$v_{\text{thermal.,H2O}} = \sqrt{\frac{8k_{\text{B}}T}{\pi \text{m}}}, \text{ (C.2)}$$

where

k_{B}, denotes the Boltzmann constant (1.380658×10^{-26} J/K),

T denotes the gas temperature [K], and

m is mean molecular mass (the mass of H_2O, computed as <mean molecular mass> × <unified atomic mass unit>, is $16 \times 1.6605 \times 10^{-27} \sim 2.6568 \times 10^{-26}$ kg)).

Moreover, from the molecular diameter and the mean free path of two-body collisions, we can estimate the number ratio of three-body collisions to two-body collisions (assuming identical molecules).

Next, I discuss the ion–molecule reactions with H_3O^+. A production number of water dimers can estimate from follows formula:

$$N[(H_2O)_2] = k_{\text{Langevin}} q_{\text{H2O}-\text{H3O+}} N[H_3O^+] N[H_2O] \quad , \text{(C.3)}$$

where

$N[(H_2O)_2]$ is the production number of $(H_2O)_2$ dimers [/s/m^3],

$N[H_2O]$ is the number density of water [/m^3]

$N[H_3O^+]$ is the number density of H_3O^+ [/m^3]

k_{Langevin} is the Langevin rate coefficient, corresponding to the reaction rate of the ion–molecular chemistry [m^3/s]

$q_{\text{H2O}-\text{H3O+}}$ is the formation rate of water dimers by the reaction of H_3O^+ and free electrons ($0 < q_{\text{H2O-H3O+}} < 1$).

Here, the Langevin rate coefficient corresponds to the crosssection between two molecules times the mean velocity of the colliders. The Langevin rate coefficient is independent of temperature.

C.2. DISSOCIATION PROCESSES OF WATER DIMERS

Water dimers are considered to dissociate by thermal evaporation. The

evaporation rate of the water clusters, determined by the unimolecular dissociation theory (UDT) (k_{UDT}), increases rapidly around 30 K (see Figure 5.1 of Bormer et al., 2013). The UDT evaporation rate is expressed as follows:

$$k_{UDT}(n) = n^{2/3}\omega_{H2O}\exp\left(\frac{H_v}{kT_c}\right), \quad \text{(C.4)}$$

where

n is the cluster size,

ω_{H2O} is the vibrational frequency of a water molecule within the cluster (proposed as 2.68×10^{12} /s by Oka & Hara, 2007),

H_v is the latent heat of vaporization of water clusters (equal to 1.46, 2.17, 1.619, 1.44, 2.13, and 2.02×10^{-20} J for n = 2, 3, 4, 6, 8, and 10 molecules, respectively),

k is the Boltzmann constant, and

T_c is the cluster temperature.

Water clusters are very sensitive to temperature because they are weakly bound and thus easily separated.

C.3. COMA ENVIRONMENT

To calculate the number density of water dimers in the coma, we require certain parameters, such as the temperature distributions (which depend on the water production rate and heliocentric distance) and the spatial distributions of H_3O^+ ions in the coma.

For the gas temperatures as a function of radial distance from the nucleus, I adopted the gas temperature distributions in the coma estimated from the water production rates of 10^{27}, 10^{28}, 10^{29} and 10^{30} /s (Bockelée–Morvan and Crovisier 1987). Once released from the nucleus, the gas temperature immediately decreases under adiabatic expansion because solar radiation exerts little effect (τ>1) in the inner coma. Relatively far from the nucleus (~100 km), the gas is heated by solar radiation.

I used the spatial distribution of H_3O^+ in comet 1P/Halley observed by the Giotto spacecraft (Ip, 1989). Based on these data, the observed water production rate in 1P/Halley is approximately 10^{30} /s.

C.4. CALCULATION OF NUMBER DENSITY OF WATER DIMERS

The formation number of water dimers is assumed to be balanced with the dissociation number of dimers in a given region. The number density of water dimers is calculated by the following system of equations:

$$k_{UDT}(2)N[(\mathrm{H_2O})_2] = q_{\mathrm{H2O-H2O}}\sigma_{\mathrm{H2O-H2O}}v_{thermal,\mathrm{H2O}}\frac{d_{\mathrm{H2O}}}{l_{\mathrm{H2O}}}N[\mathrm{H_2O}]^2 + k_{\mathrm{Langevin}}q_{\mathrm{H2O-H3O+}}N[\mathrm{H_3O^+}]N[\mathrm{H_2O}], \quad \text{(C.5)}$$

$$N[(\mathrm{H_2O})_{\mathrm{total}}] = \frac{Q[\mathrm{H_2O}]}{4\pi r v_{\mathrm{exp.,H_2O}}}\exp\left(-\frac{t}{\tau_{\mathrm{H_2O}}}\right) = N[\mathrm{H_2O}] + 2N[(\mathrm{H_2O})_2], \quad \text{(C.6)}$$

Solving the above equations, I obtainI solve the above system of equations.

$$\left\{q_{\mathrm{H2O-H2O}}\sigma_{\mathrm{H2O-H2O}}v_{\mathrm{thermal,H2O}}\right\}N[\mathrm{H_2O}]^2 + \left\{k_{\mathrm{Langevin}}q_{\mathrm{H2O-H3O+}}N[\mathrm{H_3O^+}] + \frac{1}{2}k_{\mathrm{UDT}}(2)\right\}N[\mathrm{H_2O}] - \frac{1}{2}k_{\mathrm{UDT}}(2)N[(\mathrm{H_2O})_{\mathrm{total}}] = 0 \quad \cdots \text{(C.7)}$$

(C.7) is a quadratic equation that can be solved for $N[(\mathrm{H_2O})_2]$.